INNOVATIVE ELECTROCHEMICAL SENSOR DEVELOPMENT BY USING DISPOSABLE ELECTRODES FOR ANTIBIOTIC CONCENTRATION MEASUREMENT ACROSS DIVERSE SOURCES



By

Tahmina Akter, M. Sc.

ID-21MSCHEM002F

A thesis submitted in partial fulfillment of the requirements for the degree of
MASTER of SCIENCE in Chemistry

Department of Chemistry
CHITTAGONG UNIVERSITY OF ENGINEERING AND TECHNOLOGY
March 2025

Declaration

I hereby declare that the work contained in this Thesis has not been previously submitted to meet the requirements for an award at this or any other higher education institution. To the best of my knowledge and belief, the Thesis contains no material previously published or written by another person except where due reference is cited. Furthermore, the Thesis complies with the PLAGIARISM and ACADEMIC INTEGRITY regulations of CUET.

Tahmina Akter
Student ID - 21MSCHEM002F
Department of Chemistry
Chittagong University of Engineering & Technology (CUET)

Copyright © Tahmina Akter, 2025.
This work may not be copied without permission of the author or Chittagong University of Engineering & Technology.

Dedication

To my beloved parents, siblings, teachers, and supportive life partner, and countless others who've contributed to my journey, whether through a kind word, a helping hand, or a moment of inspiration.

List of Publications

Journal Articles

1. “Advanced Ciprofloxacin Quantification: A Machine Learning and Metaheuristic Approach Using Ultrasensitive Chitosan-Gold Nanoparticle Based Electrochemical Sensor” Yunus Ahmed, Tahmina Akter, Meherunnesa Prima, Keya Rani Dutta, Sanjida Mukut, Mohebul Ahsan, Md Mahbubur Rahman, M.K. Mohammad Ziaul Hyder, Journal of Environmental Chemical Engineering. 2025, 13(1) 115094; DOI: https://doi.org/10.1016/j.jece.2024. 115094. (IF: 7.4, Q1)

Approval/Declaration by the Supervisor

This is to certify that Keya Rani Dutta has carried out this research work under our supervision, and that she has fulfilled the relevant Academic Ordinance of the Chittagong University of Engineering and Technology, so that she is qualified to submit the following Thesis in the application for the degree of MASTER of SCIENCE in Chemistry. Furthermore, the Thesis complies with the PLAGIARISM and ACADEMIC INTEGRITY regulations of CUET.

Dr. Yunus Ahmed (Supervisor)

Associate Professor

Department of Chemistry

Chittagong University of Engineering & Technology

Dr. M.K. Mohammad Ziaul Hyder (Co-supervisor)

Professor

Department of Chemistry

Chittagong University of Engineering & Technology

Acknowledgement

All praise to Merciful and Almighty Allah (SWT), who gave me the capability and opportunity to successfully complete the research and submit this thesis for the degree of Master of Science (M.Sc.) in Chemistry.

I am proud to express my heartfelt gratitude, wholehearted indebtedness, sincere appreciation, and profound regard to my honorable teacher and principal supervisor, Dr. Yunus Ahmed, Associate Professor, Department of Chemistry, CUET, Chattogram, for his academic guidance, constant untiring supervision, cordial support, endless encouragement, precious advice, guidance, enthusiasm, and helpful discussion throughout the entire period of research work and preparation of this thesis. This achievement would not be possible without his unquenched thrust of research, academic supervision, continuous encouragement, and constructive suggestions. I want to thank my co-supervisor, Dr. M.K. Mohammad Ziaul Hyder, Department of Chemistry, CUET for his guiding and mentoring me in my research.

I'd also like to thank the teachers and staff at CUET's Department of Chemistry for their collaboration, continual inspiration, and encouragement. I am also grateful to my friends in the Chemistry department, CUET, for their valuable discussion and cooperation, especially Keya Rani Dutta, Akser Alam Siddiqua Maya, Md. Mahfujur Rahman, Syed Julkar Nine, Sharmin Nahar Chowdhury Nepu and Meherunnesa Prima.

I am expressing my heartfelt gratitude to my parents, Md. Shah Alam and Johora Begum; my siblings, Md. Mohsin, Md. Motaleb, Md. Robiul Hasan Mamun and Taslima Akter; and my beloved husband, Md. Rubel, for their unwavering support, encouragement, and sacrifices during the tenure of this work.

Abstract

The prompt detection of trace amounts of antibiotics is crucial for environmental surveillance and the entire ecosystem. An electrochemical sensor has been designed to precisely detect the concentration of ciprofloxacin (CIP) utilizing gold nanoparticles coated with chitosan on a glassy carbon electrode (AuNPs/CHI/GCE). The influence of four key electrochemical parameters, viz., scan rate, pH, temperature, and electrode potential, on the satisfactory detection of CIP was also studied. The accumulated analysis generated one output parameter, which was current intensity, resulting in 2319 data points. This dataset was then used in machine learning models to predict the maximum cathodic current for CIP detection. The best model and its optimal settings of parameters were determined after comparing ten different ML models: AdaBoost, Bagging, CatBoost, Decision Tree, Extra Trees, Gradient Boosting, HistGradientBoosting, LightGBM, RandomForest, and XGBoost, the performance of the models has been evaluated by metrics Coefficient of Determination (R^2), Mean Square Error (MSE), Root Mean Square Error (RMSE), Mean Absolute Error (MAE) and Median Absolute Error (MedAE). It was concluded that CatBoost is the best model both on cumulative performance and final metrics results. These include an R^2 score of 0.9985, MSE of 1.468, RMSE of 1.225, MAE of 0.672, and MedAE of 0.375. Under optimal conditions, the cathodic current for CIP detection by the CB Model was approximately 128.51 μA, with a potential of 0.47 V, scanning rate of 98 mV/sec, temperature of 31^0C, and pH of the reaction medium at 6.75. These parameters were further used in constructing a calibration curve using differential pulse voltammetry (DPV), accurately determining the presence of CIP in known and unknown samples. The LOD, LOQ, and the specific sensitivity of the developed sensor (AuNPs/CHI/GCE) were 0.049, 0.232 μM, and 786.72 $\mu A\ \mu M^{-1}\ cm^{-2,}$ respectively. Finally, a new electrode was fabricated using disposable materials, specifically from the graphite rod of a dry cell. We evaluated how effectively the AuNPs-modified Gr electrode sensor could detect traces of CIP in ultra-pure water samples. The experiment yielded a limit of detection (LOD) of 0.0517 nM and a limit of quantification (LOQ) of 1.723 nM. The findings indicate that this newly developed electrode can quickly and accurately identify ciprofloxacin in water samples, making it valuable for rapid and sensitive analysis.

বিমূর্ত

পরিবেশগত নজরদারি এবং সম্পূর্ণ পরিবেশের জন্য অতি সামান্য পরিমাণে অ্যান্টিবায়োটিকের দ্রুত সনাক্তকরণ অত্যন্ত গুরুত্বপূর্ণ। সিপ্রোফ্লোক্সাসিন (CIP) এর ঘনত্ব সঠিকভাবে সনাক্ত করতে একটি ইলেক্ট্রোকেমিক্যাল সেন্সর ডিজাইন করা হয়েছে, যা কাচের কার্বন ইলেক্ট্রোডে (AuNPs/CHI/GCE) কাইটোসান দ্বারা আবৃত সোনার ন্যানোকণা ব্যবহার করে। CIP এর সন্তোষজনক সনাক্তকরণের উপর চারটি প্রধান ইলেক্ট্রোকেমিক্যাল প্যারামিটারের প্রভাব যথা স্ক্যান রেট, pH, তাপমাত্রা এবং ইলেক্ট্রোড পোটেনশিয়াল নিয়েও গবেষণা করা হয়েছে। সংগৃহীত বিশ্লেষণ থেকে একটি আউটপুট প্যারামিটার তৈরি হয়েছে, যা হলো কারেন্ট ইনটেনসিটি, যা মোট ২৩১৯টি ডেটা পয়েন্ট উৎপন্ন করেছে। এই ডেটাসেটটি তারপর মেশিন লার্নিং মডেলে ব্যবহার করা হয়েছে যাতে CIP সনাক্তকরণের জন্য সর্বোচ্চ ক্যাথোডিক কারেন্ট পূর্বাভাস দেওয়া যায়। দশটি ভিন্ন মেশিন লার্নিং মডেলের মধ্যে তুলনা করে সেরা মডেল এবং এর অপটিমাল প্যারামিটার সেটিংস নির্ধারণ করা হয়েছে: AdaBoost, Bagging, CatBoost, Decision Tree, Extra Trees, Gradient Boosting, HistGradientBoosting, LightGBM, RandomForest, এবং XGBoost। মডেলগুলির কর্মক্ষমতা মূল্যায়ন করা হয়েছে নিম্নলিখিত মেট্রিক্স দ্বারা: নির্ধারণ সহগ (R^2), গড় বর্গ ত্রুটি (MSE), গড় বর্গমূল ত্রুটি (RMSE), গড় পরম ত্রুটি (MAE) এবং মধ্যমা পরম ত্রুটি (MedAE)। এটা সিদ্ধান্ত নেওয়া হয়েছে যে CatBoost হলো সেরা মডেল, যা সঞ্চিত কর্মক্ষমতা এবং চূড়ান্ত মেট্রিক্স ফলাফলের উপর ভিত্তি করে। এর মধ্যে R^2 স্কোর ০.৯৯৮৫, MSE ১.৪৬৮, RMSE ১.২২৫, MAE ০.৬৭২, এবং MedAE ০.৩৭৫ অন্তর্ভুক্ত রয়েছে। অপটিমাল অবস্থায়, CB মডেল দ্বারা CIP সনাক্তকরণের ক্যাথোডিক কারেন্ট ছিল প্রায় ১২৮.৫১ μA, পোটেনশিয়াল ০.৪৭ V, স্ক্যানিং রেট ৯৮ mV/sec, তাপমাত্রা ৩১০°C, এবং বিক্রিয়া মাধ্যমের pH ৬.৭৫। এই প্যারামিটারগুলি পরবর্তীতে ডিফারেনশিয়াল পালস ভোল্টামেট্রি (DPV) ব্যবহার করে একটি ক্যালিব্রেশন কার্ভ তৈরি করতে ব্যবহৃত হয়েছে, যা জ্ঞাত এবং অজ্ঞাত নমুনায় CIP এর উপস্থিতি সঠিকভাবে নির্ধারণ করতে সক্ষম। তৈরি সেন্সর (AuNPs/CHI/GCE) এর LOD, LOQ এবং বিশেষ সংবেদনশীলতা ছিল যথাক্রমে ০.০৪৯, ০.২৩২ μM এবং ৭৮৬.৭২ $\mu A\ \mu M^{-1}\ cm^{-2}$। অবশেষে, একটি নতুন ইলেক্ট্রোড তৈরি করা হয়েছে যা ব্যবহারযোগ্য উপকরণ থেকে তৈরি, বিশেষ করে শুষ্ক কোষের গ্রাফাইট রড থেকে। আমরা পরীক্ষা করেছি যে AuNPs-পরিবর্তিত Gr ইলেক্ট্রোড সেন্সর কতটা কার্যকরভাবে অতি বিশুদ্ধ জলের নমুনায় CIP এর সনাক্তকরণ করতে পারে। পরীক্ষাটি একটি সনাক্তকরণের সীমা (LOD) ০.০৫১৭ nM এবং পরিমাপের সীমা (LOQ) ১.৭২৩ nM প্রদান করেছে। এই ফলাফলগুলি নির্দেশ করে যে এই নতুনভাবে তৈরি ইলেক্ট্রোডটি জলের নমুনায় সিপ্রোফ্লোক্সাসিন দ্রুত এবং সঠিকভাবে সনাক্ত করতে পারে, যা দ্রুত এবং সংবেদনশীল বিশ্লেষণের জন্য মূল্যবান।

Table of Contents

Declaration i

Dedication ii

List of Publications iii

Approval/Declaration by the Supervisor iv

Acknowledgement v

Abstract vi

বিমূর্ত vii

Table of Contents viii

List of Figures xi

List of Tables xiv

Nomenclature xv

Acronyms and Abbreviations xvi

Chapter 1: INTRODUCTION 1

1.1 BACKGROUND 1

1.2 CONTEXT OF THIS RESEARCH 3

1.3 AIMS AND OBJECTIVES 5

1.4 SIGNIFICANCE, SCOPE AND DEFINITIONS 6

1.5 THESIS OUTLINE 6

Chapter 2: LITERATURE REVIEW 7

2.1 BACKGROUND 7

2.2 DISCUSSION OF ELECTROMETHODOLOGIES 9

2.2.1 Cyclic Voltammetry 10

2.2.2 Square Wave Voltammetry 12

2.2.3 Differential Pulse Voltammetry 13

2.2.4 Linear Sweep Voltammetry 14

2.2.5 Electrochemical Impedance Spectroscopy 14

2.2.6 Chronoamperometric 15

2.3 MODIFICATION PROCEDURE OF ELECTRODE.....15
2.4 USES OF NANOPARTICLES IN ELECTROCHEMISTRY 19
2.4.1 Carbon Based Nanomaterials 20
2.4.2 Metal Nanoparticles 21
2.4.3 Metal Organic Framework 22
2.4.4 Quantum Dots.....24
2.4.5 Bio-Functional Materials 25
2.4.6 Others 26
2.5 ELECTROCHEMICAL BEHAVIOUR OF CIPROFLOXACIN 27
2.6 KEY KNOWLEDGE GAPS AND FUTURE DIRECTIONS 29
2.6.1 Assessment of Complex Pollution in Natural Water Bodies.....29
2.6.2 Scaling-up Application from the lab to the Pilot-scale 29
2.6.3 Development of cost-effective and high-performance plants 30
2.6.4 Comprehensive by-product analysis and toxicity assessment.....31
2.6.5 Environmental impact and sustainability assessment 31
Chapter 3: MATERIALS AND METHODOLOGY 32
3.1 CHEMICAL AND REAGENTS.....32
3.2 INSTRUMENTS.....32
3.3 FABRICATION OF WORKING ELECTRODE (WE) 33
3.4 ELECTROCHEMICAL MEASUREMENT PROCEDURE 33
3.5 DATA ANALYSIS AND COLLECTION 35
3.5.1 Coefficient of Determination (R^2) 36
3.5.2 Mean Square Error (MSE) 36
3.5.3 Root Mean Square Error (RMSE) 36
3.5.4 Mean Absolute Error (MAE) 36
3.5.5 Median absolute error (MedAE) 36
3.6 MACHINE LEARNING TECHNIQUES AND MODELLING 37
3.7 DESCRIPTIONS OF TEN MACHINE LEARNING MODELS 37
3.7.1 Gradient Boosting (GB) 37

3.7.2 HistGradientBoosting (HGB) 38
3.7.3 Extreme Gradient Boosting (XGBoost) 38
3.7.4 Light Gradient Boosting Machine (LGBM) 39
3.7.5 CatBoost (CB) 40
3.7.6 Bagging 41
3.7.7 Random Forest (RF) 41
3.7.8 Extra Trees (ET) 42
3.7.9 Decision Tree (DT) 42
3.7.10 AdaBoost 43
3.8 PREPARATION OF DISPOSABLE ELECTRODE 43
Chapter 4: RESULTS AND DISCUSSION 45
4.1 ELECTROCHEMICAL CHARACTERIZATION OF ELECTRODE 45
4.2 ELECTROCHEMICAL BEHAVIOUR OF CIPROFLOXACIN 50
4.2.1 Effect of Scan Rate 51
4.2.2 Effect of Solution pH 52
4.2.3 Effect of Temperature 55
4.3 DESCRIPTIVE STATISTICS 56
4.4 MODEL PERFORMANCE EVALUATION 58
4.5 NORMALISED IMPORTANCE OF FACTORS UNDER THE MODELS71
4.6 BEST MODEL AND ITS VALIDATION 73
4.7 ELECTROCHEMICAL QUANTITATIVE DETERMINATION OF CIP 75
4.8 QUANTITATIVE ANALYSIS USING DISPOSABLE ELECTRODE 77
Chapter 5: CONCLUSION & RECOMMENDATION 79
5.1 GENERAL CONCLUSION 79
5.2 KEY FINDINGS 80
5.3 LIMITATION OF THE STUDY 80
5.4 RECOMMENDATION FOR FURTHER STUDY 81
REFERENCES 82

List of Figures

Fig. No. **Figure Caption** **Page No.**

Figure 2.1 In CV (A) The potential (in relation to RE) is applied to the WE in CV. It shows that the potential starts at the lowest potential value (E1), increases to its greatest potential value (E2), and then decreases to its lowest potential value (E1); (B) Plotting the current caused by this potential change over time. (C) shows the current as a function of potential, is called a cyclic voltametric curve; (D) A three-electrode potentiostatic experimental setup for anodic biofilm. 11

Figure 2.2 Schematic voltammograms. To report CV data, US and IUPAC conventions are commonly used [76]. 12

Figure 2.3 Schematic illustration of electrochemical sensor for ofloxacin (OFL) detection. GCEs were directly modified using a picosecond laser 17

Figure 2.4 Various methods of nanoparticles synthesis [105] 19

Figure 2.5 Synthesis of metal-organic frameworks (MOFs) involves combining metal ions and clusters with organic linkers to create a cross-linked network. 23

Figure 4.1 Cyclic voltammograms of (a) bare and modified GCE, (b) AuNPs/ CHI-modified GCE, (c) linear plots of anodic and cathodic peak currents of AuNPs/ CHI-modified GCE and (d) EIS spectra of bare and modified GCE (Inset- Randles equivalent circuit model). The measurements were recorded in 5 mM $K_4[Fe(CN)_6$ and 0.1 M KCl at a scan rate of 100 mV/sec. 48

Figure 4.2 Cyclic voltammograms of (a) bare GCE, (c) CHI-modified GCE, and (e) AuNPs-modified GCE, recorded in a 0.1 M KCl solution containing 5 mM $Fe(CN)_6^{3-/4-}$. Corresponding linear plots of anodic and cathodic peak currents versus the square root of the scan rate are shown in (b), (d), and (f), respectively. 49

Figure 4.3 Cyclic voltametric response of GCE, CHI/GCE, AuNPs/GCE, AuNPs/CHI/GCE with 0.5 μM CIP in 0.1 M phosphate buffer at the scan rate and voltage potential was 50 m mV/sec and 0.0 to 1.2 V respectively..... 50

Figure 4.4 (a) CV responses of CIP on AuNPs/CHI/GCE at different scan rate ranging from 12.5 to 100 mV/sec in 0.5 μM ciprofloxacin (0.1 M PBS at pH 7); (b) linear plot between peak current and scan rate; (c) linear plot between potential vs log scan rate. 51

Figure 4.5 (a) Cyclic Voltammetry responses of CIP on AuNPs/CHI/GCE at different pH ranging from 3 to 11 in 0.5 μM ciprofloxacin (0.1 M PBS at 50 mV/sec); (b) the plot between peak current density and pH; c) plot between electrode potential vs pH. 54

Figure 4.6 (a) Cyclic Voltammetry responses of CIP on AuNPs/CHI/GCE at acidic pH (b) alkaline pH in 0.5 μM ciprofloxacin (0.1 M PBS at 50 mV/sec) and (c) linear plot between potential vs pH data obtained ranging pH from 6 to 11. 54

Figure 4.7 (a) Cyclic voltammetry responses of CIP on AuNPs/CHI/GCE at different temperatures ranging from 25 to 65 ^{0}C in 0.5 μM ciprofloxacin (0.1 M PBS at pH 7); (b) linear plot between peak current density and temperature; (c) linear plot between electrode potential vs temperature 55

Figure 4.8 Pearson correlation coefficient of experimental parameters. 58

Figure 4.10 The radar plot for the models: (a) AdaBoost, (b) Bagging, (c) CatBoost, (d) Decision Tree, (e) Extra Trees, (f) Gradient Boosting, (g) HistGradientBoosting, (h) LightBoost, (i) Random Forest and (j) XGBoost. 67

Figure 4.11 The residual plot for (a) AdaBoost, (b) Bagging, (c) CB, (d) DT, (e) ET, (f) GB, (g) HGB, (h) LGB, (i) RF and (j) XGBoost. 70

Figure 4.12 The Feature importance for the models: (a) AdaBoost, (b) Bagging, (c) CB, (d) DT, (e) ET, (f) GB, (g) HGB, (h) LGB, (i) RF and (j) XGBoost..... 72

Figure 4.13 (a) Global feature importance assessed through SHAP values, (b) The summary plot (beeswarm plot) illustrates the distribution of feature impacts on the output of the CatBoost. 74

Figure 4.14 (a) DPV responses of AuNPs/CHI/GCE sensor for diverse conc. of CIP in 0.1 M KCl (scan rate: 50 mV/sec), b) CIP's calibration curve. 76

Figure 4.15 (a) Differential pulse voltammetry (DPV) responses of AuNPs/Gr sensor for diverse concentrations of CIP in 0.01 M KCl (scan rate: 25 mV/sec); (b) CIP's calibration curve 78

List of Tables

Table No.	Table Caption	Page No.
Table 4.1	The components of the Randles equivalent circuit for both bare and modified electrodes.	48
Table 4.2	Statistical analysis of the experimental data.	57
Table 4.3	Hyper-parameters' optimal values	60
Table 4.4	Feature importances for the studied models	61
Table 4.5	Performance matrices of studied ML models	64
Table 4.6	Input parameters optimization using the novel framework.	75
Table 4.7	Comparison of various developed electrodes and their performance for the determination of CIP.	77

Nomenclature

Symbols	Elaborations
e.g.	for example
etc.	Etcetera
et al	And Others
Eq	Equation
Fig.	Figure
Min	Minimum
Max	Maximum
ppm	Parts per million
uM	micromolar
nm	nanomolar
λ	Wavelength
eV	Electron volt
ppb	Parts per billion
^{0}C	Degree Celsius
ppt	Parts Per Thousand
AuNPs	Gold Nanoparticals

Acronyms and Abbreviations

AB	AdaBoost
CA	Chronoamperometric
CB	CatBoost
CE	Counter Electrode
CHI	Chitosan
CV	Cyclic Voltammetry
DT	Decision Tree
DPV	Differential pulse voltammetry
EIS	Electrochemical Impedance Spectroscopy
GB	Gradient Boosting
Gr	Graphite
GCE	Glassy Carbon Electrode
HGB	Hist Gradient Boosting
LGB	Light GBM
LSV	Linear sweep voltammetry
ML	Machine Learning
MSE	Mean Square Error
MAE	Mean Absolute Error
MedAE	Median Absolute Error
RE	Reference Electrode
RF	Random Forest
SHAP	Shapley Additive Explanations
SWV	Square wave voltammetry
WE	Working Electrode
XGB	Extreme Gradient Boosting

Chapter 1: INTRODUCTION

1.1 BACKGROUND

Antibiotics are pharmaceutical drugs that treat bacterial illnesses in humans, animals, aquaculture, and livestock feed. Since their discovery, they have contributed to the treatment of bacterial diseases. The widespread and misuse of antibiotics has raised public concern because they are being detected as environmental contaminants from human and animal waste [1]. These antibiotics can persist without change or as active metabolites in the environment, posing significant aquatic and human health risks [2, 3]. Alarming projections in the USA anticipate antimicrobial resistance-related deaths exceeding the combined toll of cancer and diabetes, with approximately 23,000 deaths annually [4]. The overuse, abuse, and improper disposal of antibiotics have contributed to the development and dissemination of antibiotic-resistant microorganisms posing a significant threat to global public health [3, 5-7]. Their global use has increased significantly, reaching an estimated 100,000 to 200,000 tonnes between 2010 and 2019 [8], with approximately half designated for human use, projected to escalate to 105,596 tonnes by 2030 [9]. In 2018, the Science and Knowledge Service of the European Commission released a technical report [10] stating that the thirteen antibiotics including ciprofloxacin, ofloxacin, and sulfamethoxazole found nearly or equivalent to 10 μg/L or 27.2 nM in wastewater treatment plant (WWTP) effluents. The high concentration of antibiotics was mainly due to the incomplete removal of WWTP treatment process that could not completely remove the antibiotics. These antibiotics are not completely metabolized and are excreted into the environment, contaminating surface water, groundwater, and drinking water [11, 12].

Ciprofloxacin (CIP), a versatile fluoroquinolone antibiotic, is frequently detected in contaminated water sources as a result of its extensive use and persistent nature [13]. Accurate detection of persistent antibiotic drugs is imperative to address antibiotic resistance issues effectively. Various analytical and electroanalytical approaches have been extensively employed to detect and quantify these compounds in biological and environmental samples [14]. The methods used in this study are liquid chromatography-mass spectroscopy (LC-MS) [15-18], capillary electrophoresis [19], spectrophotometry [20], and chemiluminescence [21]. These instruments are only possible to handle with skilled personnel, require costly equipment, large quantities of organic solvents, more time for operation, extensive procedures, and require standardization. Thus, there is a pressing need for quick and sensitive technology. Electroanalytical determination methods have gained increasing recognition as a cost-effective and straightforward option for qualitatively and quantitatively determining different electroactive compounds in medicines and environmental contexts. These methods offer quick reactions, strong selectivity, sensitivity, consistency, reliability, stability, and user-friendliness [14].

Carbon-based electrodes are commonly used in electroanalytical techniques because they are inexpensive, have a vast potential range, have low electrical resistance, and can be easily modified chemically. Different carbon-based electrodes have been used as bare electrodes, including graphite, glassy carbon, carbon nanotubes, activated carbon, carbon fiber, and diamond-like carbon electrodes [22]. Ciprofloxacin contains numerous functional groups that are capable of being absorbed onto the substrate's surface. A bare glassy carbon electrode (GCE) is a low-cost and easily modified electrode that can be utilized to identify CIP. Bare electrodes exhibit inadequate electrochemical properties, making them unsuitable for CIP detection. However, GCE-modified electrodes can enhance the detection capabilities of electrodes, resulting in heightened

sensitivity, selectivity, and compatibility. This, in turn, requires a comprehensive examination. Modification of GCE electrodes with conducting polymers for detecting antibiotics, such as chitosan (CHI), has shown significant promise. CHI is a polyamine saccharide derived from chitin through deacetylation processes commonly found in biological materials [23]. It belongs to the category of cationic polymers and holds significant potential across diverse fields such as wastewater treatment, drug delivery, biomedical sciences, pharmaceuticals, cosmetics, and food science [24]. It is favorable for biocompatibility and strong adsorption tendencies, the ability to quickly form thin films on electrode surfaces, and sufficient mechanical strength. It is a non-conductive material and is often mixed with conductive substances to enhance sensitivity and selectivity [25] through increased surface area and catalytic activity [26, 27]. Gold nanoparticles (AuNPs) have been widely utilized for modifying electrodes over the past twenty years and possess exceptional adsorption and catalytic properties [28]. This approach improves the electrochemical performance of GCEs and expands their applicability in sensing applications. Some semiconductor materials, such as TiO_2, ZnO, ZrO_2, and doped metal oxides, among others, have shown great promise in improving the sensitivity and performance of electrochemical sensors for the detection of organic contaminants like antibiotics in various environments [29, 30]. These materials, upon incorporation into electrochemical sensors, enhance sensor response by facilitating charge transfer and enhancing the redox activity of analytes, which is essential for detecting low concentrations of antibiotics.

1.2 CONTEXT OF THIS RESEARCH

Machine learning models are crucial in predicting ecological toxic substances such as antibiotics in contaminated water. These models offer valuable insight into environmental monitoring, risk assessment, and the design of appropriate remedies [31]. Therefore, developing predictive models with

accuracy is relevant for fully protecting human health and ecosystem integrity against the growing concerns about antibiotic pollution in water bodies. These are implemented through several ML approaches for the mentioned purpose, including Linear Regression, Support Vector Machines, Gaussian Processes, K-Nearest Neighbors, Artificial Neural Networks, and tree-based models. Among these models, the tree-based models will serve the problem related to both linear and nonlinear features. These are highly used to predict contaminant levels owing to their ensemble nature in which they are less prone to overfitting while offering increased predictive performance, according to Ahmed and coworkers [32, 33]Where algorithms like AdaBoost-AB, CatBoost-CB, LightGBM, HistGradientBoosting-HGB, and Extreme Gradient Boosting-XGB [34, 35] had been brought forth with continuous research. CatBoost, a gradient boosting algorithm, offers distinct advantages compared to other models, such as XGBoost and LightGBM. It allows nonlinear relationships and categorical data handling more efficiently. It works well on categorical features using its target-based encoding without much preprocessing, at least without heavy risk of data leakage and overfitting [36]. The ordered boosting approach of the algorithm enhances generalization, ensuring that predictions are only based on previously observed data, reducing overfitting risks and improving model robustity. CatBoost does a great job in capturing complex, non-linear interactions due to its optimized tree structure, making it highly suitable for tasks with intricate dependencies. It also requires very little in the way of hyperparameter tuning, often performing competitively well out of the box and is optimized for CPU and GPU for faster training. Offering native support for imbalanced datasets, advanced regularization techniques, and integrated interpretability tools such as SHAP, CatBoost helps improve prediction accuracy, simplify model development, and can fit into a wide range of machine learning scenarios.

Differential Evolution (DE) seems to be a promising algorithm for model hyperparameter calibration, such as Random Forest and Gradient Boosting used in high-dimensional and complex search spaces. This approach performs the exploration and exploitation by applying the mutation, crossover, and selection operators in an interleaved way to ensure the robustness of better model performance. DE does not require gradient information, which is advantageous for tree-based models handling non-differentiable datasets. Compared to other evolutionary algorithms, DE is friendly to the user and efficient [37, 38]. DE optimization methods will improve model parameter selection and predictive performance to enable an accurate prediction of contaminant concentration in aqueous media. Despite conducting a comprehensive review of the literature, no studies have been found that employ machine learning to compare and predict ciprofloxacin adsorption by using AuNP/CHI-modified GCE sensor and to evaluate the effect of individual parameters on its quantitative determination.

1.3 AIMS AND OBJECTIVES

This study focuses on the following specific objectives

- To develop and characterize an ultrasensitive and selective sensor for accurately detecting the trace amount of antibiotic using gold nanoparticles with the help of chitosan as a binder.
- To evaluate the efficiency of the sensor through analysis of major electrochemical parameters such as scan rate, solution pH, and temperature with the help of the cyclic voltammetry technique.
- To optimize obtained electrochemical parameters with the aim of enhancing the performance of the sensor using ten different machine-learning models.
- To construct the calibration curve through DPV to precisely quantify the concentrations of CIP in both known and unknown aqueous samples.

1.4 SIGNIFICANCE, SCOPE AND DEFINITIONS

This study will help educate future researchers for developing a highly sensitive and selective electrochemical sensor which helps to detect the trace amount of antibiotics in water sample. This research will provide an outline on electrochemical process in detecting antibiotics. The research can also be used to find out the way in establishing optimal parameter in antibiotic detection. The study's final phase will involve the use of machine learning models specifically the CatBoost model for predicting the highest cathodic current.

1.5 THESIS OUTLINE

Chapter 1 outlines the background, and key objectives of the study, emphasizing the role of the development of electrochemical sensor for detecting antibiotics from wastewater.

Chapter 2 outlines the brief literature review focusing on the development procedure of electrodes, modification techniques, uses of various nanomaterials in electrode modification, discussion of different electromethodologies, roles of nanomaterials in the detection of antibiotics, lab-scale, and full-scale applications.

Chapter 3 describes the materials and instruments used during the research work and the procedures followed for the range of tests conducted.

Chapter 4 briefly describes the characterization of the materials used in the study and its outcomes, such as developed AuNP and CHI modified GCE electrodes, Parameter optimization by ten tree-based ML algorithms, determining the value of LOD and LOQ as well as the sensitivity assessment.

Chapter 5 summarizes the whole study and gives a clear picture and future direction of this study.

Chapter 2: LITERATURE REVIEW

2.1 BACKGROUND

Antibiotics constitute a critical therapeutic category, significantly influencing human health [39]. Semisynthetic and synthetic derivatives have to be included in the definition because of the progress medicinal chemists had made in modifying naturally occurring antibiotics and creating synthetic analogues. Antibiotics are therefore defined as substances that are a byproduct of metabolism (though they may be replicated or even predicted by chemical synthesis), are synthesised as a structural analogue of a naturally occurring antibiotic, inhibit the growth or survival of one or more microorganism species, and are effective at low concentrations [40]. Both human and animal bacterial infections are treated and prevented with antibiotics [41]. They have prevented the majority of infectious diseases that have afflicted humanity for centuries and spared millions of lives [42]. However, because of their ability to accumulate throughout food cycles and produce a number of dangerous issues like organ poisoning and hearing loss, ATBs have detrimental effects on human health and in tiny amounts [43-46]. Additionally, excessive use of ATBs increases the prevalence of resistance genes, which decreases the efficacy of treatments for health concerns [47]. In addition, animals and people might be disclosed to the genuine threat posed by the growth of ATBs-resistant bacteria, which is projected to spread to other microbial groups [48]. FAs are one of the several families of antibiotics that merit special consideration. These well-known medications are widely used to treat bacterial infections of the urinary system in humans and are also regularly used to treat animals, including as "preventive" feed additives. The latter is particularly dangerous since it contains FA residues in livestock food items or is released into the environment. FAs are extremely common [49]. The WHO reports that, depending on the nation, the success rate of using CIP to treat urinary tract infections caused by Escherichia coli ranges from 8% to 65% [50]. FAs (i)

prefer to reside in both terrestrial and aquatic habitats due to their limited biodegradability, (ii) may move to and live in plants from the environment (soil), (iii) are only advised for the treatment of severe illnesses since they are regarded as dangerous (FAs have been linked to several negative side effects when ingested by humans). Methodologies that enable FAs to manipulate the environment and/or bodily fluids on-site and in-situ are desperately needed [51]. The most widely used methods for identifying antibiotics in biological fluids and pharmaceuticals formulation are spectroscopy [52], microbiological assays [53], high performance liquid chromatography (HPLC) [54], high performance liquid chromatography- mass spectroscopy (LC/MS) [55]. These methods have several drawbacks, including the requirement for derivatization or labour-intensive extraction processes, a significant amount of typically organic solvent for extraction, costly equipment and skilled workers [56]. Compared to analytical techniques, electrochemical techniques are now widely used in the field of pharmaceuticals, environmental and biological sample analysis primarily because of their high sensitivity, low instrumentation cost, relatively quick response time and elimination of laborious extraction procedure. Determining the biomolecular interaction and electrode mechanism of medicines, which offer insight into the metabolic fate of drag molecules, is an advantage of electrochemical approaches [56-60]. The two most used electroanalytical methods are polarography and voltammetry [57, 61]. For the detection of drugs, a variety of voltametric methods, including square wave voltammetry, differential pulse voltammetry, linear sweep voltammetry and cyclic voltammetry were successfully used with great sensitivity [56, 57, 59, 61]. Modification of electrode surfaces has emerged as a key field of electrochemistry study in recent year. NMTs are a crucial part of analytical techniques used to analyse drugs because of their excellent surface area and strong electrical, physical and chemical characteristics, which could enhance the interaction with the analyte [62-65]. The efficiency of NMT based sensors, which measure the degree of contact and the rate of electron transport is influenced by shape, dimensions, crystallographic axis orientation, crystal structure quality and chemical distribution

[66]. Because of their exceptional potential, NMTs were used as sensor in clinical and analytical system. To better serve their intended uses, all contemporary sensor based on different operation (potentiometric, electrochemical impedance spectroscopy, amperomatric) have been developed. In contrast, the utilization of NPs in an electrochemical sensor allows for selectivity to a particular analyte and signal maximization, detecting sensor performance. The application of NPs for antimicrobial electrochemical was examined in a number of earlier research [67, 68]. In this review, I tried to make a comprehensive overview on the uses of nanomaterials in developing sensor properties. Therefore, this review would serve as a starting point for scientists interested in studying NMTs-based ATBs sensors. Additionally, there is seldom reports to summarize the latest different modification techniques and the electromethodologies.

2.2 DISCUSSION OF ELECTROMETHODOLOGIES

Due to its benefits, which include high sensitivity, quick processing times, and the potential for miniaturization, electrochemical sensors have demonstrated tremendous promise in the detection of antibiotic residues in recent decades (through the combination between potential (E), current (I), charge (Q) and time (t)) [69]. Voltammetry, electrochemical impedance spectroscopy (EIS), and chronoamperometry (I-t) are electroanalytical techniques for the electrochemical detection of antibiotics [70]. Four voltammetry methods are frequently employed in antibiotic detection [71, 72]. (i) Cyclic Voltammetry (CV), whose ability to simultaneously view the redox peak potential and current makes it useful for researching reversible redox reactions. (ii) square wave voltammetry (SWV), this is more sensitive than CV and applies a rapidly scanning stepped voltage to the electrode. (iii) Differential pulse voltammetry (DPV), it is quite sensitive and can offer pertinent analyte information on the chemical form. (iv) Linear sweep voltammetry (LSV), it involves supplying the electrode with a voltage that varies linearly. EIS can be used to evaluate electrode performance and is also a useful technique for detecting antibiotics [73]. Antibiotics are commonly detected using the I-t method, which involves subjecting a test sample to an oxidation-reduction reaction at a

constant potential and tracking the change in current over time. Because of their enhanced electroanalysis performance, voltametric techniques (DPV, CV, SWV, and LSV) have been used most frequently to date for the electrochemical detection of antibiotic residues. Furthermore, the well-known benefits of voltametric techniques include automation, easy measurement and preparation, mass-transport amplification, and the potential for miniaturisation. Other benefits of this approach are its large linear range, low detection limits, selectivity, and quick reaction. But as a backup method for detecting antibiotics, chronoamperometry and electrochemical impedance spectroscopy have also drawn a lot of interest. The part provided specifics on these techniques, such as their principles, applicability, and detection limit.

2.2.1 Cyclic Voltammetry

One of the most often used electrochemical methods for identifying antibiotics is the CV. In order to create a current flow between the working and counter electrodes, cyclic voltammetry applies potential to the working electrode in a triangular waveform that sweeps forward and backward at a steady pace. This causes the electroactive analyte that is present in solution or adsorbed on the electrode surface to oxidise and then reduce [74]. This approach measures the generated current because the voltage is too high. The x-axis shows a parameter that is applied to the system, in this case the applied potential (E), and the y-axis shows the response, in this case the resulting current (i) passed. The working electrode's (WE) voltage is cycled and the resulting current is measured. The components of a typical CV electrochemical cell are an electrolytic solution that provides the ions needed for the redox reaction, a reference electrode that keeps the potential constant, a counter electrode that cuts the circuit between the WE and the signal source, and a WE where the reaction takes place. In order to draw a modest current signal, the cell is connected to a potentiostate, which produces a precise potential. A current to voltage converter measures the resulting current, and the data acquisition system creates the final voltammogram. For a sample under analysis, the current versus potential graph is shown [75]. Figure 2.1 shows the standard

configuration used for CV, along with the waveform and typical voltammogram shape. The equation O+ne ↔ R, in which O stands for the oxidised form and R for the reduced form, illustrates the reversible system.

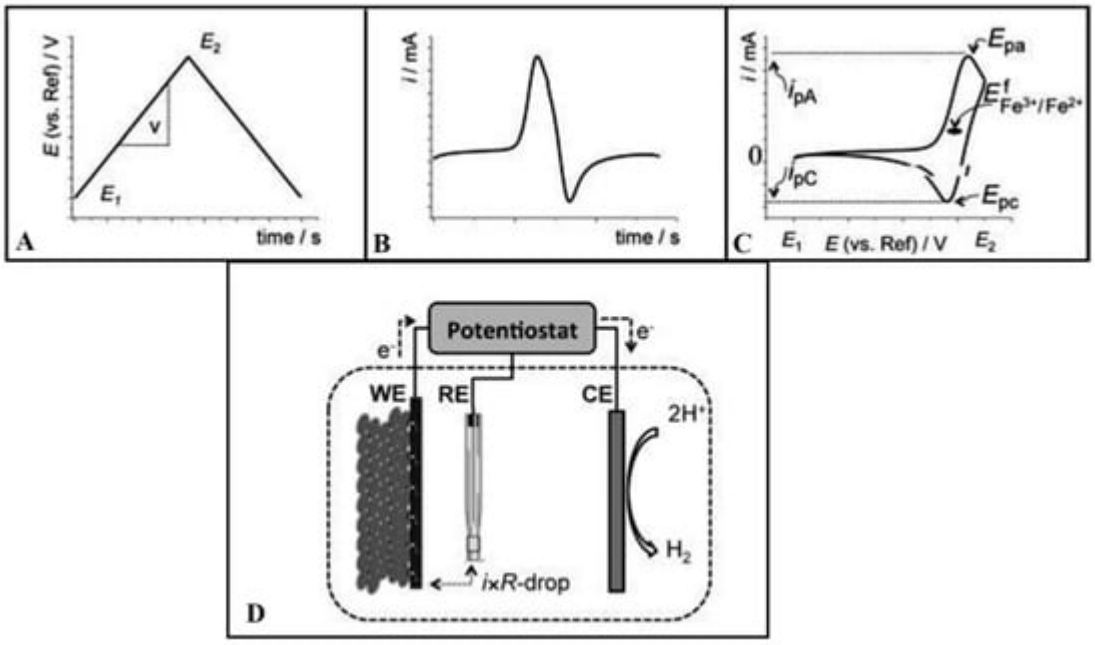


Figure 2.1 In CV (A) The potential (in relation to RE) is applied to the WE in CV. It shows that the potential starts at the lowest potential value (E1), increases to its greatest potential value (E2), and then decreases to its lowest potential value (E1); (B) Plotting the current caused by this potential change over time. (C) shows the current as a function of potential, is called a cyclic voltametric curve; (D) A three-electrode potentiostatic experimental setup for anodic biofilm.

CV data is typically reported using two conventions: the IUPAC convention and the US convention (Figure 2.2). Every trace has an arrow that shows which way the potential was scanned to capture the data, and the experiment's circumstances are mentioned in the description. If the potential is swept negatively from the starting potential (E1) to the switching potential (E2) in the forward scan. It is known as the cathodic trace. The potential is then swept positively back to E1 by reversing the scan direction; this is known as the anodic trace [76]. In order for chemical and electrochemical processes to occur to a substantial degree during CV studies, the scan rate needs to be long enough [74]. Consequently,

data regarding the system's redox potential and diffusion kinetic parameters associated with the electrochemical reactions could be obtained. Additionally, it provides details on the number of redox states, their stability, and the characterisation of redox systems.

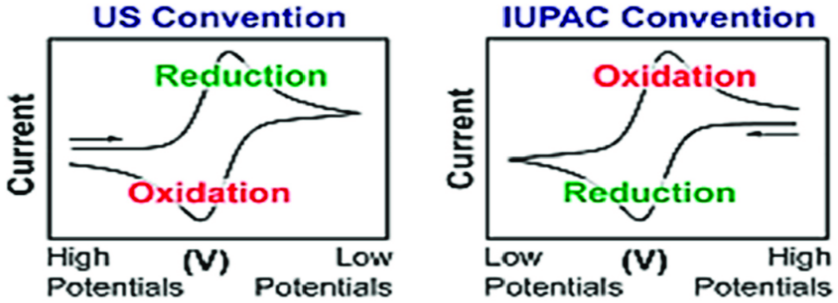


Figure 2.2 Schematic voltammograms. To report CV data, US and IUPAC conventions are commonly used [76].

2.2.2 Square Wave Voltammetry

One effective electrochemical method for electroanalytical measurements is SWV [77]. SWV is an intensive differential approach that applies a waveform to the working electrode that consists of a symmetrical square wave superimposed on a staircase. Each square-wave cycle involves two samples of the current: one at the conclusion of the forward pulse and one at the conclusion of the reverse pulse. Plotting of the two measurements' difference against the staircase potential has been performed. Excellent sensitivity and successful background contribution discrimination are displayed by the following peak-shaped voltammogram [78].

SWV offers the electroanalyst a number of benefits. The first benefit of using the SWV waveform is that it can significantly boost the scan rate by mitigating the negative impacts of charging current. The second benefit of SWV is that oxygen does not have to be removed from the analyte solution; as long as the voltametric peak is more cathodic than the one for oxygen reduction, the forward and reverse current magnitudes will include an equal amount of current from the reduction of oxygen. The other benefit of SWV is that because the current difference is greater than the forward or reverse current, it is typically easier to read the peak's height, improving accuracy. Several drug active

compounds were subjected to the SWV technique. SWV is helpful for drug analysis in dosage forms and biological specimens due to its sensitivity and speed. It is possible to analyse traces of drug compounds due to the low detection and determination limitations.

2.2.3 Differential Pulse Voltammetry

A very helpful method for determining the trace amounts of pharmaceutically active substances is DPV. This electrochemical approach has also been used to study the kinetics, thermodynamics, processes, and quantitative chemical analysis of chemical reactions [79]. In basic terms, the excitation waveform is the stairs. The key parameters of pulse techniques are the pulse amplitude, pulse width, sample period, and, for certain techniques, the pulse period or drop time. The DPV approach applies fixed-magnitude pulses to the working electrode shortly prior to the drop's termination, superimposed on top of a linear potential ramp. In each pulse period, the current is sampled twice: once prior to the pulse and again at the conclusion of the pulse. The DPV voltammogram is obtained by recording the difference between these two current values as a function of the potential (DPV) and plotting the current difference against the potential [80]. These measures are useful because they can reduce the impact of the charging current, which increases the sensitivity of current measurements [81]. Due to its high faradaic to charging current ratio and good charging current discrimination, the DPV technique is among the most sensitive voltametric methods [82]. Due to their peak shape, differential pulse curves are ideal for analytical applications. The DPV method is very helpful for trace analysis, such as for drug active chemicals, forensic, or environmental science, because of its great sensitivity. Because of these advantages and the availability of low-cost instruments, DPV is generally the choice for the identification of drug active chemicals in their dosage forms and in bodily fluids. The improved sensitivity of the DPV technique, which permits low LOD values for a variety of chemicals, is its greatest benefit.

2.2.4 Linear Sweep Voltammetry

When using LSV, an electroanalytical method, the working electrode potential changes linearly over the course of the analysis. With this method, a potential (E_i) is swept in which there is no reaction towards a higher potential value in relation to oxidation or a more negative potential value in relation to reduction of the electroanalyte under study. During this analysis, the measured current intensity generates the current-potential (I-E) curve named voltammogram with a typical shape indicating the analyte's red/ox characteristics as well as the main parameters of the involved phenomenon [83].

2.2.5 Electrochemical Impedance Spectroscopy

The EIS investigates the sensitive events occurring on the electrode surface as well as the changes in electrical characteristics at this surface during an electrochemical process. The foundation of the EIS is the control, within a specific frequency range, of the interactions generated on the detection platform during a reaction between the electroactive analyte dissolved in the solution and the modifier at the electrode surface, resulting in equivalent electrical circuits of the phenomena involved on the electrode/solution interface [74]. Ohms (as resistance unit) are used in this method to measure a circuit's impedance. EIS has a number of advantages over the other electrochemical techniques, depending on its steady-state nature, use of small signal analysis, and ability to use commercially available electrochemical working stations (potentiostate) to probe signal relaxations over a very wide range of applied frequencies, from less than 1 mHz to greater than 1 MHz. Using graphical techniques to visualise and interpret the impedance data is the first step in the data analysis process in EIS. Impedance data must be presented in a variety of formats to highlight a particular feature or behaviour. These formats include the complex-capacitance format for the capacitive behaviour of a dielectric system, the admittance format for capacitive behaviour at high frequencies, the Nyquist representation for mass transfer and kinetic behaviour, and the Bode representation for frequency-dependent behaviour. Frequency (f), modulus ($|Z|$), and phase (f) for the Bode diagram or frequency, real part (Z), and

imaginary part (Z) for the Nyquist diagram are the three-dimensional representations of the experimental results that are obtained over a wide frequency range (usually between 100 kHz and 10 mHz). EIS is extensively used in a variety of electrochemical cells, devices, and systems, including as biomedical systems, corrosion, energy storage and conversion, and sensors. This technique can be used to extract specific physical and chemical information about a process of interest, detect the presence and assess the relative relevance of several processes, and offer basic system diagnostics both in-situ and in-operando.

2.2.6 Chronoamperometric

The potential is initially set to potential E_0 in chronoamperometric (CA) tests, where no electrochemical action takes place. After that, redox activity takes place when the voltage is stepped from E_0 to E_1 [84]. The current is then measured at constant potential E_1 as a function of time. Because the concentration of the electroactive species falls close to the electrode surface and the concentration gradient falls, the current reduces. In order to create the CA potential-time graph, the response current variation is recorded in relation to time. Furthermore, given a reversible process, the Cottrell equation describes the current's time-dependence:

$$I(t)=n*F*A*c*\pi \qquad (2.1)$$

where t is the time, c is the starting concentration, D is the diffusion coefficient, A is the electrode area, F is the Faraday constant, and n is the number of electrons.

2.3 MODIFICATION PROCEDURE OF ELECTRODE

The detection performance can be enhanced by altering the bare electrode's surface. One way to enhance the hydrophilicity of the interface between the electrode and the solution and raise the concentration of antibiotics in the reaction area is to physically or chemically trim and modify the electrode surface [85-87]. Conversely, self-assembly, coating, electrodeposition, electro-polymerization, and other modifications are used to create single-layer or multi-layer functional materials, such as nanomaterials, organic

materials, enzymes, or antibodies, on the electrode surface [88-90]. Following modification, the electrode will exhibit unique catalytic activity, surface effect, size effect, and quantum tunnelling effect. These particular characteristics can lower the redox overpotential of antibiotics, speed up electron transfer at the interface, increase the electrode's electrical conductivity, and encourage the electrochemical reaction. The sensitivity of antibiotic detection can be significantly increased by combining the two aforementioned factors in a way that works well together. The two primary categories of preparation techniques needed for modified electrodes are top-down and bottom-up, which are based on the various processes that take place inside or on the surfaces of working electrodes.

Top-down is a modification that uses a laser or other etching techniques to etch a solid electrode's surface [85, 86, 91]. To enhance the electrode's adsorption capabilities and electrochemical activity, top-down modification can be used to appropriately raise the electrode's surface roughness and add surface functional groups. Feng et al. etched directly onto GCE using a laser one-step process, and the modified electrode can identify ofloxacin in actual water samples [85]. Figure 2.3 shows that while the crystal structure remains unchanged, the electrode's surface roughness rises, increasing the reaction area following alteration. Increased oxygen-containing functional groups on the surface can enhance the electrode's surface reactivity. For the first time, Chen et al. bombarded the surface of GCEs using the nitrogen plasma approach, appropriately enhancing the specific surface area and adding nitrogen reactive functional groups. Ciprofloxacin was successfully detected in real water samples using this modified electrode [86].

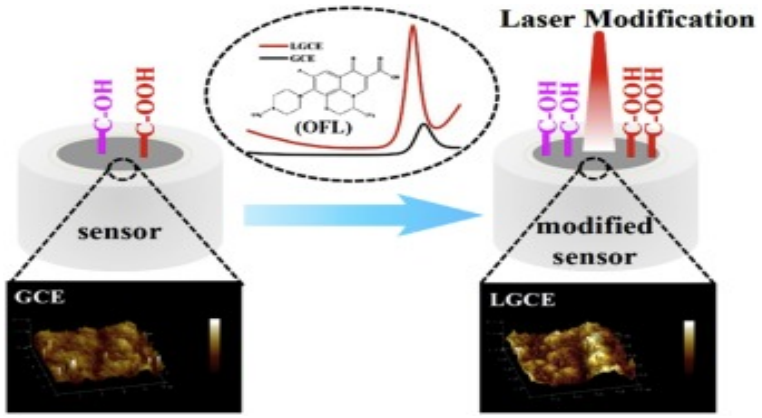


Figure 2.3 Schematic illustration of electrochemical sensor for ofloxacin (OFL) detection. GCEs were directly modified using a picosecond laser

To increase the sensitivity and specificity of electrodes, bottom-up modification involves adding more active materials to the electrode surface through self-assembly [92], coating [93], electrochemical polymerisation [94, 95], and electrochemical deposition [96], among other methods. The process by which fundamental structural units—molecules, nanomaterials, microns, or larger—spontaneously create ordered structures is known as self-assembly. Modified electrodes for electrochemical sensors are frequently prepared using this technique [97]. One of the most popular modification techniques is coating. Although it is simpler to use than the self-assembly approach, it is still an adsorption process. Drop coating and dip coating are two of the coating techniques. Applying a quantitative mixture of material and modified solution to the exposed electrode's surface is known as drop-coating. Sun et al. coated the pretreatment GCE surface with their own Zn-Mt colloidal solution and dried it under an infrared lamp to create a customised electrode that could be used to detect oxytetracycline in meals [98]. The electrode is submerged in the electrode modification solution using the dip coating technique, although it is difficult to regulate the quantity. Electrodes must be dried before using either of these coating techniques.

Two widely utilised modification techniques are electrochemical polymerisation and electrochemical deposition. To perform the polymerisation reaction by electrolysis, the electrode in the electrochemical polymerisation method is submerged in a monomer solution. In order to determine the amount of levofloxacin in medications, Wen et al. produced PoAP/MWCNTs/GCE by electrochemically polymerising an aminophenol and MWCNT mixed solution on the GCE surface at cyclic potentials ranging from -0.20 to 0.84 V [95]. Molecularly imprinted sensors frequently use electrochemical polymerisation. A molecularly imprinted electrochemical sensor was developed by Jafari et al. to identify azithromycin in serum. The sensor, which can selectively detect azithromycin, was created by electropolymerizing aniline on graphene oxide (GO) and gold nanoparticle-modified GCE using azithromycin as the template [99]. An external electric field causes the positive and negative ions in the electrolyte solution to migrate, and a redox reaction takes place on the electrode to create a coating. This process is known as electrochemical deposition. Jiang et al. [100] used electrochemical reduction to deposit Pt-Au onto the GCE surface. Ofloxacin can be found in pills and human urine samples using GCE/rGO/Pt-Au, according to the actual sample analysis. When metal or metal oxide nanoparticles modify the electrode, the electrochemical deposition process is typically employed.

In addition to the aforementioned modification techniques, there are other ways to prepare electrodes, such as carbon paste electrodes (CPEs) and screen-printed electrodes (SPEs). SPEs are prepared by using a screen board to deposit ink into a thin layer on a solid substrate. As needed, other elements can be added to the ink [101]. SPEs can be inexpensively mass-produced using predetermined processes, or they can be substantially altered with additional materials as required after manufacture [102]. Incorporation is also a popular technique for creating CPEs. To create a chemically modified electrode, a certain quantity of modifier, binder, and graphite powder are combined and ground in a glass tube [103, 104].

2.4 USES OF NANOPARTICLES IN ELECTROCHEMISTRY

The most appealing option for creating effective electrochemical sensors is nanomaterials because of their remarkable optical, thermal, chemical, electrical, and physical characteristics. According to Figure 2.4, the various methods used to create the nanomaterials give them a range of sizes, shapes, and physical and chemical characteristics that enable their use in various industries. The effectiveness of these nanomaterial-based sensors in detecting antibiotic residues has increased due to their simplicity of functionalisation and modification. This section discusses the many kinds of nanoparticles used in antimicrobial electrochemical sensing.

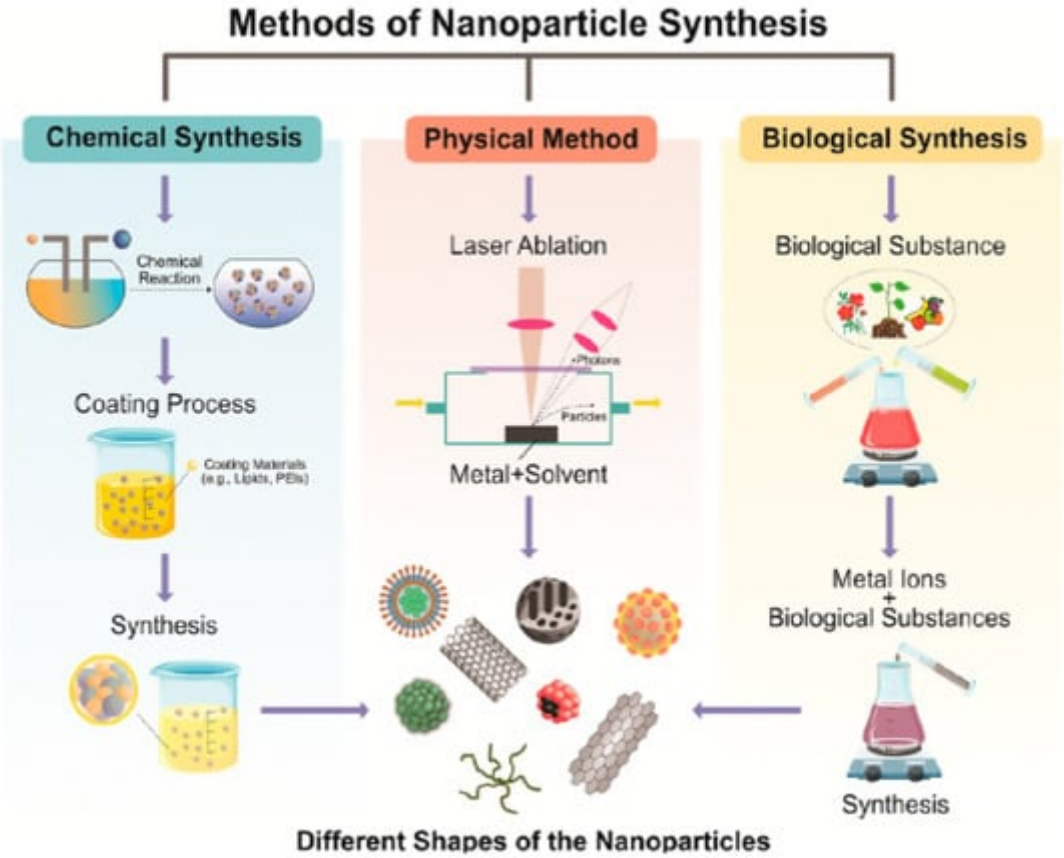


Figure 2.4 Various methods of nanoparticles synthesis [105]

2.4.1 Carbon Based Nanomaterials

Carbon nanoparticles have garnered a lot of interest as a class of material to change electrodes using bottom-up approaches. They are appropriate for the detection of antibiotic electrochemistry devices because of their special qualities, which include a large specific surface area, low background current, a wide electrochemical window, strong electronic conductivity, good chemical stability, selectivity, and reproducibility. Carbon nanotubes (CNTs), graphene oxide (GO), carbon nanospheres, and other carbon nanomaterials are frequently employed in the electrochemical detection of antibiotics [106]. Among these, GR and CNTs have been extensively employed in electrochemical sensors for antibiotic detection.

In addition to having exceptional chemical stability and mechanical strength, one-dimensional (1D) carbon nanotubes (CNTs) have a large surface area and a high electron transfer rate, which allow electrons to travel quickly from the analyte to the electrode surface. CNTs have a lot of potential for use in electrochemical sensors because of their properties. CNTs can be broadly classified as single-wall carbon nanotubes (SWCNTs) or multi-wall carbon nanotubes (MWCNTs) based on the number of layers in the tube wall. For instance, Liu et al. created the MWCNTs-CPE/prGO-ANSA/Au composite electrode, which can efficiently detect norfloxacin, using MWCNTs and additional materials [107]. Since its initial isolation in 2004, GR has emerged as a trailblazer in the field of novel materials and has found effective applications in a number of sectors, including sensors. GR is a two-dimensional (2D) nano-thin film with a high specific surface area and strong conductivity. He et al. suggested a modified GCE using functionalised graphene and gold nanoparticles to identify sulfonamides [108]. Sulfonamide molecules have a tendency to gather on the electrode surface due to the large specific surfaces and strong conductivity of both gold and graphene oxide (GR) nanoparticles. This suggests that the electrode can improve the electrochemical response signal. After oxidising GR to GO using H_2SO_4/HNO_3, Santos et al. electro

dedeposited nickel oxide nanoparticles (NiO-NPs) and modified GO onto the GCE. They developed a straightforward, extremely selective electrochemical technique for determining ciprofloxacin (CIP) and paracetamol (PAR) simultaneously [109]. Wong et al. investigated CPE modulated by GO and ionic liquids (ILs). Ofloxacin's analytical sensitivity was 8.2 times higher with the modified CPE than with the unmodified CPE [110]. Researchers have created a number of methods for producing 3D GR in recent years, and this technology has also been used consistently in the field of sensors. Zhang et al. assembled GO by reducing zinc foil spontaneously at room temperature and then washing it with diluted hydrogen chloride solution to create 3D rGO. The resulting 3D rGO/GCE can be used to detect chloramphenicol [111]. Many methods for creating 3D GR have been established thus far, including laser-induced GR [112]. 3D GR has shown promise in the electrochemical detection of antibiotics and has produced positive results in the electrochemical detection of other chemicals.

2.4.2 Metal Nanoparticles

The structure, shape, composition, and size of metal nanoparticles are what give them their favourable chemical and physical characteristics. Metal nanoparticles are the most popular options for electrochemical sensor-based NPs due to their superior conductivity, structural stability, mechanical and electrical characteristics, biocompatibility, and catalytic capabilities. The creation of new metal nanostructures and their successful use in a variety of industries, including electronics, sensing, medicine, and catalysis, have advanced significantly in recent years. Because of their large surface area, quick electron transfer kinetics, and several adsorption sites to antigen, enzymes, and antibodies, metal nanoparticles have drawn interest for use in the electrochemical detection of antibiotics [113]. In the investigation of electrochemical sensors to detect antibiotics, noble metal nanoparticles—such as gold, silver, and platinum—are frequently utilised to raise the detection limit [114, 115]. For instance, Roushani et al. investigated the use of AgNPs and 3-aminomethylpyridine functionalised graphene oxide (3-Ampi-GO) as electrochemical detection amplifiers to

build an electrochemical sensor for chloramphenicol using aptamers and molecularly imprinted dual recognition systems [116]. Additionally, a novel concept of support-less electrochemical platform for ultra-sensitive metronidazole (MNZ) detection was proposed using molecularly imprinted polymer (MIP) [117]. In order to identify and quantify MNZ simultaneously, electropolymerized molecularly imprinted polymer (MIP) was altered using porous Au–Ag microrods. The sensor demonstrated an ultra-low DL of 0.02 pM towards MNZ because of the special combination of free-standing and nanoporous microelectrodes with MIP coatings. In addition to AuNPs, Pt nanoparticles and MWCNTs were mixed to create Pt-MWCNTs, a voltametric ceftriaxone sensor in the presence of lidocaine [118]. Due to the combined actions of Pt NPs and MWCNTs, the sensor demonstrated a detection limit of 9.01 nM (range: 0.01–10 μ M) towards ceftriaxone. The catalytic impact of transition metals is as effective as that of precious metals. Transition metals are more affordable and accessible than precious metals. Gan et al. created an electrochemical sensor for tetracycline (TC) detection by modifying the montmorillonite (MMT) with iron/zinc (Fe/Zn-MMT) via cation exchange and applying it on the surface of GCE [119]. Fe/Zn can increase the catalytic activity, while MMT's extended layer structure offers a large specific surface area. When the two are combined, the electrode's electrocatalytic and enrichment capabilities can be significantly increased.

2.4.3 Metal Organic Framework

Metal-organic frameworks (MOFs) polymers are among the most porous materials; they have huge internal pore volumes, well-defined pore diameters, and high specific surface areas [120]. Furthermore, as illustrated in Figure 2.5, the extended crystalline structures of MOFs, which combine metal ions with linker organic molecules [121], enable a variety of sensing applications because of the wide range of organic linker and metal ion modification options and the good tunability of MOFs in terms of pore size from nanometres to angstroms.

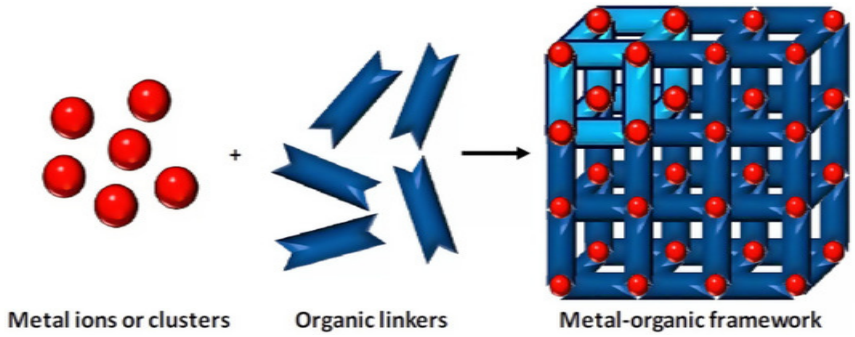


Figure 2.5 Synthesis of metal-organic frameworks (MOFs) involves combining metal ions and clusters with organic linkers to create a cross-linked network.

Despite the many benefits of employing MOFs in sensor fabrication, MOF-based electrochemical sensors have a number of drawbacks, including a lengthy response time, poor target selectivity, poor target binding to the MOF sensing surface, and challenges in synthesising conductive MOFs because MOFs are semiconductors or insulators. The creation of MOF-based sensors is made possible by a post-synthetic chemical alteration that gets beyond all of these restrictions. The use of MOFs for the possible detection of various antibiotics was covered in the next section. For the first time, molecularly imprinted polymer (MIP) microporous MOFs were used to detect tetracycline in honey samples [122]. This study used imprinted composite to modify the gold (Au) electrode surface by electro-polymerizing imprinted molecules with Au NPs functionalised with p-amino-thiophenol. The scientists examined the effects of several parameters, including elution conditions, washing conditions, incubation time, and extraction time, in order to attain the maximum electrochemical reaction towards tetracycline antibiotics. In a concentration range of 225 fM to 22.5 nM, this sensor displayed a detection limit of 0.23 fM for tetracycline. Similar compounds like doxycycline have no effect on the sensor's response, which likewise yielded a respectable recovery rate (102–107%) for tetracycline detection in honey samples. Therefore, even at extremely low concentrations, this sensor is suitable for monitoring tetracycline in food samples and the environment. Similarly, chromium-containing

MOF was used to detect the antibiotic chloramphenicol [123]. Because of the extremely low conductivity of chromium-containing MOF, the authors combined it with highly conductive carbon black XC-72 to create a novel hybrid composite that has a detection limit of 1.6 nM for chloramphenicol in the concentration range of 0.01 to 21 μM. Additionally, by examining the effects of several parameters like pH, scan rate, accumulation duration, and the ratio of chromium, the authors were able to maximise the sensor's responsiveness to the antibiotic. The sensor's response to chloramphenicol was found to be greater than that of a glassy carbon electrode (GCE) that had been separately modified by chromium-containing MOF or carbon black XC-72. A number of interfering antibiotics, including amikacin, gentamycin, neomycin, penicillin, kanamycin, kiasamycin, tetracycline, and chlortetracycline, were tested for their effects on the manufactured sensor. When carbon black XC-72's high conductivity and chromium-containing MOF's large surface area were combined, the sensor's response to the detection of the antibiotic chloramphenicol enhanced. This manufactured sensor is thought to be ideal for analysing actual samples, such as milk, honey, and eye drops.

2.4.4 Quantum Dots

Because of their numerous well-known advantages, QDs are popular candidates for a variety of biosensing applications (e.g., intrinsic high aspect ratio, excellent biocompatibility, outstanding interfacial characteristics, high electron transfer efficiency, and flexibility for surface modification) [124-126]. QDs use the oxidation potentials of the related metal ions to function as signal tags in multiplexed electrochemical biosensing applications [127]. The severe toxicity of heavy metal-based QDs, lengthy and time-consuming synthesis processes, lack of size repeatability, and potential for agglomeration all hinder their biosensing applications despite their immense potential [128]. Thus, the purpose of this section was to provide an overview of the latest developments in QD-based electrochemical antibiotic sensing. For the detection of ciprofloxacin (CIP), a simple electrochemical sensing method based on complex formation between CIP from CdS QDs and insitu produced Cd (II) ions was

developed [129]. With a DL of 22 nM, the sensor demonstrated excellent detectability for CIP. Nevertheless, superior selectivity of CIP against interfering substances (such as ofloxacin, chloramphenicol, kanamycin, erythromycin, and gentamicin) was also noted using this sensor design. Furthermore, acceptable recoveries in human urine samples ranging from 99.1% to 109.6% further validated its usefulness for CIP analysis. A sophisticated method for the voltametric measurement of levofloxacin (LEV) was created utilising composites of poly(o-aminophenol) and GQDs produced by electropolymerization in order to get around the toxicity of CdS quantum dots [130]. A very low DL of 10 nM towards LEV was found to be made possible by the exceptional electrical conductivity and electron transfer efficiency of GQDs. Santos et al. added carbon black and CdTe QD to the chitosan membrane to modify GCE. Norfloxacin was effectively detected using this electrode [131]. According to Roushani et al., a streptomycin aptamer sensor with good selectivity for streptomycin was created using ZnS QDs and gold nanorod composites.

2.4.5 Bio-Functional Materials

With the exception of a few inorganic chemical components, biofunctionalized materials like enzymes, nucleic acids, and antigens (antibodies) are utilised in the production of electrochemical sensors. They can precisely identify substances that have been discovered and have a high degree of specificity. The catalytic reaction of the enzyme on pertinent antibiotics allows for the detection of the particular reaction in an electrochemical sensor that uses enzyme biomacromolecule as modified material. Que et al. electropolymerized aniline and o-phenylenediamine on a gold electrode substrate to create molecular imprinted polymer (MIP), and they used glucose oxidase signal amplification to detect streptomycin [132]. Enzyme biomacromolecules broaden the electrochemical domain of antibiotic detection to some degree, however the simplicity of enzyme inactivation still has some drawbacks. An electrochemical immunosensor is a particular kind of sensor that responds to an analyte by immobilising an antigen (antibody) and then detecting changes in an electrical signal. Using a screen-printed

carbon electrode and a selective capture of the antibody surface immobilised protein G-functionalized magnetic beads, Conzuelo et al. created an amperometric immunological sensor to identify tetracyclines in milk samples [133]. A biosensor known as an electrochemical aptamer sensor alters the appropriate antibiotic's nucleic acid aptamer on a substrate material that has high electrical conductivity. Traditional aptamers have a limited signal gain, therefore Yu et al. added a displacement probe and examined how the sensor's performance was affected by the length of the displacement probe and the melting temperature. The findings demonstrated the necessity of utilising the ideal displacement probe length [134]. The created biosensor's sensitivity can be further increased by modifying its metal, carbon, and other components. Long-term reuse of the sensor will be facilitated by increasing the electrode surface's effective active area to load more biological macromolecules.

2.4.6 Others

In addition to the components listed above, MIP electrodes are frequently prepared using organic compounds like polyaniline. Additionally, when preparing electrodes, conductive organic substances like chitosan and Nafion reagent are frequently included. Polyaniline is a conductive polymer that has found extensive application in electrochemical sensing. In order to create materials with high conductivity and numerous electroactive reaction sites for the electrochemical detection of chloramphenicol, Chen et al. investigated combining MoS_2 with aniline [135]. Nevertheless, polyaniline also has drawbacks, including high brittleness and insolubility. Derivatives of aniline have been researched to address these issues [132]. Nafion is a perfluorosulfonated cation exchanger, which is an electrode modifier. On the electrode surface, it can create a layer with strong antifouling properties [136]. In order to measure norfloxacin, Huang et al. built MWCNTs/Nafion/GCE and demonstrated that the modified electrode has a quick response time, high stability, and repeatability [137]. Additionally, chitosan possesses the qualities of conductivity, biocompatibility, and film-forming potential. Additionally, it has a lot of hydroxyl and

amino functional groups [138]. On the surface of the carboxy-Fe_3O_4MNPs chitosan composite membrane, Liu et al. reported a label-free tetracycline electrochemical immunosensor that immobilises tetracycline monoclonal antibody [119]. Since the performance of electrodes is limited by the solitary nature of bare electrode materials, we typically alter the electrode surfaces to enhance performance. Nowadays, the materials listed above are frequently changed for use in antimicrobial electrochemical sensors. The discipline of sensing will employ more novel materials as research advances. It is challenging for a single modified material to accomplish the intended aims since different materials each have unique advantages. Consequently, we can combine several materials in some way to improve the electrode's performance even more. For instance, GR's layered structure can offer several binding sites that can efficiently distribute metal or metal oxide nanoparticles, which are rather easy to agglomerate. The sensitivity of the electrode can be increased by combining metal and carbon materials, which have good catalytic activity and biocompatibility, with bio-functional elements, which have strong specificity.

2.5 ELECTROCHEMICAL BEHAVIOUR OF CIPROFLOXACIN

Pharmaceutical chemicals in dosage forms (tablets, capsules, injections, and solution) and biological samples (blood, serum, and urine samples) have been identified using electrochemical techniques, particularly voltametric techniques. The most often described methods for quantification are linear sweep, differential pulse voltammetry, and square wave voltammetry, but cyclic voltammetry is employed for the electrochemical characterisation of medicinal substances [56, 57, 59, 60]. This section of the review examines recent advancements in the use of modified and unmodified electrodes for the electrochemical determination of ciprofloxacin in pharmaceutical formulations.

Ciprofloxacin (1-cyclopropyl-6-fluoro-4-oxo-7-piperazin-1-ylquinoline-3-carboxylic acid) is classified as a second-generation fluoroquinolone [139]. Ciprofloxacin (CF) is a synthetic chemotherapeutic agent utilised for the treatment of severe and life-threatening bacterial infections. Its clinical application is favoured due to its low toxicity, broad antibacterial spectrum, and minimal propensity to induce bacterial resistance. CF is particularly effective against infections of the urinary tract, respiratory tract, gastrointestinal tract, as well as skin and soft tissues [93, 139-141]. Despite its approval for exclusive use in humans, the recent misuse of antibiotics in food-producing animals has raised significant public concern regarding the transmission of antibiotic-resistant bacteria from animals to humans [96]. Using various electrodes, numerous investigations on the electrochemical characterisation of CF have been carried out. Cyclic voltammetry was used to examine the electrochemical behaviour of CF at a multi-walled nanotube film-modified glassy carbon electrode (MWCNT/GCE) [93]. Cyclic voltammograms of CF were recorded at a bare GCE and MWCNT/GCE in pH 7 PBS in order to assess the electrocatalytic effect of MWCNT towards CF oxidation. The Cotterll equation was used to calculate the diffusion coefficient (D) of CF across the solution-modified electrode interface using the chromatoamperometric method of analysis. The approach demonstrated a linear dependency of the oxidative peak current on the concentration of CF in the range of 40–1000 μM with LOD 6 μM under the optimised solution and method parameters. This technique was effectively used to identify CF in serum and urine samples. Additionally, Kingsley et al. [139] reported using a modified carbon paste electrode (CZF-CPE) with copper zinc ferrite nanoparticles to simultaneously measure CF and paracetamol (PA). Cyclic voltammetry was used to examine the electrochemical behaviours of CF and PA at CZF-CPE. Using the CFZ-CPE, a differential pulse adsorptive voltametric technique was created for the simultaneous measurement of CF and PA. For CF and PA, the reported linear working ranges were 0.909–4700 μM and 0.185–476 μM, respectively, with detection limits of 0.0026 μM and 0.0885 μM. The created technique was effectively used to the simultaneous and individual measurement of CF and PA in pharmaceutical formulations, serum, and

urine samples [139]. Additionally, cyclic voltammetry was used to examine the electrochemical behaviour of CF in pH 6 BRB solution at a chemically reduced graphene oxide modified GCE (CRGO/GCE) [140]. A square wave voltametric method was reported with a linear dynamic range LOD, and LOQ of 6–40 μM, 0.21 μM, and 0.70 μM, respectively, under optimised solution and method parameters.

2.6 KEY KNOWLEDGE GAPS AND FUTURE DIRECTIONS

2.6.1 Assessment of Complex Pollution in Natural Water Bodies

Current studies on electrochemical detection that use nanomaterials to fabricate electrodes usually concentrate on controlled, simplified settings that fall short of capturing the complexity of actual water pollution. The existence of several contaminants in natural water bodies, such as surface and groundwater greatly hampers the evaluation and efficacy of this procedure. To assess the effectiveness of electrochemical methods in detecting a wide range of pollutants, not just antibiotics, future research should focus on following real-world settings and clarifying the interactions between numerous pollutants in natural water habitats. This calls for an exhaustive examination of the electrochemical detection matrices, including investigating the impact of various factors such as pH of the solution, potential, scan rate, nature of supporting electrolyte, temperature, reaction time on efficiency of this process. Future research can offer a more realistic evaluation of electrochemical processes and their potential for practical applications by taking a more comprehensive approach that takes into account the complex structure of environmental water systems.

2.6.2 Scaling-up Application from the lab to the Pilot-scale

The majority of research on electrochemical methods for antibiotic detection is carried out in lab settings, which leaves little knowledge on how well they operate at larger pilot or full scales, especially in terms of operational stability, cost-effectiveness,

and scalability. The development and testing of pilot-scale reactors should be the top priority for research in order to move electrochemical processes from laboratory to industrial applications. Electrochemical flow reactors (EFR), batch electrochemical reactors (BER), and membrane electrochemical reactors (MER) that are combined with electrochemical processes are examples of these reactors. Optimising reactor design to increase sensitivity, scalability, conducting thorough cost-benefit evaluations, and closely assessing long-term operational stability under real-world circumstances should be major areas of study. These initiatives are essential for proving the industrial-scale feasibility and economic viability of these methods, which would enable their wider use in wastewater treatment.

2.6.3 Development of cost-effective and high-performance plants

Addressing issues including improving electrode stability, decreasing electrode fouling, raising the electrode's sensitivity, selectivity, repeatability, and dependability, as well as making sure that cost and material limits are met, is crucial to moving from laboratory to real-world applications. In order to make Fenton procedures competitive with alternative treatment technologies, additional advancements are necessary, according to economic estimates. Notwithstanding these achievements, there are still issues with Fenton and modified Fenton processes in pilot-scale applications that need to be resolved before they can be used on a large scale. These enhancements include developing inexpensive electrodes, lowering chemical requirements, improving efficiency under environmentally relevant pH values, and minimising the development of byproducts at the electrode surface. These developments are intended to make electroanalytical-based systems more scalable and commercially viable, enabling them to effectively treat actual wastewater that contains antibiotic contamination.

2.6.4 Comprehensive by-product analysis and toxicity assessment

Investigations into the detection pathways of specific antibiotics, including how reactions affect the stability and toxicity of resulting breakdown products, are essential for improving the safety and efficacy of electrochemical processes. The detection of antibiotics through electrochemical processes can result in the formation of a variety of by-products, some of which may exhibit unknown or increased toxicity. There are currently no comprehensive studies on the identification, quantification, and toxicity assessment of these by-products. Future research should employ to identify and quantify the by-products generated during antibiotic detection. Additionally, it is critical to prioritise the evaluation of the toxicity of these by-products to avoid the unintentional production of more harmful compounds during the processes.

2.6.5 Environmental impact and sustainability assessment

Despite the effectiveness of electrochemical techniques in the detection of antibiotics, little is known about their sustainability and wider environmental effects. This includes factors including long-term ecological effects, the production and disposal of nanoparticle waste, and the role of supporting electrolyte. Comprehensive life cycle assessments (LCAs) and environmental impact studies are necessary to examine the sustainability profile of electrochemical processes in order to fill in these information gaps. Future studies should focus on minimizing the waste of nanoparticles, cutting down on energy use, preventing the production of secondary contaminants, and encouraging the creation of environmentally friendly treatment techniques. Recycling electrode materials and integrating renewable energy sources—especially solar power—offer a promising way to increase the sustainability and environmental advantages of these treatments.

Chapter 3: MATERIALS AND METHODOLOGY

3.1 CHEMICAL AND REAGENTS

The following chemicals were purchased from various suppliers and used as received: ciprofloxacin (Sigma Aldrich). $HAuCl_4$ and chitosan (Sisco Research Laboratories Pvt. Ltd, India), disodium hydrogen phosphate (Na_2HPO_4), sodium dihydrogen phosphate (NaH_2PO_4), acetic acid (CH_3COOH), sodium acetate (CH_3COONa), sulfuric acid (H_2SO_4) and sodium hydroxide (NaOH) were of analytical reagent grade (Research Lab Fine Chem Industries, India). Chemical solutions were prepared with ultrapure water (≥18.2 MΩ-cm) obtained using a Direct-Q® 3 UV water purification system (Merck Milipre, UK).

3.2 INSTRUMENTS

Electrochemical analysis was performed using a μStat-i 400 portable Bipotentiostat/ Galvanostat/Impedance Analyser (EIS) manufactured by Metrohm DropSens, Switzerland. Experiments were controlled by a personal computer with DropView 8400 application. The experimental arrangement consisted of a cell of 100 mL capacity fitted with a three-electrode system: counter or auxiliary (platinum wire electrode), reference (Ag/AgCl electrode) and working electrode. The working electrode was connected to the anode, and the reference/counter electrode to the cathode. The experiment employed unmodified glassy carbon electrodes (GCE) of 3 mm diameter and modified working electrodes that consisted of AuNPs and chitosan-modified GCE. A pH meter-Lutron WA-2015, Taiwan, was used to determine the reaction medium. In addition, an ultrasonic cleaner (Hwashing Powersonic 405, Korea) was employed to cleanse the surface of the electrode and prepare different reagent solutions. Meanwhile, a water-shaking bath was employed to uphold the desired temperature.

3.3 FABRICATION OF WORKING ELECTRODE (WE)

Prior to modification with chitosan and AuNPs, the bare GCE surface was polished using various grades of alumina powder on smoothing pads to achieve a shiny appearance. Subsequently, the object was cleansed using distilled water and ethanol to eliminate contaminants, and later air-dried at ambient temperature. The electrode underwent pretreatment by conducting ten cyclic voltammetry scans (scan rate100 mV/sec), within an electrode potential range of -0.2 to +1.6 V in a 0.5 M sulphuric acid solution. Consistent with the prior research [142], we utilized a comparable approach to construct the working electrode with slight modifications. By employing a micropipette, a 0.5% chitosan (CHI) solution (consisting of 50 mg of CHI dissolved in 10 mL of 1% acetic acid (CH_3COOH)) was applied onto the pre-treated GCE. The solution is then allowed to dry naturally at ambient temperature, resulting in the formation of a thin film of chitosan. Afterwards, we performed electrodeposition of AuNPs onto the electrode by applying 0.2 mM $HAuCl_4$ precursor in a 0.5M H_2SO_4 solution through five voltametric cycles within an electrode potential range of -1.5 to 0.5 V at a scan rate of 30 mV/sec. A vivid crimson electrode surface provided evidence for the deposition of AuNPs. The AuNPs/CHI/GCE was subsequently rinsed with distilled water and exposed to five CV cycles (0.2 to 1.2 V) in phosphate buffer solution (PBS) (pH 7) to establish a stable peak response [143, 144]. AuNPs/GCE and CHI/GCE were modified using identical techniques to facilitate comparability.

3.4 ELECTROCHEMICAL MEASUREMENT PROCEDURE

The electrochemical characteristics of an unmodified and AuNPs and/or CHI-modified GCE were assessed using cyclic voltammetry (CV), electrochemical impedance spectroscopy (EIS), and differential pulse voltammetry (DPV) for the quantification of CIP in aqueous solution. CV is a very powerful technique in the analysis of electro-active species and especially in the studies of the redox reactions of

the analytes. In this study, the preliminary electroactive properties of the bare and modified GCE electrode were characterized in the potential range from +0.6 to - 0.3 V. This was conducted in a solution comprising 5.0 mM potassium ferrocyanide [$K_4Fe(CN)_6$] with 0.1M KCl. On the other hand, the detection of ciprofloxacin (CIP) on the AuNPs/CHI/GCE electrode was conducted individually by running CV scans in a 0.1M PBS solution within a potential range of 0.2 to +1.2V. An investigation into the effect of scan rate, pH and temperature on the detection of CIP was performed. To test the effect of temperature, the voltametric cell was placed in a water bath until the desired temperature was reached and stabilized at the set value.

EIS is a valuable methodology in electrochemistry that provides insight into the conductivity of electrode surfaces during either oxidation or reduction reactions. This technique also yields information about an electrode's alteration in conductance or impedance after its modification. In this regard, EIS was conducted using four different electrodes: Bare GCE, CHI-modified GCE (CHI/GCE), AuNPs-modified GCE (AuNPs/GCE), and AuNPs/CHI-modified GCE (AuNPs/CHI/GCE). The measurements were made in the frequency range from 1000 Hz to 500000 Hz, using a modulation amplitude of 40 mV in applied electrode potential. The Nyquist plots of bare and modified electrodes were recorded in the solution of 5.0 mM $[Fe(CN)_6]^{3-/4-}$ and 0.1 M KCl. In this plot, two-time constants may be well distinguished: a semicircular portion at high frequency due to electron transport processes and a linear portion at low frequency due to mass transport processes.

The choice of DPV for sensitivity testing was based on its superior sensitivity and rapidity. The DPV parameters chosen for CIP determination were Step Potential (Estep), Pulse Amplitude (Epuls), Pulse Time (tpuls), and Scan rate (Srate). In these tests, an initial CIP solution with a concentration of 27.19 μmol (10 mg/L) was prepared to adjust the other tested CIP concentrations. The selection was conducted univariately, using the

highest analytical response within the optimal range of experimental input parameters. The concentration range of CIP was analyzed from 0.0 to 1.25 µM. Specific concentrations evaluated included 0.0, 0.1560, 0.3125, 0.6250, and 1.25 µM. Analyzed in an electrochemical cell, the experiment utilized a 50 mL solution of supporting electrolyte, specifically 0.1 M KCl.

3.5 DATA ANALYSIS AND COLLECTION

A grand total of 2319 data sets were gathered from the experimental studies using a fabricated AuNPs/CHI-modified GCE electrochemical sensor to forecast the presence of the ciprofloxacin antibiotic in an aqueous solution. The data was acquired by systematically adjusting four parameters: voltage electrode potential, scan rate, pH, and temperature. The input variables include five scan rates, seven different pH conditions, and five temperature points. Two output currents: anodic and cathodic current, were achieved in the experiment, but this study was more focused on analyzing the cathodic current entirely. The comprehensive experimental protocol for data collecting and analysis is illustrated in Figure 3.1.

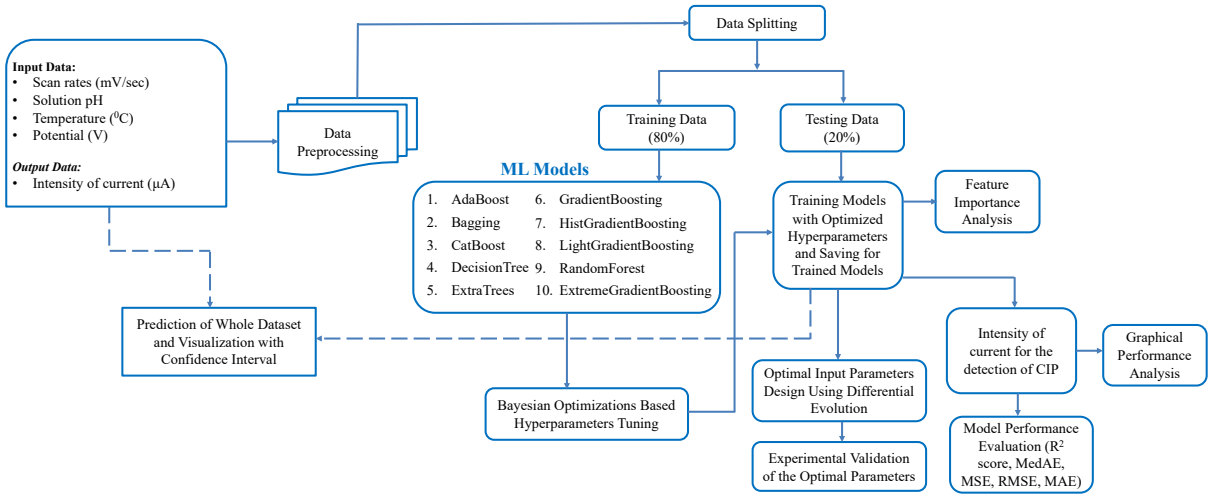


Figure 3.1 Complete block diagram of the proposed approach

A range of statistical metrics including the Coefficient of Determination (R^2), Mean Square Error (MSE), Root Mean Square Error (RMSE), Mean Absolute Error (MAE) and Median Absolute Error (MedAE) were employed to evaluate the predictive performance of the models [33, 145].

$$\text{Normalised Value } (X_{norm}) = \frac{X_i - X_{min}}{X_{max} - X_{min}} \quad (3.1)$$

Where Xi is any data.

Various statistical metrics, such as R^2, MSE, RMSE, MAE and MedAE, as defined by equations 3.2 to 3.6, were used to evaluate the model's predictive performance.

3.5.1 Coefficient of Determination (R^2)

$$R^2 = 1 - \frac{\sum_{i=1}^{n}(y_i - \hat{y}_i)^2}{\sum_{i=1}^{n}(y_i - \bar{y})^2} \quad (3.2)$$

Where y_i is the actual value, $\hat{y}_i$ is the predicted value, $\bar{y}$ is the mean of actual values, n is the number of observations, R^2 values range from 0 to 1, with higher values indicating better model performance.

3.5.2 Mean Square Error (MSE)

$$MSE = \frac{1}{n}\sum_{i=1}^{n}(y_i - \hat{y}_i)^2 \quad (3.3)$$

3.5.3 Root Mean Square Error (RMSE)

$$RMSE = \sqrt{\frac{1}{n}\sum_{i=1}^{n}(y_i - \hat{y}_i)^2} \quad (3.4)$$

3.5.4 Mean Absolute Error (MAE)

$$MAE = \frac{1}{n}\sum_{i=1}^{n}|y_i - \hat{y}_i| \quad (3.5)$$

3.5.5 Median absolute error (MedAE)

$$\text{Median Absolute Error} = \text{median}(|y_i - \hat{y}_i|) \quad (3.6)$$

3.6 MACHINE LEARNING TECHNIQUES AND MODELLING

Ten different tree-based machine learning models possess their unique performance characteristics. Using the default hyperparameters, models were used from the Scikit-learn library (https://scikit-learn.org/ stable) in the Python programming language. These approaches were AdaBoost (AB), Bagging (B), CatBoost (CB), Decision Tree (DT), Extra Trees (ET), Gradient Boosting (GB), HistGradientBoosting (HGB), LightGBM (LB), Random Forest (RF), and extreme Gradient Boosting (XGB) [146, 147]. These models and their hyperparameter tuning are discussed in more detail in the next section. The dataset was divided randomly into two sets: 80% of the data for training and the rest (20%) for testing [32, 33, 145]. The selected ML algorithms' hyperparameters were tuned by using a Bayesian optimization technique. After the tuning of hyperparameters, the models were trained on the training dataset and tested on the test dataset. The best model was selected through performance evaluation, which was used to design the optimal experimental parameters with DE for maximum CIP detection. This optimization technique provides practical insights to optimize time-based settings to achieve maximum predictability of CIP detection, further enhancing the practical utility of research.

3.7 DESCRIPTIONS OF TEN MACHINE LEARNING MODELS

3.7.1 Gradient Boosting (GB)

Gradient boosting is a widely utilized machine learning model that employs an ensemble method of decision trees known as boosting. The core concept of boosting involves the sequential addition of new decision trees by calculating the residuals of the entire ensemble model. This process continues until the model achieves the highest accuracy. Additionally, these models can be customized by adjusting the structure, such as the loss function and tree addition method [148]. The fundamental algorithm for gradient boosting used in this study can be generalized by the following equation.

$$f(x) = \sum_{k=1}^{K} f^k(x) \qquad (3.7)$$

Where $f(x)$ and $f^k(x)$ indicate entire ensemble model and k-th independent decision tree. N indicates the number of decision trees.

3.7.2 HistGradientBoosting (HGB)

Histogram-based gradient boosting is an advanced method that enhances the speed and performance of gradient boosting models [149]. This technique efficiently combines decision trees on large datasets by dividing input features into a specified number of intervals. As a result, the models can quickly find the optimal split, unlike traditional gradient boosting methods. Additionally, histogram-based gradient boosting can handle missing values by using one of the partitions for training, eliminating the need to preprocess the input data for missing values before applying the model.

3.7.3 Extreme Gradient Boosting (XGBoost)

XGBoost, short for Extreme Gradient Boosting, is an advanced gradient boosting algorithm that assigns weights to the learning errors of weak models and sequentially incorporates them into the next model to create a prediction model[150]. XGBoost models support parallel processing, resulting in faster computing speed compared to traditional gradient boosting models. Additionally, XGBoost models utilize a technique to prevent overfitting by training the tree using a regularized loss function, defined by the following mathematical equation.

$$L^t = \sum_{i=1}^{n} l\left(y_i, \hat{y}_i^{t-1} + f_t(x_i)\right) + \Omega(f_t) \qquad (3.8)$$

$$\Omega(f_t) = \gamma T + \frac{1}{2}\lambda \|w\|^2 \qquad (3.9)$$

Where L^t and $f^t(x)$ indicate the loss function and decision tree at the t-th iteration. The l is convex loss function. The y_i, $\hat{y}_i$ and x_i indicate true value, predicted value and input data at i-th data instance. The Ω is regulation term calculated with the number of leaves (T) in the decision tree and the Euclidean distance of each leaf ($\|w\|^2$).

3.7.4 Light Gradient Boosting Machine (LGBM)

Light gradient boosting machine (LGBM) is an enhanced version of the Gradient Boosting model. It achieves this by including two techniques that effectively decrease the computational workload [34]. LGBM utilises gradient-based one-side sampling (GOSS) and exclusive feature bundling (EFB) methods. The GOSS methodology is a method that decreases the sample size of a dataset. The fundamental premise of GOSS is that cases with substantial gradients exert a considerable influence on predictions, and the model is inadequately trained for such instances. The GOSS algorithm curates the training data set by selectively including examples that exhibit significant gradients. Hence, cases exhibiting negligible gradients can be disregarded, thereby minimising their contribution to the training process and reducing the dataset's sample count. The EFB is a data analysis technique that aims to reduce the dimensionality of a dataset by minimising the number of input features. The EFB employs a technique of consolidating variables that have a strong correlation into a single category under the assumption that data with a large number of dimensions is sparsely populated. Reducing the number of samples and features in the dataset using these two approaches significantly reduces the time it takes to compute the model. Furthermore, as stated by Guolin et al., the creators of LGBM, they found a maximum limit to the decrease in performance due to the decrease in sample size and number of features [34]. Therefore, while using the LGBM model, the issue of decreased prediction accuracy should not be overlooked. In addition, the LGBM model utilises a leaf-wise approach during the tree partitioning process. Compared to the level-wise technique, which considers the tree's balance, the leaf-wise tree development in LGBM selects the best possible node to split, reducing prediction error.

The LGBM technique employs a weighted summation to amalgamate predictions from individual trees within the ensemble. During the training iteration, these weights are established through evaluations of the loss function’s gradients. The subsequent

equation can be employed to predict the target variable using LGBM:

$$\hat{y} = \sum \alpha i \; hi(x) \qquad (3.10)$$

Where, $\hat{y}$ forecasts the goal value, the weight assigned to the i^{th} tree is denoted by αi, and the forecast made by the i^{th} tree for the input attributes x is represented by $hi(x)$. The LGBM can handle massive datasets, and it excels at capturing intricate non-linear connections between features and the target variable. Through gradient-based optimization, it constructs a set of trees that collectively yield accurate predictions, thus enhancing the performance of the loss function.

3.7.5 CatBoost (CB)

CatBoost is a machine learning technique that use gradient-boosted decision trees to predict continuous variables. The CatBoostRegressor is widely recognized for its efficacy, precision, and capacity to handle categorical data [36]. For the CatBoostRegressor method to function, it is necessary to design a set of relatively weak decision trees initially. Subsequently, these trees are amalgamated to construct a robust model. The method employed to link the trees is gradient boosting. Gradient boosting addresses the mistakes created by the previous trees by incorporating additional trees into the model. Equation (3.11) presents the mathematical expression utilised by CatBoost to predict continuous values:

$$y = f(x) = \sum_{i=1}^{n} \alpha i \; hi(x) \qquad (3.11)$$

Here, y represents the predicted value while x denotes the input features. The resultant function $f(x)$ is a linear amalgamation of fundamental functions, $hi(x)$. The coefficients αi ascertain the significance of individual base functions within this linear amalgamation.

The model coefficients are calculated using the gradient descent method. In CatBoost, the loss function must be minimised. The loss function quantifies the

difference between predicted and observed values. The ML approach CatBoost can effectively address a wide range of regression problems. It is especially effective at addressing issues that pertain to categorical attributes.

3.7.6 Bagging

Bootstrap aggregation, also known as Bagging, integrates the concepts of bootstrap and aggregation [151]. The Bagging model generates multiple datasets with slight variations in noise and distribution by randomly sampling from the original training data. Each dataset is used to train a model independently, and the models are then combined into an ensemble model. This approach reduces the risk of models making predictions based solely on specific noise patterns in the original data. Additionally, the out-of-bagging data not included in the bootstrap process can be used to validate individual models during the model aggregation process. This validation helps the Bagging model achieve high generalization performance

3.7.7 Random Forest (RF)

Random Forest is a model that utilizes the bagging technique among ensembles of independent decision trees [152]. In the bagging approach for regression, multiple decision trees are created by randomly sampling data from the original dataset. The final prediction is then generated by averaging the predictions of the individual trees. Random forests offer performance benefits by reducing variance while maintaining the bias of the models, which is a key advantage of the bagging model. Additionally, random forests randomly select input features for each decision tree from the pool of all input features. This variance in the input variables used in individual decision trees reduces the correlation between the trees. An analysis has shown that ensemble models consisting of low-correlation trees reduce generalization errors and improve prediction performance [152].

3.7.8 Extra Trees (ET)

ExtraTrees, also known as extremely randomized trees, are models that utilize an ensemble algorithm with significant randomness incorporated into the decision tree growth process [153]. The fundamental concept behind ExtraTrees is to introduce strong randomization in the selection of input features and cut points when splitting the nodes of the decision tree. Due to the high level of randomness in this model, the decision tree may not provide an optimal cutting point, resulting in suboptimal predictive performance as a standalone model. However, when combined with multiple decision tree models, ExtraTrees can effectively explore the data and enhance predictive performance. Furthermore, the model's randomness allows it to utilize all the data in the training process, reducing prediction bias. Additionally, the time required to build the model is reduced since it does not compute the optimal split.

3.7.9 Decision Tree (DT)

Decision trees are models that use a series of logical rules organized into a tree-like structure. Each test typically involves comparing data to a threshold value or specific category. This model makes predictions by segmenting the data into smaller groups using a series of decision rules arranged along a tree structure. Therefore, the order and placement of rules are crucial for the predictive accuracy of decision tree models [154]. Compared to complex artificial intelligence algorithms like artificial neural networks and convolutional neural networks, decision trees have a simple structure and prediction technique. This simplicity allows decision tree models to offer interpretability of predictions. Recently, many studies have focused on enhancing the performance of decision trees by improving their simple structure. As a result, studies have frequently emphasized using a combination of multiple independent decision trees rather than a single decision tree as a model [155].

3.7.10 AdaBoost

The AdaBoost model can be utilized for both regression and classification scenarios. It is an ensemble learning technique that iteratively improves weak classifiers by learning from their errors. AdaBoost uses sequential ensembling instead of the parallel ensembling used in the RandomForest model. Combining numerous weak classifiers can achieve a strong classifier with high accuracy. However, it's important to note that while AdaBoost is an adaptive classifier, it can lead to overfitting. It is sensitive to outliers and noisy data but shows great promise in enhancing the performance of decision trees in binary classification problems. In our analysis, hyperparameter optimization and tuning were done using grid search to identify the best loss function. The key hyperparameters considered were the learning rate (ranging from 0.1 to 5) and the number of boosted trees (n_estimators) from 20 to 500.

3.8 PREPARATION OF DISPOSABLE ELECTRODE

The graphite rod was extracted from used zinc-carbon battery of commercial brand. After separating the dismantling products (casing, plastic films, sealing, graphite rod, scraps), the retrieved graphite rod was cleansed using a paper towel to remove the adhesive and were consequently cleansed with deionized water and dried to remove moisture [156]. The rod was then polished by a metallographic method that included grinding with sandpaper, rinsing with water and alcohol and finally polishing with alumina slurry (0.3-micron). The polished rod was adhered to a copper rod. The copper-incorporated graphite rod was used as the working electrode. The electrode surface was polished using 0.3-micron alumina slurry on smoothing pads to achieve a shiny appearance. Subsequently, the electrode was sonicated using distilled water and ethanol to eliminate contaminants and later air-dried at ambient temperature. The prepared graphite electrodes were subjected to cyclic voltammetry (CV) as a pretreatment to enhance their electrochemical properties and modification with chitosan and AuNPs,

were followed the same previous procedure for GCE (see section 3.3).

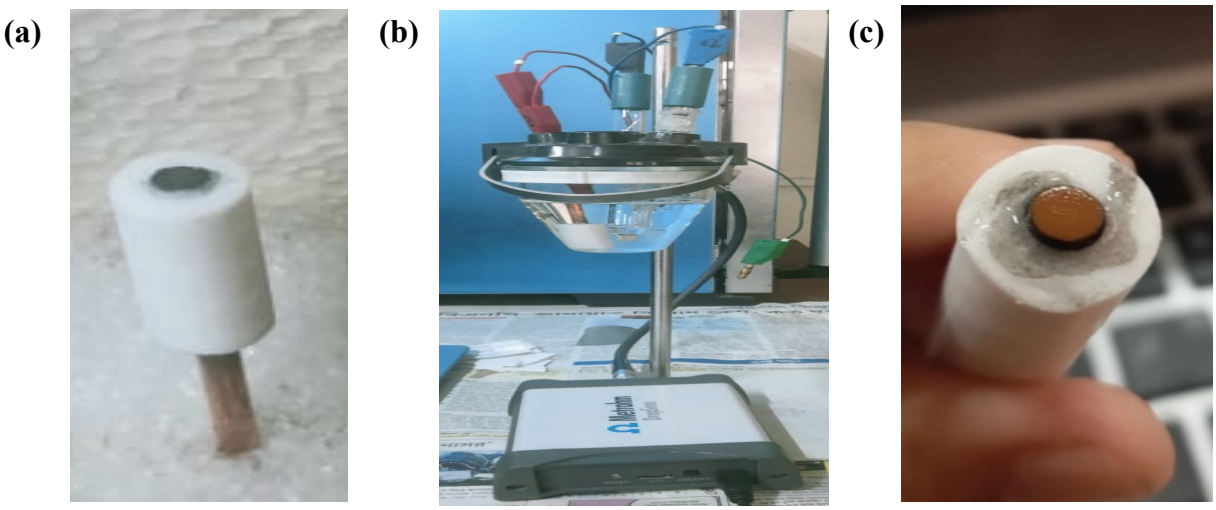


Figure 3.2 The preparation of (a) disposable electrode from dry cell, (b) drop casting of AuNPs and (c) final working electrode (AuNPs/ CHI-modified graphite)

Chapter 4: RESULTS AND DISCUSSION

4.1 ELECTROCHEMICAL CHARACTERIZATION OF ELECTRODE

Cyclic voltammetry (CV) and EIS studies were exploited for the electrochemical characterization of the bare and modified GCE electrodes. A set of cyclic voltammograms were recorded for the bare and modified electrodes and presented in Figures 4.1a, 4.1b, and 4.2a, 4.2b respectively. Figure 4.1a clearly elucidates that there is a remarkable increment in the magnitude of current and reasonable peak-to-peak separation (ΔE_p) for the Au-CHI-modified GCE as compared to bare GCE, CHI modified GCE and AuNPs-modified GCE. The superior performance of Au-CHI-modified GCE can be reasonably explained by the increased surface area and improved conductivity. This can also be attributed to the synergistic effect of AuNPs and CHI onto the GCE electrode. On top of that, the bare and modified GCE performances were assessed using scan rates from 12.5 to 100 mV/sec. The results are provided in Figure 4.1b and the Figures 4.2a, 4.2c, and 4.2e. From Figure 4.1c, it is seen that the redox peak currents increase linearly with a rise in the scan rate. This indicates that the mass transfer at the electrodes was predominantly governed by diffusion. That means, electroactive species diffuses from the electrode surface to bulk solution. Furthermore, Figure 4.2b, 4.2d, and 4.2f display the redox peak currents for the bare electrode, CHI/GCE and AuNPs/GCE electrodes, respectively. The electroactive surface area of the bare and modified electrodes was also calculated using the Randles-Sevcik equation (4.1) [157].

$$I_p = 2.69 \times 10^5 AC \sqrt{D} (\sqrt{n})^3 \sqrt{\nu} \qquad (4.1)$$

Where I_p, A, C, D, n, and ν are the peak current, surface area of the electrode, concentration of $[Fe(CN)_6]^{3-/4-}$ (mol cm^{-3}), diffusion coefficient (cm^2/s), number of electrons, and scan rate (mV/sec), respectively. Here in, the reported diffusion coefficient of $[Fe(CN)_6]^{3-/4-}$ is 7.63×10^{-6} cm^2/s [158], corresponding to a single electron transfer phenomena at a scan rate of 100 mV/sec.

The GCE, CHI-modified GCE, AuNPs-modified GCE, and AuNPs and CHI-modified GCE regression equations were derived from CV and are as follows: $I_{pa} = 6.129 \times v^{1/2} + 6.280$ ($R^2 = 0.9986$), $I_{pa} = 12.70 \times v^{1/2} - 5.861$ ($R^2 = 0.9993$), $I_{pa} = 12.90 \times v^{1/2} - 10.23$ ($R^2 = 0.9976$), and $I_{pa} = 27.21 \times v^{1/2} - 57.13$ ($R^2 = 0.9940$), respectively (Figure 4.2b, d, f and c). The effective surface areas of the following modifications were determined to be 0.0571 cm^2, 0.1026 cm^2, 0.1036 cm^2, and 0.1877 cm^2, respectively. Here, the AuNPs/CHI/GCE electrode demonstrated a significantly larger electroactive surface area by over three times, exceeding that of bare GCE. The greater surface area leads to the heightened current intensity during cyclic voltammetry (CV), indicating a more labile electron transfer process. The change significantly enhances the performance of the electrode, resulting in increased sensitivity and responsiveness. This is clearly demonstrated by the enhanced peak currents detected in the CV profiles (Figure 4.1a).

For further verification, electrochemical impedance spectroscopy (EIS) data were recorded to confirm the changes in impedance on the electrode surface. This technique provides information about the characteristics of interfacial electron transfer at the electrode surface for oxidation or reduction processes during its modification. Electrochemical impedance spectra are typically represented on a Nyquist plot, where the real component (Z') and imaginary component (Z'') of the impedance are plotted on the x- and y-axes, respectively. Figure 4.1d displays the Nyquist plots of bare and modified electrodes. It can be depicted using Randles's equivalent circuit (Figure 4.1d, Inset), which consists of the Warburg impedance (W or Z_w), charge transfer resistance (R_{ct}), solution resistance (R_s), and double-layer capacitance (C_{dl}) and their corresponded values are tabulated in Table 4.1. Typically, a smaller semicircle diameter indicates a higher rate of electron transfer, while a larger diameter suggests a slower rate of electron transfer [159]. The R_{ct} values of bare GCE, CHI/GCE, AuNPs/GCE and AuNPs/CHI/GCE were 81.6 Ω, 72.2 Ω, 71.6 Ω and 60.4 Ω, respectively. The EIS results indicate that the

AuNPs/CHI-modified GCE electrode shows significantly enhanced electrochemical characteristics compared to the bare GCE and GCE modified with only one component. Here, bare GCE and GCE-modified AuNPs or CHI are highly resistive with high charge transfer resistance and larger semi-circles. Besides, the decreased R_{ct} observed in the AuNPs/CHI-modified GCE electrode signifies enhanced electron transfer kinetics, which is essential for promoting fast and efficient electrochemical reactions. The enhancements in R_{ct}, C_{dl}, and W together demonstrate the efficacy of the surface modification in enhancing the electrical conductivity and overall performance of the electrode. The rate constant (k^0) of bare and modified electrodes was determined from its EIS and CV data using Equation (4.2) as described by Randviir [2]

$$K^0 = \frac{RT}{Rct\ ACF2} \qquad (4.2)$$

where k^0, F, Rct, T, C, A, and R, are the standard heterogeneous electron transfer rate constant (cms^{-1}), Faraday constant (96,485 $Cmol^{-1}$), the electron transfer resistance (Ω), temperature (303 K), the concentration of $[Fe(CN)6]^{3-/4-}$ solution ($molcm^{-3}$), the electrode surface area (cm^2), and gas constant (8.314 $JK^{-1}mol^{-1}$), respectively. The k^0 values recorded for the bare GCE, CHI/GCE, AuNPs/GCE and AuNPs/CHI- modified GCE were 3.54×10^{-4} and 6.89×10^{-4} cms^{-1}, respectively. The AuNPs/CHI-GCE exhibits a greater k^0 value, indicating enhanced electron transport and a larger active surface area than the bare and single modified.

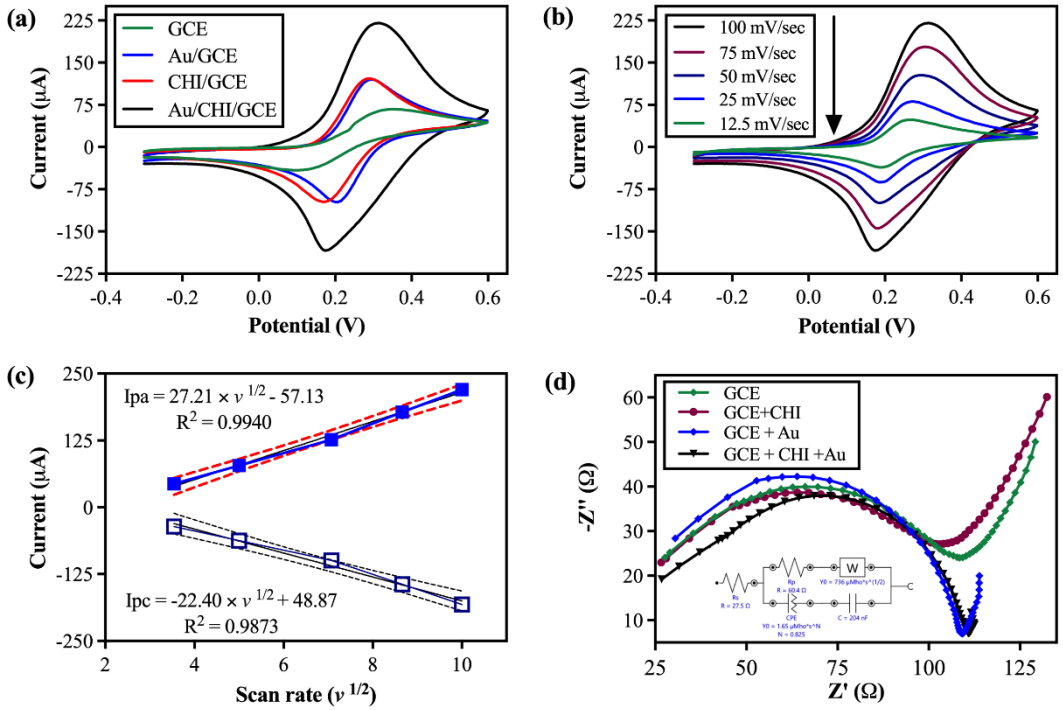


Figure 4.1 Cyclic voltammograms of (a) bare and modified GCE, (b) AuNPs/ CHI-modified GCE, (c) linear plots of anodic and cathodic peak currents of AuNPs/ CHI-modified GCE and (d) EIS spectra of bare and modified GCE (Inset- Randles equivalent circuit model). The measurements were recorded in 5 mM $K_4[Fe(CN)_6$ and 0.1 M KCl at a scan rate of 100 mV/sec.

Table 4.1 The components of the Randles equivalent circuit for both bare and modified electrodes.

Electrode	**R_s (Ω)**	**R_{ct} (Ω)**	**C_{dl}(F)**	**W($\Omega s^{-1/2}$)**
GCE	19.7	81.6	7.8×10^{-7}	0.000170
CHI/GCE	20.7	72.2	8.81×10^{-7}	0.000125
AuNPs/GCE	18.4	71.6	9.57×10^{-9}	0.000100
AuNPs/CHI/GCE	27.5	60.4	1.41×10^{-7}	0.000736

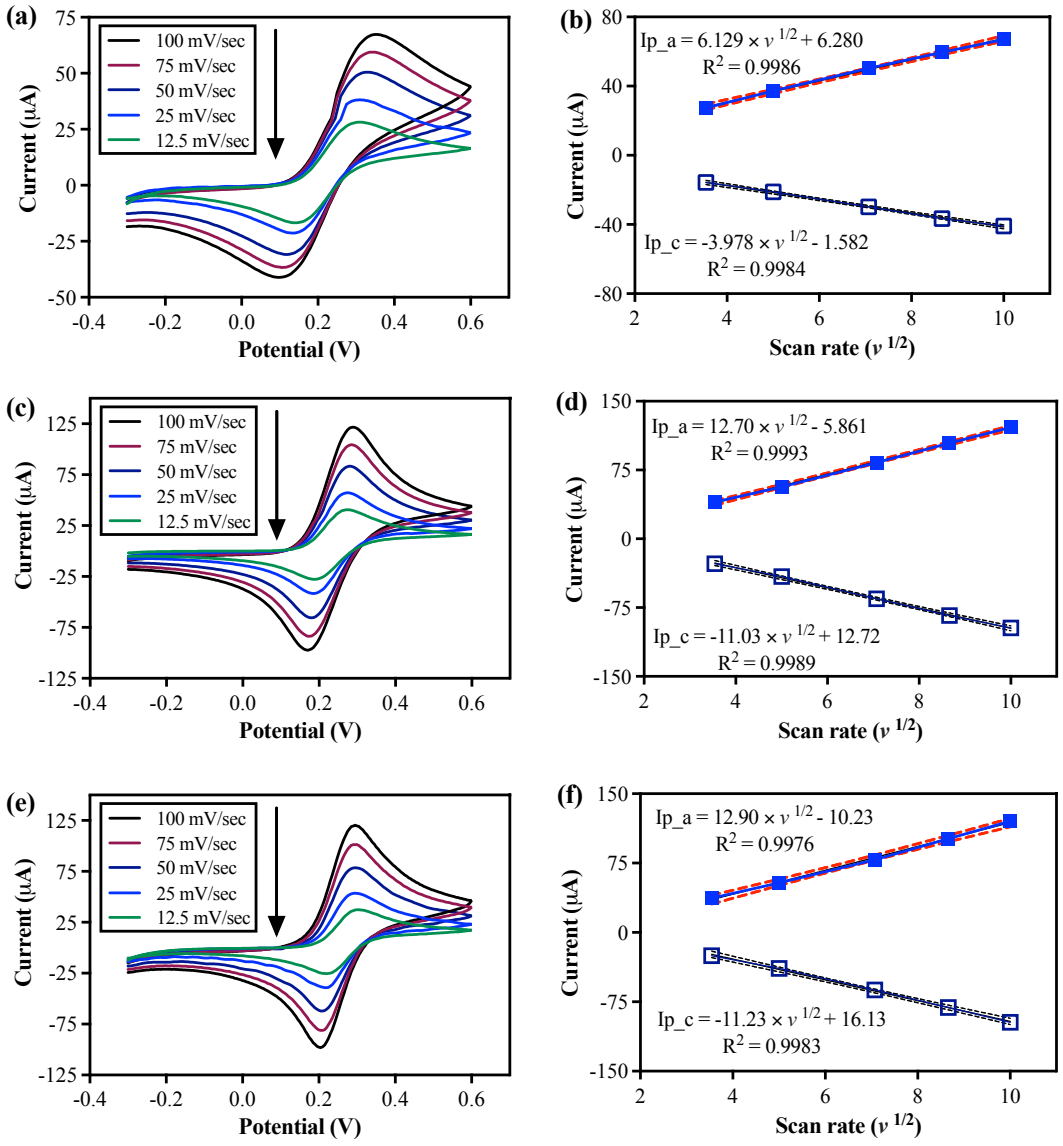


Figure 4.2 Cyclic voltammograms of (a) bare GCE, (c) CHI-modified GCE, and (e) AuNPs-modified GCE, recorded in a 0.1 M KCl solution containing 5 mM $Fe(CN)_6^{3-/4-}$. Corresponding linear plots of anodic and cathodic peak currents versus the square root of the scan rate are shown in (b), (d), and (f), respectively.

4.2 ELECTROCHEMICAL BEHAVIOUR OF CIPROFLOXACIN

The CV behaviours of CIP were examined at bare and modified GCE electrodes in PBS solution (pH 7.0) containing 0.5 µM of CIP. The scan rate was set at 50 mV/sec within the electrode potential range of 0.2 to 1.2 V. Bare and CHI-modified GCE electrodes didn't show any obvious CV response for detecting CIP (Figure 4.3). This phenomenon can be ascribed to inadequate electron transport occurring at both the unmodified and CHI-modified GCE electrodes. An enhanced CV response was observed for AuNPs modified electrode, where the transformation of Au (III) to Au (0) occurred. The oxidation peak was detected at 0.91 V, and the reduction peak was observed at 0.47 V due to the electron transformation of Au ions [158, 160]. Interestingly, the CV response was significantly increased when the CHI binder was used with AuNPs to modify the bare GCE electrode for the detection of CIP. This enhancement can be attributed to the combined effect of CHI and AuNPs on the electrode's surface, which synergistically contributed to the electrode surface [76, 161]. The influence of modified GCE on both oxidation and reduction peaks was observed for detecting CIP in an aqueous solution. For subsequent analysis, it is desirable to explain only the reduction peaks (cathodic current), which give sharper peaks than anodic currents and make it easier to evaluate the effect of scan rate, pH and temperature.

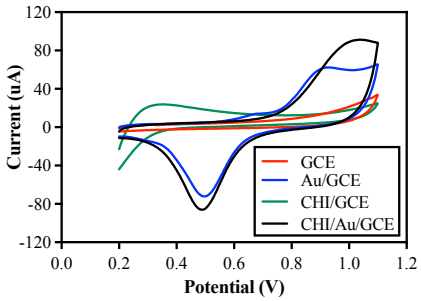


Figure 4.3 Cyclic voltametric response of GCE, CHI/GCE, AuNPs/GCE, AuNPs/CHI/GCE with 0.5 µM CIP in 0.1 M phosphate buffer at the scan rate and voltage potential was 50 m mV/sec and 0.0 to 1.2 V respectively.

4.2.1 *Effect of Scan Rate*

Fundamentally, the scan rate is a crucial parameter for unveiling the electron transfer kinetics and mechanism on the electrode. On a theoretical aspect, increasing the scan rate effectively decreases the diffusion layer thickness, resulting in a corresponding increase in peak current [162]. Herein, the electrochemical mechanism was studied by investigating the influence of five different scan rates (v) 12.5, 25, 50, 75, and 100 mV/sec - on the cathodic current and electrode potential for detecting CIP. Figure 4.4 demonstrates a gradual rise in cathodic current as the scan rates increase from 12.5 to 100 mV/sec. This is accompanied by a shift in electrode potential towards a more positive value, indicating the irreversibility of the lowering of CIP at the surface of AuNPs/CHI/GCE. The graph in Figure 4.4b demonstrates a linear regression relationship between I_p and v $^{1/2}$. The equation is $I_p = -15.01 \times v^{1/2} + 22.98$, and the correlation coefficient (R^2) is 0.9990. This indicates that the process is regulated by adsorption [76]. The reduction of CIP occurred through chemisorption, where ionic bonds formed between CIP and the surface of AuNPs/CHI/GCE. This process involves the exchange of electrons. The electrode potential (E_p) is directly proportional to the logarithm of scan rate (v), as described by the equation: $E_p = -0.06426 \times \log(v) + 0.5796$. This relationship is highly accurate, with a correlation coefficient (R^2) of 0.9989. This behavior aligns with an electrode process that cannot be reversed [163].

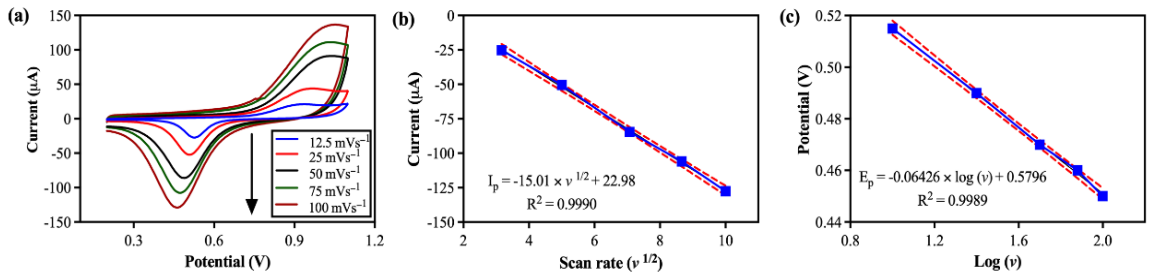
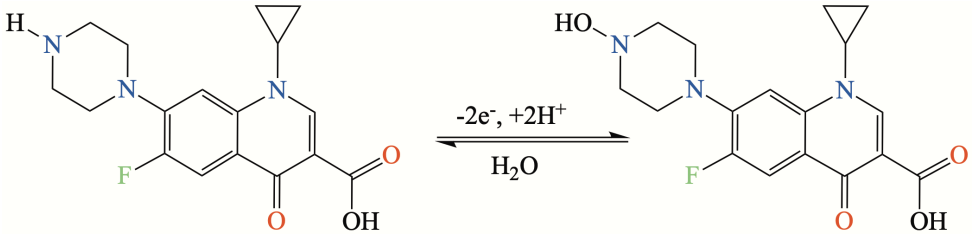


Figure 4.4 (a) CV responses of CIP on AuNPs/CHI/GCE at different scan rate ranging from 12.5 to 100 mV/sec in 0.5 µM ciprofloxacin (0.1 M PBS at pH 7); (b) linear plot between peak current and scan rate; (c) linear plot between potential vs log scan rate.

The Laviron equation was used to determine the number of electrons involved in the irreversible electrode reactions [157]. Electrode potential (Ep) is given by the equation (4.3):

$$Ep = E^0 + \frac{2.303\ RT}{\alpha nF}\log\frac{RTk^0}{\alpha nF} + \frac{2.303\ RT}{\alpha nF}\log\ \nu \qquad (4.3)$$

Where E^0, α, n, k^0, v, F, R, and T denote the formal potential, electron transfer coefficient, number of electrons, heterogeneous rate constant, scan rate, Faraday constant (96,485C/mol), universal gas constant (8.314 J/K mol), and temperature (298 K). According to Eq. (4.3), the plot of Ep versus log v shows very good linearity. The slope (0.0643) corresponds to 2.303RT/αnF, yielding αn = 0.920. For an irreversible electrode process, it is assumed that α is equal to 0.5 [157]. Therefore, the electron count was calculated to be 1.84, which is a value in close proximity to 2. This indicates that the electrochemical redox process entailed the transfer of two protons and two electrons. This discovery is consistent with the values that have been previously recorded in literature [164].



Scheme 1. Proposed reaction mechanism of Ciprofloxacin

4.2.2 Effect of Solution pH

The solution pH plays a crucial role in the development of electrochemical sensors, particularly in influencing the sensor's response and sensitivity for the detection of CIP. The solution's pH might influence the antibiotic molecules' ionization state, affecting their interaction with the electrode surface. The current investigation focused on analyzing the electrochemical behaviour of 0.5 µM CIP in 0.1 M PBS. This was achieved using cyclic voltammetry (CV) with a 50 mV/sec scan rate. The pH range

explored was 3.0 -11.0. The outcomes of this analysis are presented in Figure 4.5. The electrode potential and current intensity for detecting CIP exhibited significant variations as the pH increased from 3.0 to 11.0, as illustrated in Figure 4.5a. This demonstrates that the pH of the supporting electrolyte solution influences the oxidation and reduction of CIP. The decrease peak exhibited a distinct sharpness at pH levels of 3, 7, and below 9, indicating that the sensor demonstrates superior performance in acidic, neutral, and alkaline environments. Two pK_a values were observed for ciprofloxacin (5.90 ± 0.15 and 8.89 ± 0.11). This antibiotic can exist in several forms depending on the pH level. At a pH below 5.90, the substance can function as a cation (positively charged). When the pH is between 5.90 and 8.89, it acts as a zwitterion (containing both positive and negative charges). At a pH higher than 8.89, it becomes an anion (negatively charged) [145, 165]. It was noted that any well-defined peak was not observed at pH values 4 and 5 (Figure 4.5a and Figure 4.6a); this could be due to the cationic nature of CIP, which is positively charged in acidic solutions and was blocked from reaching the anode surface to get oxidized. However, at a higher pH greater than 8.89, where CIP exists as an anionic species, there was a decline in peak intensity for the adsorption of CIP in the sensor. As a result, the current density at pH 9 exhibited a decreased peak intensity compared to both neutral and extremely acidic pH (3.0). Conversely, a more prominent peak was seen under highly alkaline conditions (pH = 11), as shown in Figure 4.5a and Figure 4.6b. The highest peak current was also seen at a pH of 7.0. Thus, it was selected as the most favourable reaction medium condition for the following experiments. The study revealed that the peak intensity for the detection of CIP was increased as the pH of the reaction medium increased and reached a maximum at pH 7.0 (I_{pc} = 86 μA). After that, there was a modest decline in cathodic peak until pH 11.0 (I_{pc} = 75.58 μA), as depicted in Figure 4.5b. Furthermore, the impact of pH on the electrode potential for the detection of CIP was examined, and the findings are displayed in Figure 4.5c. As the pH increased from 3.0, the electrode potential went towards a higher positive value until reaching pH 5.0 (E_p = 0.690 V). After that, it declined dramatically until pH 11.0 (E_p = 0.435 V), indicating the presence of protons in

the electrochemical process. The relationship between E_p and pH can easily explained by the Nernst equation [157].

$$E_p = \frac{0.0592\, m}{n}\, pH + b \qquad (4.4)$$

Where Ep, m, n and b denote electrode potential (V), protons and electrons number involved in the electrochemical process and intercept of the equation, respectively. Figure 4.6c presents the linear regression for the cathodic electrode potential vs pH: Ep = −0.01381 pH + 0.5877 (R^2 = 0.9985).

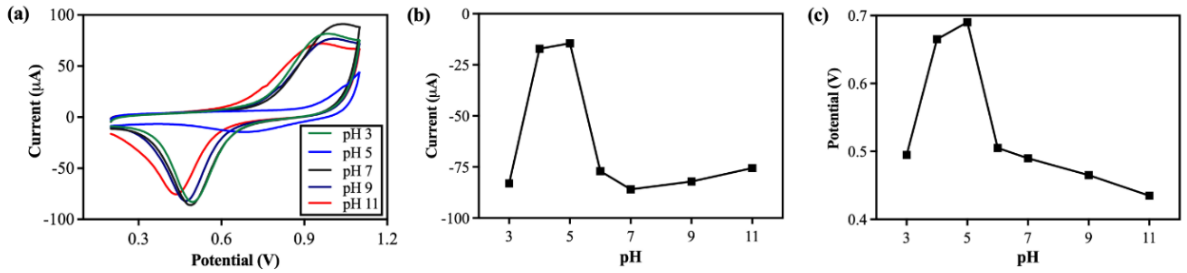


Figure 4.5 (a) Cyclic Voltammetry responses of CIP on AuNPs/CHI/GCE at different pH ranging from 3 to 11 in 0.5 µM ciprofloxacin (0.1 M PBS at 50 mV/sec); (b) the plot between peak current density and pH; c) plot between electrode potential vs pH.

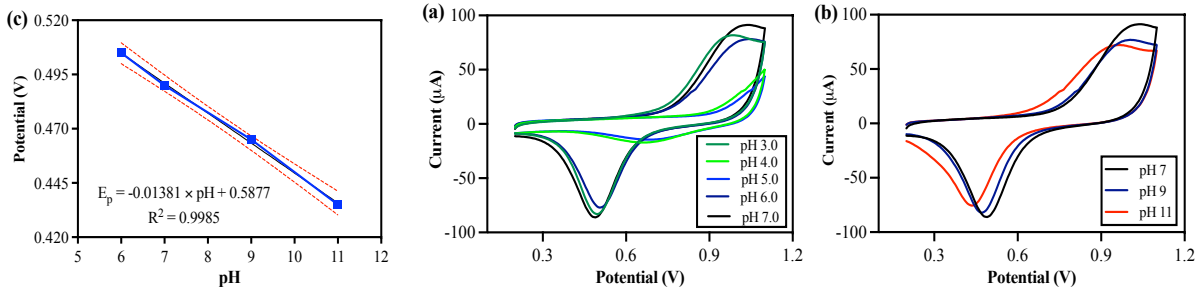


Figure 4.6 (a) Cyclic Voltammetry responses of CIP on AuNPs/CHI/GCE at acidic pH (b) alkaline pH in 0.5 µM ciprofloxacin (0.1 M PBS at 50 mV/sec) and (c) linear plot between potential vs pH data obtained ranging pH from 6 to 11.

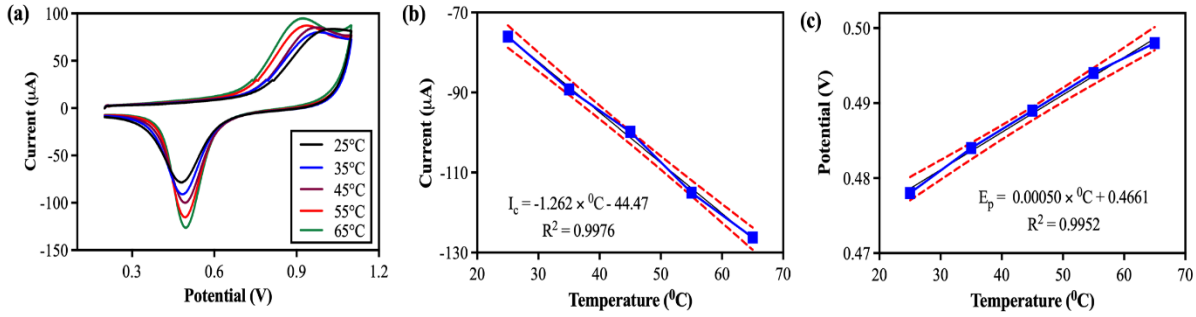


Figure 4.7 (a) Cyclic voltammetry responses of CIP on AuNPs/CHI/GCE at different temperatures ranging from 25 to 65 ^{0}C in 0.5 μM ciprofloxacin (0.1 M PBS at pH 7); (b) linear plot between peak current density and temperature; (c) linear plot between electrode potential vs temperature

4.2.3 Effect of Temperature

In order to examine the impact of temperature on CIP, the cathodic peak current was measured utilizing electrodes made of AuNPs/CHI/GCE. The cyclic voltammograms were measured throughout a range of temperatures (25 - 65 °C) using a potential range of 0.2 to 1.2 V and a scan rate of 50 mV/sec as shown in Figure 4.7. It is evident that there is a consistent rise in peak current as the temperature increases. The peak location exhibited a progressive movement towards negative values as the temperature increased, and the cathodic current peaks shifted from 25 to 65°C. The cathodic reduction peak was observed at a maximum potential of 0.49 V at a temperature of 65°C. However, the enhancement in peak current suggests that the higher reaction kinetics, higher rate of mass transfer and/or the number of active sites had risen as a result of the rise in the temperature of the reaction medium. The decrease in CV potentials at higher temperatures indicates the formation of noble catalytic pathways. These pathways require less energy to carry out the CIP. Additionally, the cathodic electrode potential remains constant, indicating the occurrence of the reduction phase of CIP.

4.3 DESCRIPTIVE STATISTICS

The statistical characteristics of the dataset used to predict ciprofloxacin (CIP) detection using sensors fabricated with AuNPs and CHI-modified GCE are presented in Table 4.2. The analysis computed various statistics based on four input parameters: reaction medium pH, scan rate (mV/sec), temperature (^{0}C) and potential (V). The output parameter reflected the cathodic current (μA). The mean values of each parameter refer to its average level such as scan rate of 50 mV/sec, solution pH of 7, temperature of 30 ^{0}C, and the cathodic currents were measured in microamperes (μA) as specified in Table 4.2. The standard deviation quantifies the dispersion of data around the mean. Minimum and maximum values establish the range of the data, hence showing the amount of variability. Percentiles, namely the 25th, 50th, and 75th, divide the data into quartiles, which give a better view of the distribution of the data and help in identifying any skewness or outliers. Skewness is a measure of asymmetry, with values closer to zero indicating greater symmetry of the data distribution. Kurtosis gives an indication of the shape of the distribution, with negative kurtosis values indicating a flatter-than-normal distribution. The measures of central tendency, variability, and distribution characteristics give comprehensive information about the dataset.

Figure 4.8 displays a Pearson correlation coefficient that comprehensively represents the correlation matrix between important variables, including pH, scan rate, temperature, electrode potential, and cathodic current. The correlation coefficient for each cell indicating the magnitude and direction of the linear relationships. The coefficient values range from -0.37 to 0.25. The diagonal elements consistently display a value of 1.00, indicating a perfect correlation between each variable and itself. Shades of brown are used to represent negative correlations, with darker shades indicating greater inverse associations. For instance, the pH has a moderate negative association with the scan rate (-0.33), temperature (-0.28), potential (-0.33), and current (-0.35). In contrast, shades of blue are used to depict positive correlations, with darker tones indicating

greater direct associations, such as the correlation between scan rate and current (0.25). Lighter hues like light blue suggest weak or insignificant correlations, such as the weak positive correlation (0.14) between electrode potential and cathodic current. The heatmap is a crucial instrument for researchers, offering a straightforward and precise method of recognizing and comprehending the connections within the dataset, facilitating more knowledgeable decision-making and deeper exploration of the factors involved.

Table 4.2 Statistical analysis of the experimental data.

Statistics	**pH**	**Scan rate (mV/sec)**	**Temperature (^{0}C)**	**Potential (V)**	**Cathodic current (μA)**
Count	2319	2319	2319	2319	2319
Mean	7	50	37.79	0.44	34.828
Std	1.29	14.95	12.65	0.139	30.519
Min	3	12.5	25	0.20	1.587
25%	7	50	30	0.32	10.956
50%	7	50	30	0.44	21.458
75%	7	50	45	0.56	53.468
Max	11	100	65	0.68	128.929
Skewness	0	0.679	1.09	6.18×10^{-17}	1.107
Kurtosis	5.128	4.943	-0.234	-1.200	0.210
Correlation with output	-0.35	0.25	-0.32	0.14	1

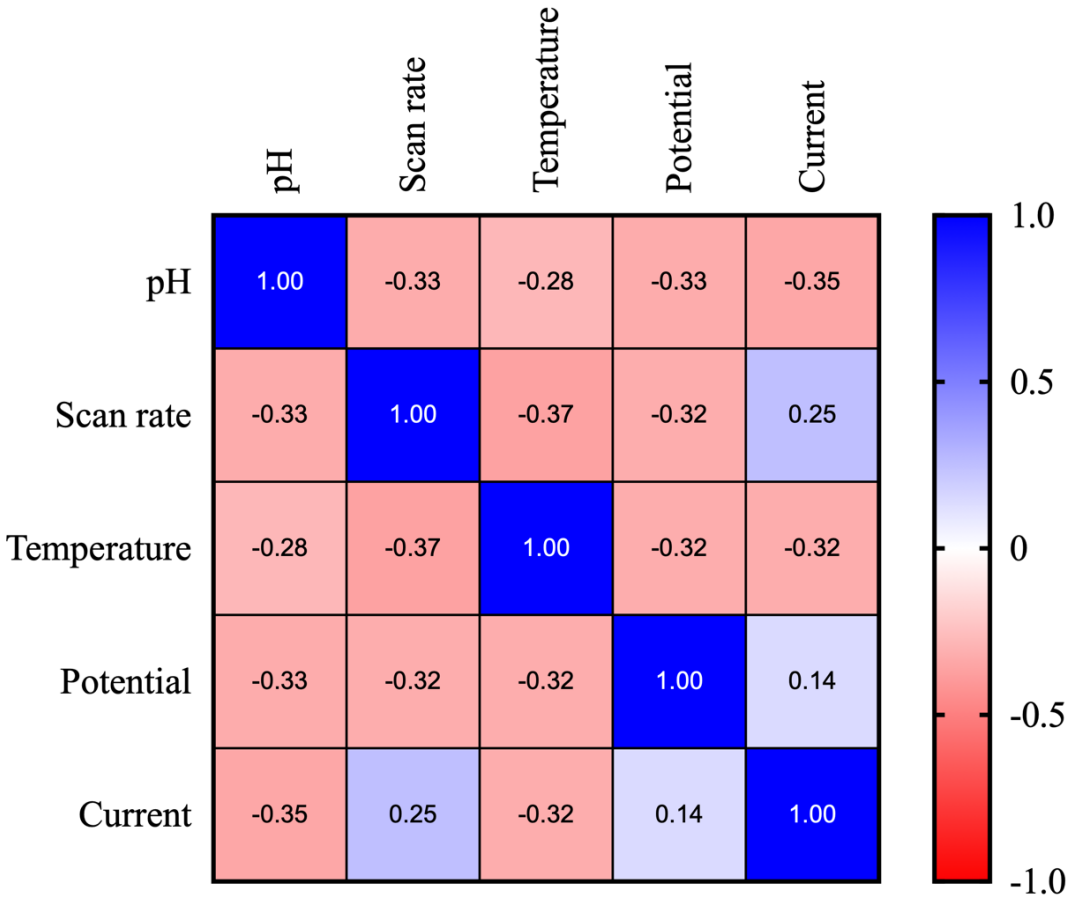


Figure 4.8 Pearson correlation coefficient of experimental parameters.

4.4 MODEL PERFORMANCE EVALUATION

The hyperparameters for the AdaBoost, Bagging, CatBoost, Decision Tree, Extra Trees, Gradient Boosting, HistGradientBoosting, LightGBM, Random Forest, and XGBoost models are optimized using Bayesian optimization. Figure 4.9 shows the scatter plots of training and test datasets, enabling a comparison between experimental and predicted values for all these models. From the scatter plots, it can be observed that the experimental and predicted values of the training data for the chosen models are highly correlative; the points gather closely around the 45-degree reference line. Each model was trained and evaluated with a dataset consisting of 2,319 data points. The hyperparameter setting in machine learning models has a direct and considerable

impact on the model's prediction performance [166]. Consequently, optimizing the hyperparameters before the AI model's prediction process is necessary. This study employed the Bayesian optimization (BO) technique to determine the most suitable parameter configuration for 10 machine learning models. The BO technique used the bayes_opt module in the Python computer language [167]. Furthermore, the BO fine-tuned the hyperparameters across all models, conducting 200 iterations. The optimal hyperparameter values for all 10 models were computed, resulting in the values presented in Table 4.3.

This study utilizes BO technique, which treats the objective function as an unknown black box function and aims to identify the optimal solution that maximizes the function value. This technique necessitates the implementation of two fundamental algorithms to carry out the process of optimization. At first, a surrogate model uses probability to approximate the shape of an objective function that is not known. The acquisition function identifies the most advantageous candidate values for determining the best solution by using a probabilistic estimation of the objective function. The BO repeatedly executes the two algorithms a specified number of times, consistently identifying potential values that are progressively closer to the accurate solution. Stochastic analysis-based optimization techniques can track the optimal hyperparameters much faster than other automated optimization approaches[168]. Table 4.3 summarizes the ranges of hyperparameters with their optimal values.

Table 4.3 Hyper-parameters' optimal values

Adaboost	max_depth= 10, learning_rate= 0.09879773, n_estimators= 198
Bagging	max_features= 1.0, max_samples= 1.0, n_estimators= 88
CatBoost	bagging_temperature= 0.0, depth, 16, iterations= 281, l2_leaf_reg=1e-08, learning_rate= 0.02064, random_strength= 0.1
Decision Tree	ccp_alpha= 0.0, max_depth= 150, max_features= None, max_leaf_nodes= 500, min_impurity_decrease= 0.0, min_samples _leaf = 1, min_samples_split= 2
ExtraTree	max_depth= 17, max_features= 0.370818, min_samples_leaf= 1, min_samples_split= 2, n_estimators= 300
GradientBoosting	learning_rate= 0.039622, max_depth= 19, max_features= 0.508653, min_samples_leaf= 4, min_samples_split= 18, n_estimators= 300, subsample= 0.535356
HistGradientBoost	l2_regularization= 0.033512, learning_rate= 0.119708, max_bins= 114, max_depth= 14, max_iter= 300, max_leaf_nodes= 15, min_samples_leaf= 4
LightBoost	colsample_bytree= 0.867014, learning_rate= 0.244097, max_depth= 6, min_child_samples= 5, n_estimators= 242, num_leaves= 124, subsample= 0.729512
Random forest	max_depth= 28, max_features= 0.1, min_samples_leaf= 1, min_samples_split= 2, n_estimators= 300
XGBoost	colsample_bytree= 1.0, learning_rate= 0.044654, max_depth= 8, min_child_weight= 1, n_estimators= 300, subsample= 0.5

Table 4.4 Feature importances for the studied models

Adaboost	pH = 0.043207 Scan rate = 0.101468 Temperature = 0.073699 Potential = 0.781627
Bagging	pH = 0.055323 Scan rate = 0.118522 Temperature = 0.041543 Potential = 0.784612
CatBoost	pH = 0.257002 Scan rate = 0.209474 Temperature = 0.059205 Potential = 0.474319
ExtraTree	pH = 0.045035 Scan rate = 0.089873 Temperature = 0.057564 Potential = 0.807528
GradientBoosting	pH = 0.052876 Scan rate = 0.115172 Temperature = 0.042673 Potential = 0.789279
HistGradientBoosting	pH = 0.058429 Scan rate = 0.115706 Temperature = 0.039392 Potential = 0.786472
LightBoost	pH = 0.109330 Scan rate = 0.102843 Temperature = 0.140431 Potential = 0.647396
Random Forest	pH = 0.048265 Scan rate = 0.091247 Temperature = 0.052577 Potential = 0.807911
XGBoost	pH = 0.056426 Scan rate = 0.112253 Temperature = 0.043694 Potential = 0.787627

In scatter plots, the black dotted lines represent the ideal regression line. The scatter plots shown in Figure 4.9 illustrate the effectiveness of ten studied models during the detection of CIP in an aqueous solution. Each scatter plot differentiates between the training (pink markers) and the test datasets (blue markers). The points that closely coincide with the diagonal line (black dotted line) of the scatter plot exhibited a correlation with the predictions and actual values that show the accuracy of the model [32, 33, 145]. Out of the models mentioned, CatBoost (Figure 4.9c), LightGBM (Figure 4.9h), and XGBoost (Figure 4.9j) showed the highest level of alignment with the diagonal line. This implies that the predictive performance is strong and consistent with low variability across both the training and testing datasets. The strong correlation shows their robustness and outstanding ability to predict cathodic current efficiency. AdaBoost (Figure 4.9a), Bagging (Figure 4.9b) and Decision Tree (Figure 4.10d) show that their data points extend from the standard regression line (black dotted line) to a wide scattered area, especially in the test dataset. This suggests reduced prediction accuracy and the possibility of overfitting during the training phase. The scatter plots for these models demonstrate less accurate predictions, with greater variability between the experimental and anticipated values. The scatter plots of the Extra Trees (Figure 4.9e), Gradient Boosting (Figure 4.9f), HistGradientBoosting (Figure 4.9g) and Random Forest (Figure 4.9i) models exhibit a reasonable prediction performance, considered by relatively close gathering points around the ideal regression line. However, this clustering is less compact than the top-performing models. These models offer accurate forecasts with moderate precision, recommending a well-balanced CIP prediction performance across the train and test datasets.

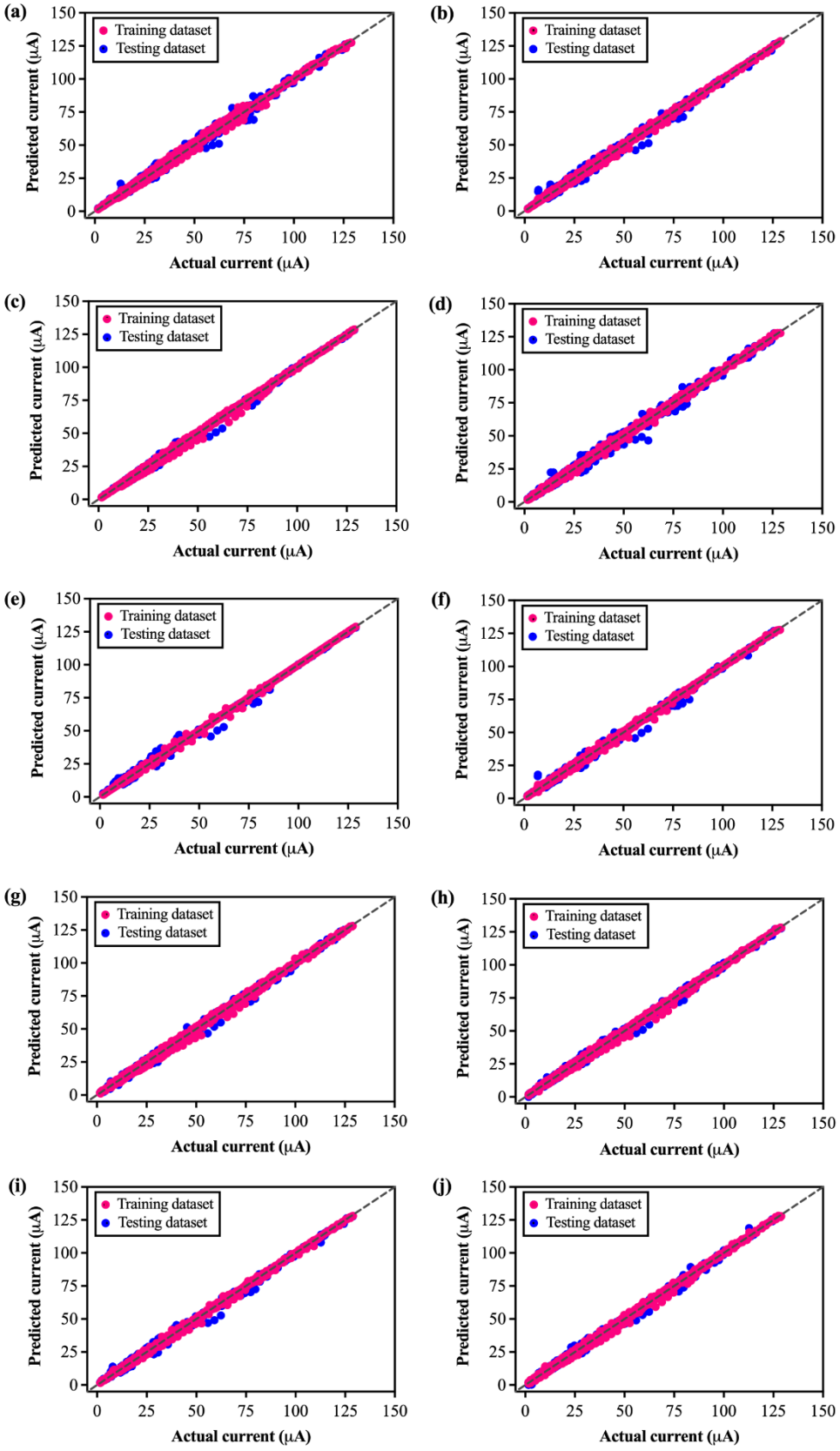


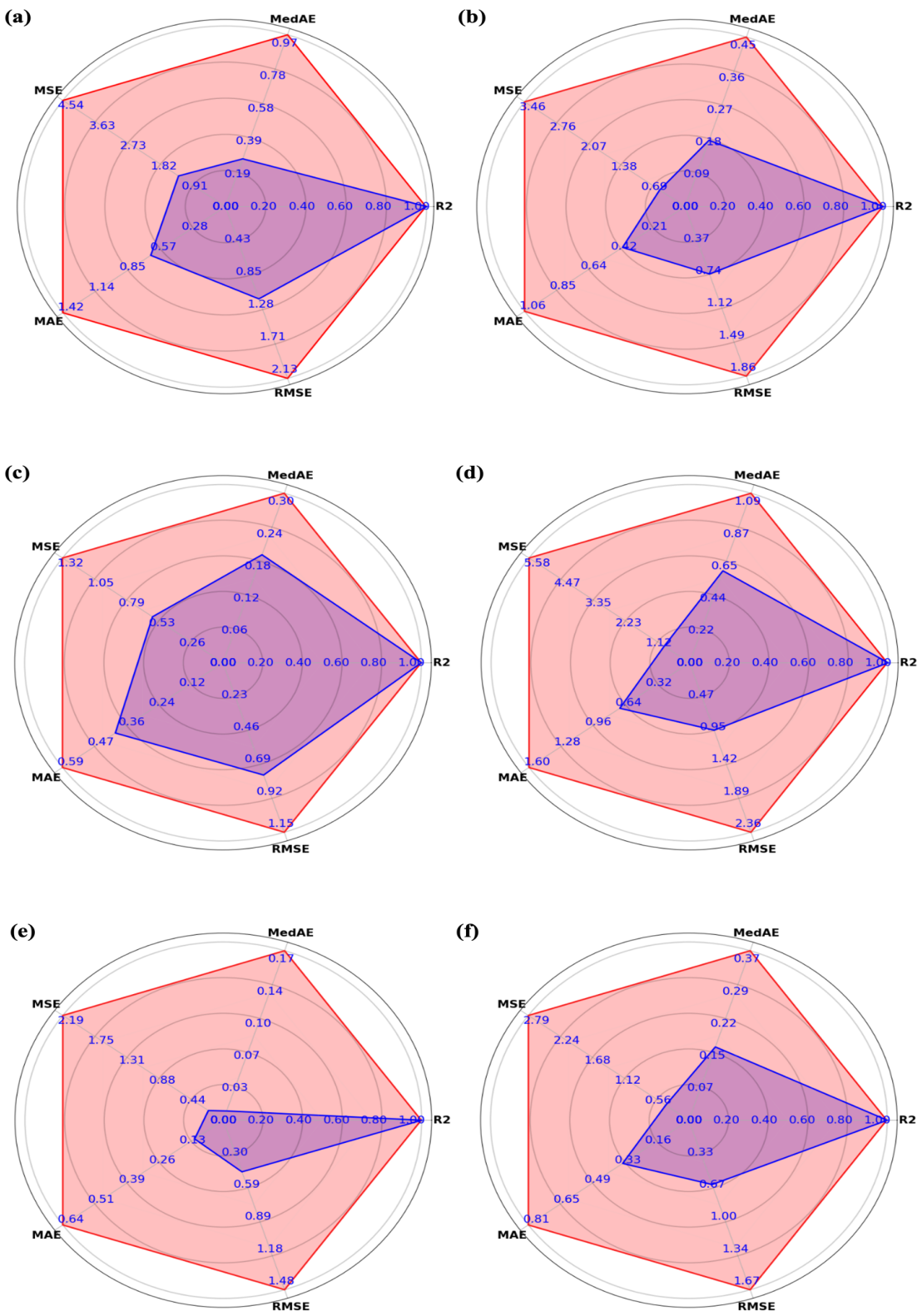
Figure 4.9 The scatter plot for the models: (a) AdaBoost, (b) Bagging, (c) CB, (d) DT, (e) ET, (f) GB, (g) HGB, (h) LGB, (i) RF and (j) XGBoost.

Table 4.5 Performance matrices of studied ML models

Model		R^2 Score	MSE	RMSE	MAE	MedAE
AdaBoost	Training	0.9985	1.3112	1.14509	0.6532	0.2699
	Testing	0.9952	4.5426	2.13135	1.4217	0.9709
Bagging	Training	0.9994	0.5465	0.7393	0.4131	0.1769
	Testing	0.9963	3.4558	1.8589	1.0604	0.4523
CatBoost	Training	0.9993	0.5781	0.7603	0.3973	0.1881
	Testing	0.9986	1.31706	1.1476	0.5923	0.2954
Decision Tree	Training	0.99904	0.8838	0.9401	0.6961	0.5904
	Testing	0.99412	5.5831	2.3628	1.6019	1.0885
Extra Trees	Training	0.9997	0.2030	0.4505	0.1147	0.0092
	Testing	0.9976	2.1885	1.4793	0.6426	0.1696
Gradient Boosting	Training	0.9995	0.4023	0.6343	0.3359	0.1580
	Testing	0.9970	2.7942	1.6715	0.8143	0.3654
HistGradient Boosting	Training	0.9989	0.9477	0.9735	0.6021	0.3404
	Testing	0.9976	2.2142	1.48804	0.9333	0.51906
LightGBM	Training	0.9993	0.6378	0.7967	0.4736	0.2632
	Testing	0.9978	2.02302	1.4223	0.9232	0.5799
Random Forest	Training	0.9994	0.4854	0.6967	0.3785	0.1717
	Testing	0.9972	2.6448	1.6262	0.9152	0.4382
XGBoost	Training	0.9991	0.7636	0.8738	0.5476	0.3291
	Testing	0.9978	2.0753	1.4406	0.93505	0.5928

The assessment of machine learning models entailed the comparison of essential metrics, such as R^2, MSE, RMSE, MAE, and MedAE. These measures offer vital insights into the capacity of each model to accurately fit the training data and make precise predictions on unknown data, providing a thorough evaluation of their overall performance. The comprehensive outcomes have been summarized in Table 4.5. Figure 4.10 displays radar plots that depict the assessment metrics of different classical and ensemble machine-learning models. The value of R^2 quantifies the degree to which the predictions match with the actual values. A score close to 1 signifies a robust correlation and a precise fit of the model. The training dataset exhibits near-perfect R^2 values, indicating successful hyperparameter fine-tuning using Bayesian optimization. The mean squared error (MSE) applies a greater penalty to larger deviations by calculating the average of the squared errors. Mean absolute error (MAE) measures the average absolute difference between predicted and actual values, assigning equal weight to all variances. On the other hand, median absolute error (MedAE) emphasizes the median of these absolute differences, hence limiting the influence of outliers. Superior model performance and low model-data discrepancy are indicated by low MSE, MAE, and MedAE values. Smaller RMSE values also signify more precise forecasts [169, 170].

CatBoost has outstanding performance on both the training and testing datasets. CatBoost (Figure 4.10c) gets an exceptional R^2 score of 0.9993 on the training set, along with the lowest error metrics - MSE of 0.5781, RMSE of 0.7603, MAE of 0.3973, and MedAE of 0.1881. The results demonstrate a strong correlation between the training data and low discrepancies in predictions. The testing set exhibits a strong R^2 value of 0.9986 and demonstrates relatively low error metrics, including an MSE of 1.3171, RMSE of 1.1476, MAE of 0.5923, and MedAE of 0.2954. This demonstrates the capacity of CatBoost to achieve a balance between high accuracy and effective generalization to unseen data.


(a)
MedAE
MSE
MAE
RMSE
R2
0.97
0.78
0.58
0.39
0.19
0.00 0.20 0.40 0.60 0.80 1.00
4.54
3.63
2.73
1.82
0.91
1.42
1.14
0.85
0.57
0.28
2.13
1.71
1.28
0.85
0.43
(b)
MedAE
MSE
MAE
RMSE
R2
0.45
0.36
0.27
0.18
0.09
0.00 0.20 0.40 0.60 0.80 1.00
3.46
2.76
2.07
1.38
0.69
1.06
0.85
0.64
0.42
0.21
1.86
1.49
1.12
0.74
0.37
(c)
MedAE
MSE
MAE
RMSE
R2
0.30
0.24
0.18
0.12
0.06
0.00 0.20 0.40 0.60 0.80 1.00
1.32
1.05
0.79
0.53
0.26
0.59
0.47
0.36
0.24
0.12
1.15
0.92
0.69
0.46
0.23
(d)
MedAE
MSE
MAE
RMSE
R2
1.09
0.87
0.65
0.44
0.22
0.00 0.20 0.40 0.60 0.80 1.00
5.58
4.47
3.35
2.23
1.12
1.60
1.28
0.96
0.64
0.32
2.36
1.89
1.42
0.95
0.47
(e)
MedAE
MSE
MAE
RMSE
R2
0.17
0.14
0.10
0.07
0.03
0.00 0.20 0.40 0.60 0.80 1.00
2.19
1.75
1.31
0.88
0.44
0.64
0.51
0.39
0.26
0.13
1.48
1.18
0.89
0.59
0.30
(f)
MedAE
MSE
MAE
RMSE
R2
0.37
0.29
0.22
0.15
0.07
0.00 0.20 0.40 0.60 0.80 1.00
2.79
2.24
1.68
1.12
0.56
0.81
0.65
0.49
0.33
0.16
1.67
1.34
1.00
0.67
0.33

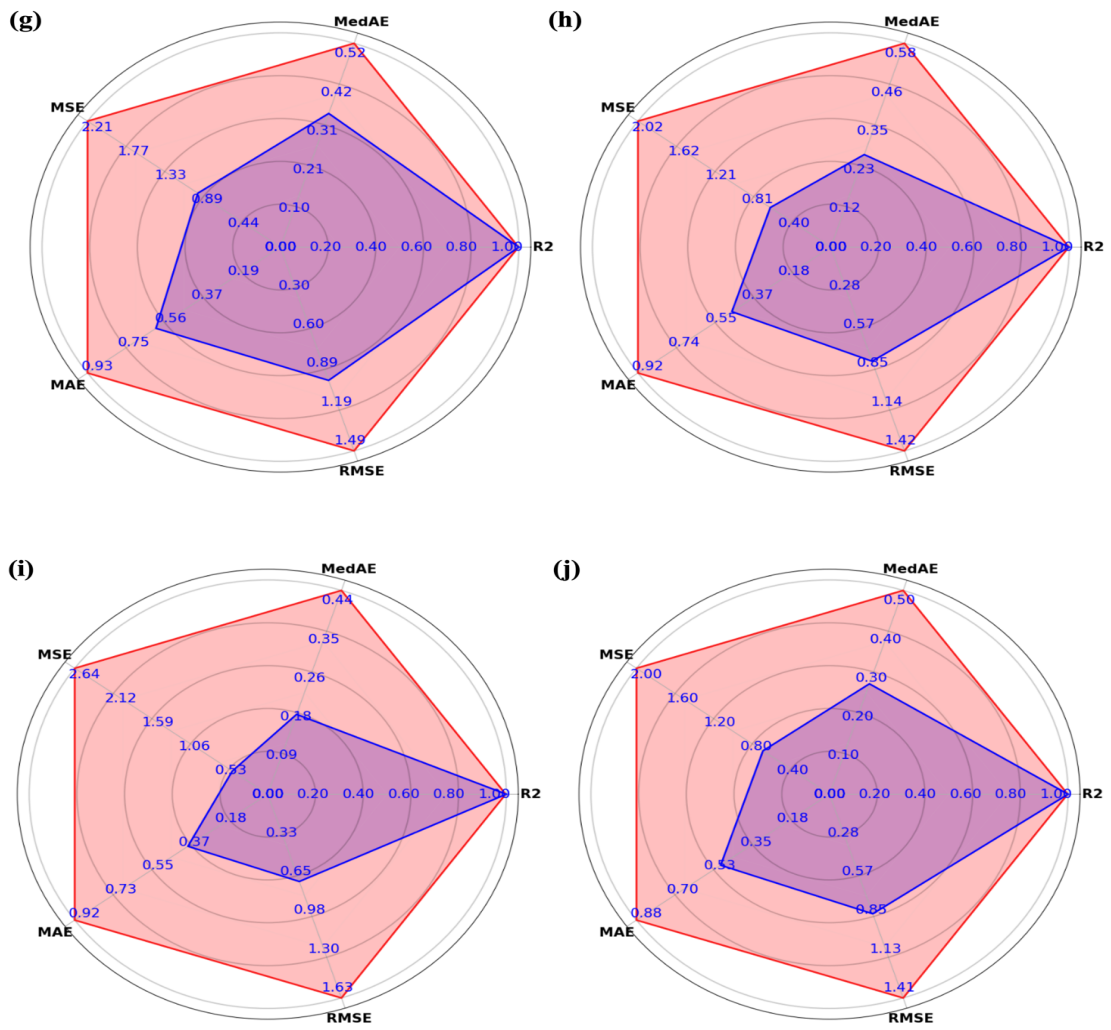


Figure 4.9 The radar plot for the models: (a) AdaBoost, (b) Bagging, (c) CatBoost, (d) Decision Tree, (e) Extra Trees, (f) Gradient Boosting, (g) HistGradientBoosting, (h) LightBoost, (i) Random Forest and (j) XGBoost.

LightGBM (Figure 4.10h) and XGBoost (Figure 4.10j) exhibit impressive performance, attaining high R^2 scores and relatively low error metrics. LightGBM demonstrates a high R^2 value of 0.9993 on the training set and a slightly lower R^2 value of 0.9978 on the testing set. Additionally, it achieves low values for MSE, RMSE, MAE, and MedAE, indicating good performance. XGBoost achieves a R^2 of 0.9991 on the training set and 0.9978 on the testing set. Although both models demonstrate exceptional training accuracy, their performance on the testing set, while still strong, is

not as optimum as that of CatBoost. This indicates strong overall generalization, however with marginally higher error rates compared to CatBoost. The Extra Trees model (Figure 4.10e), Gradient Boosting model (Figure 4.10f), HistGradientBoosting model (Figure 4.10g), and RandomForest model (Figure 4.10i) demonstrate exceptional training performance ($R^2 > 0.999$) on the training set. However, they experience a smaller performance decline on the test set, with an $R^2 > 0.997$. AdaBoost, Bagging, and Decision Tree, as shown in Figures 4.10a, 4.10b, and 4.10d, respectively, exhibit high performance in training with an R^2 value of more than 0.999. However, they face challenges in effectively generalizing their performance. More precisely, the R^2 value of Bagging decreases from 0.9994 during the training phase to 0.9963 during the testing phase. On the other hand, AdaBoost and Decision Tree demonstrate the lowest performance compared to other models. The R^2 of the Decision Tree model decreases dramatically from 0.999 during the training phase to 0.994 during the testing phase. Additionally, the model exhibits high values for the MSE at 5.5821, RMSE at 2.3628, MAE at 1.6019, and MedAE at 1.089. Similarly, the R^2 of AdaBoost experiences a significant decrease from 0.9985 during the training phase to 0.9952 during the testing phase. This decrease is accompanied by high error values, including an MSE of 4.5426, RMSE of 2.1314, MAE of 1.4217, and MedAE of 0.9709. The three models exhibit significant drops in performance when tested, with radar plots indicating smaller optimal ranges and larger areas showing poorer performance. The current situation indicates a risk of overfitting to the training data and challenges in generalizing to unseen data. The differences in prediction skills can be ascribed to the properties of the data, the sensitivity of the electrodes, the nature of the contaminants, the input factors, and the algorithms used. The high R^2 values across all ten models indicate a high level of accuracy and a strong correlation between the observed and projected data. This demonstrates their appropriateness for predicting cathodic current in the detection of ciprofloxacin antibiotic in water-based solutions.

To better illustrate the forecasted results from the models developed, a residual plot was drawn showing the differences between the various predicted and observed values. Figure 4.11 shows the data points arranged in ascending order along the x-axis and then refined using Bayesian techniques. A model is considered stronger if the residual errors are located as close to the zero line as much as possible [32, 146]. The CatBoost model exhibits a far more compact clustering of residuals centered around the zero line, with the y-axis spanning from -10 to +10. This suggests a significant degree of precision and low margin of error in its forecasts. The residuals exhibit a uniform distribution over the projected cathodic current range, indicating that these models possess the ability to consistently forecast larger currents with minimal bias or volatility (Figure 4.11c). The even distribution of residuals indicates that these models are able to effectively handle the intricacies of the dataset, making them extremely dependable for real-world use. The other models likewise exhibit a rather compact clustering of residuals data points around zero, with a little wider distribution in comparison to CatBoost. The residual plots display a predominantly uniform distribution, indicating that these models typically excel in their predictive tasks. However, they appear to be sensitive to specific outliers or variations within the dataset. Although these outliers are infrequent, their occurrence suggests that the models are generally robust. Nonetheless, further fine-tuning or modification to the models could potentially enhance their predictive effectiveness.

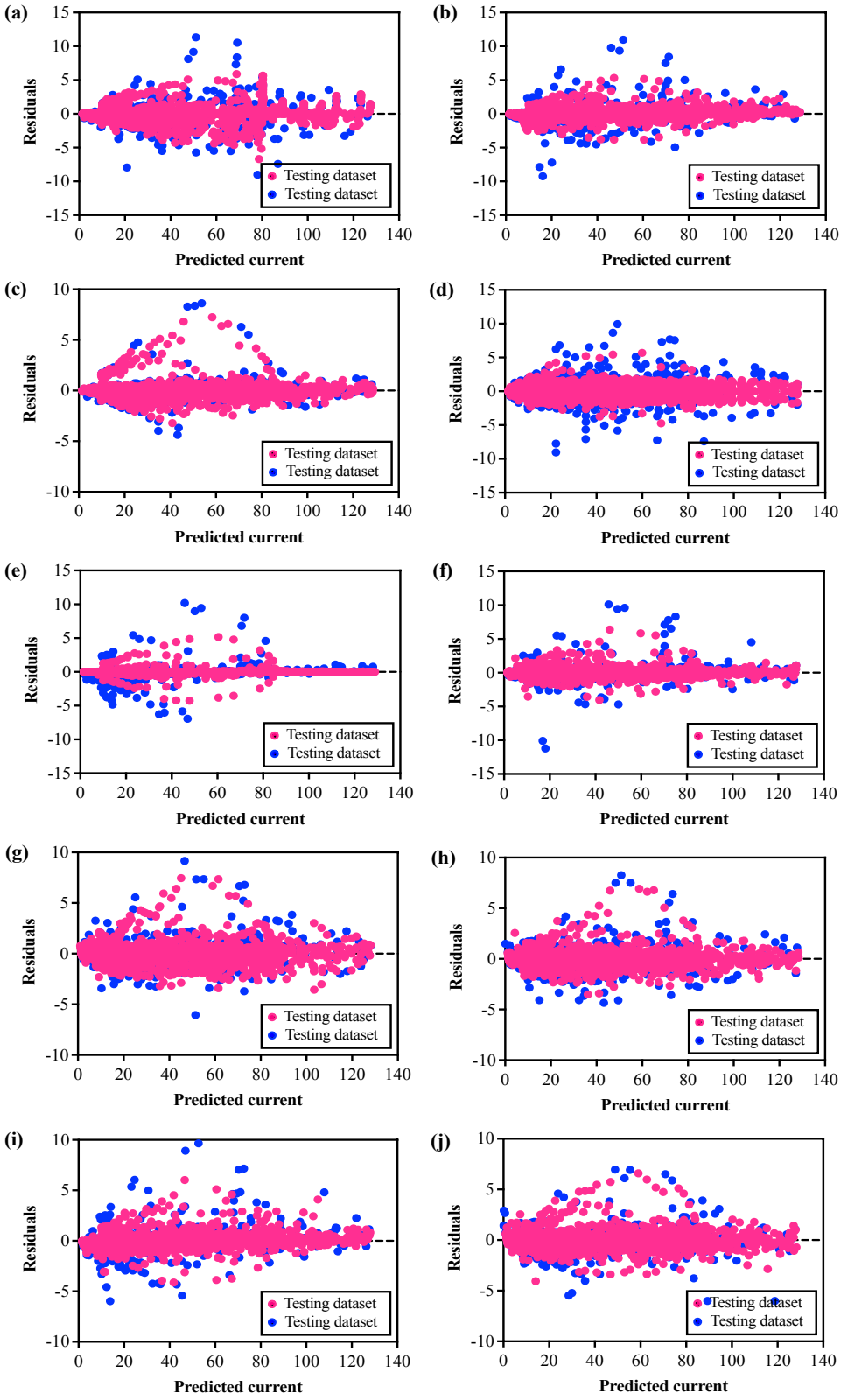


Figure 4.10 The residual plot for (a) AdaBoost, (b) Bagging, (c) CB, (d) DT, (e) ET, (f) GB, (g) HGB, (h) LGB, (i) RF and (j) XGBoost.

4.5 NORMALISED IMPORTANCE OF FACTORS UNDER THE MODELS

Multiple factors affect the cathodic current in detecting CIP, and it is clear that their effects vary. Figure 4.12 and Table 4.4 present the statistical importance of the input features in relation to the cathodic current efficiency. The results showed that all models have substantial potential, with values exceeding 0.50. The Extra Trees and Random Forest models exhibit the highest normalised importance (0.81) for potential, suggesting that potential considerably impacts cathodic current efficiency. The scan rate is a critical factor that applies to all models. An increased scan rate results in higher cathodic peak current efficiency. The efficiency performance of the current is influenced by the pH and temperature of the system, which can impact the effectiveness of currents [171, 172]. Evaluating the comparative significance of input characteristics can offer valuable insights into understanding the effectiveness of forecasting antibiotics. Table 4.3 presents the spectrum of hyperparameters and their most effective values, which were identified using Bayesian optimization calculations. Deliberate choices were made when fine-tuning the machine learning model for individual tasks, finding a middle ground between the network's intricacy and regularization to maximize its learning performance.

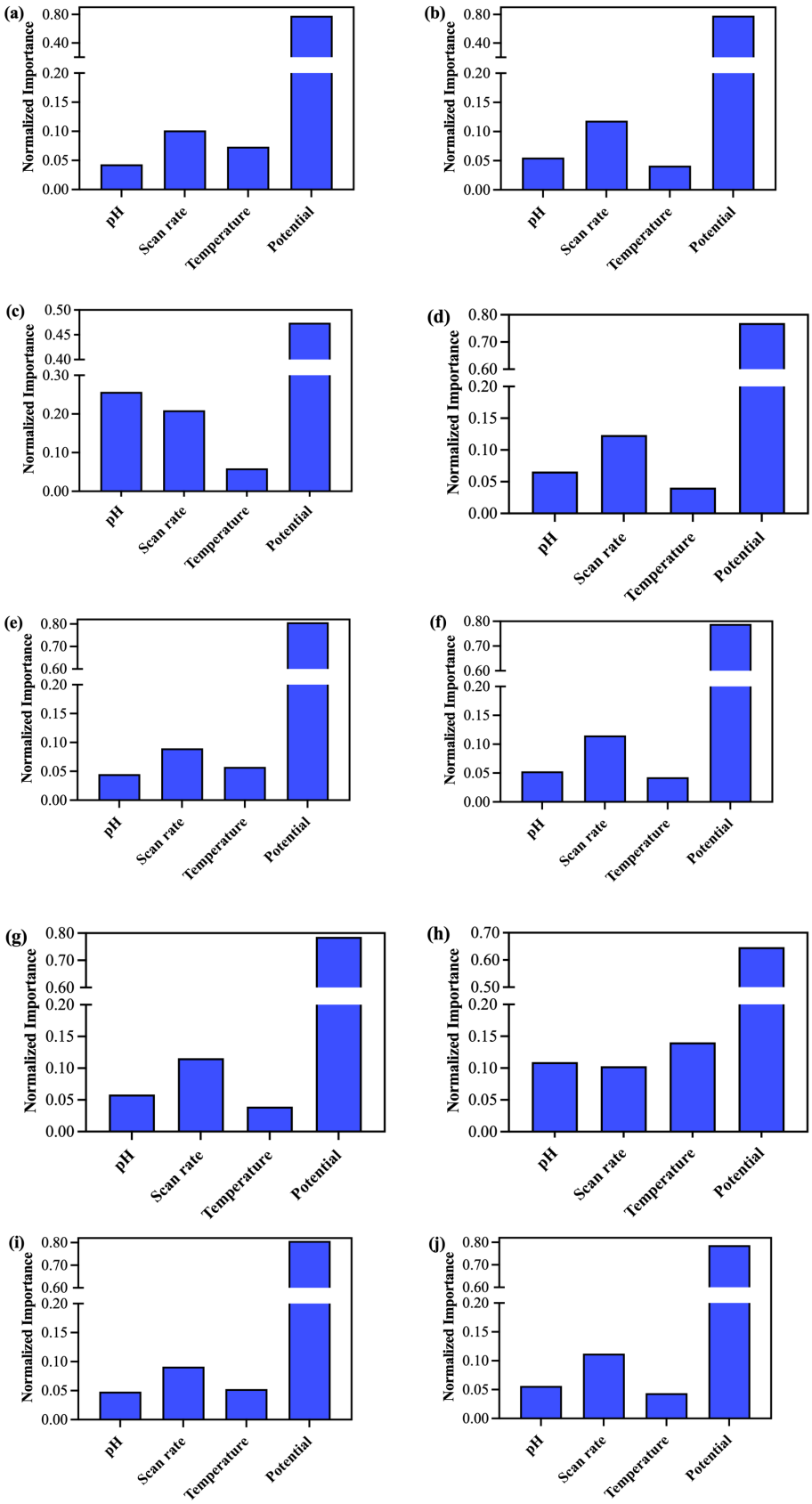


Figure 4.11 The Feature importance for the models: (a) AdaBoost, (b) Bagging, (c) CB, (d) DT, (e) ET, (f) GB, (g) HGB, (h) LGB, (i) RF and (j) XGBoost.

4.6 BEST MODEL AND ITS VALIDATION

SHapley Additive exPlanations (SHAP) analysis offers a reliable and precise assessment of each feature by assigning its influence on the model output. This approach comprehensively comprehends how each parameter contributes to forecasts for the identification of CIP depending on cooperative game theory. SHAP provides a means to visually represent and understand how each attribute affects the predictions made by the model. Traditional feature importance values in tree-based models reflect just the overall significance of a model's inputs and do not account for nuanced and specific impacts of these variables. In contrast, the SHAP provides insights into local feature impacts both in a direction and magnitude. While both approaches generally agree on potential as the main predictor, SHAP analysis reveals subtler details, especially for cases where effects are different due to interactions with other features. This promotes transparency and confidence in the model's behaviour. Figure 4.13a illustrates the significance of the global feature of the best CB model in predicting current efficiency by sensing CIP. The potential had the greatest influence, with a significance value of +21.90, followed by the scan rate with a score of +3.28. The temperature of the reaction medium had a moderate impact, with a score of +2.5, while the solution pH had a relatively smaller effect, with a score of +2.29. This visualization provides useful information about the fundamental characteristics of the model's decision-making process. Additionally, the SHAP summary plot in Figure 4.13b validates the impact of these results on various variables in the output of the CB model. The SHAP values demonstrate that the potential, scan rate, temperature and pH of the reaction medium considerably impact the model's predictions, matching the observed rankings of feature relevance in Figures 4.13.

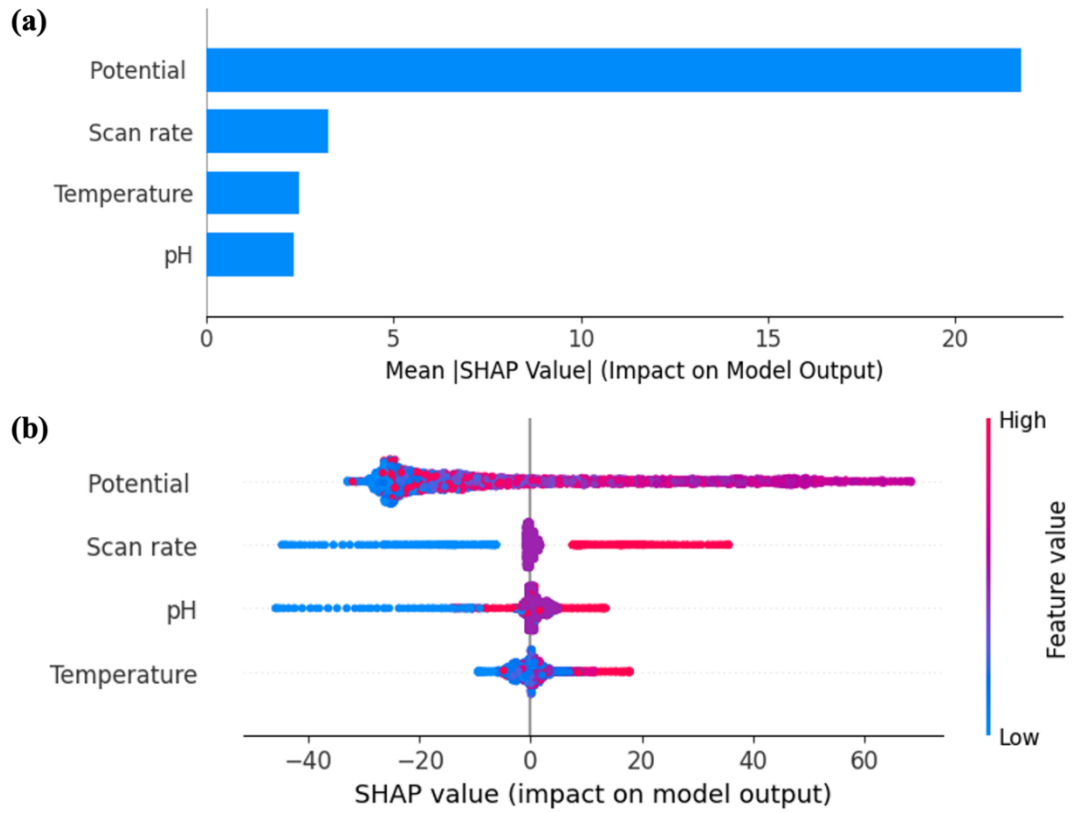


Figure 4.12 (a) Global feature importance assessed through SHAP values, (b) The summary plot (beeswarm plot) illustrates the distribution of feature impacts on the output of the CatBoost.

Model robustness refers to a model's ability to consistently achieve high performance when presented with new data, rather than just test data. It is crucial for the model to maintain stability in order to perform well. The experimental validation was conducted under conditions identified by the CB model's optimization process, which determined the optimal values for key parameters: potential, scan rate, temperature, and pH of the reaction medium. The CB model identified an optimal predicted value (Table 4.6) for experimental validation, forecasting a maximum CIP detection cathodic current of 128.51 μA under the following conditions: potential of 0.47 mV, scan rate of 98 mV/sec, temperature of 31°C, and pH of the reaction medium at 6.75. Experimental results showed a slightly lower current efficiency of 128.07 μA under the same conditions. The final model metrics, including an R^2 score of 0.9985, MSE of 1.468,

RMSE of 1.225, MAE of 0.672, and MedAE of 0.375, indicate that the Bayesian-optimized model accurately predicts ciprofloxacin from contaminated sources. These successful outcomes, achieved using the CB model with differential evolution, are further illustrated in Table 4.6.

Table 4.6 Input parameters optimization using the novel framework.

Potential (V)	Scan rate (mV/sec)	Temperature (^{0}C)	pH	Predicted current (μA)	Experimental current (μA)
0.47	98	31	6.75	128.51	128.07

4.7 ELECTROCHEMICAL QUANTITATIVE DETERMINATION OF CIP

The AuNPs/CHI-modified GCE electrode sensor was evaluated to measure trace amounts of CIP in ultra-pure water samples accurately. The detection and quantification performance of developed electrode was evaluated using differential pulse voltammetry (DPV) following the determination of optimized parameters by machine learning (ML) modelling. The specified conditions also encompassed instrumental settings for DPV, including an Estep of 5 mV, Epuls of 100 mV, pulse duration of 50 ms, and a scan rate of 98 mV/sec. The measurements were directed in a 0.1 M KCl solution to determine the concentration of CIP at each level. The analysis concentration range was 0.0 to 1.25 μM, with specific concentrations tested at 0.0, 0.1560, 0.3125, 0.6250, and 1.25 μM. Figure 4.14 illustrates that an increase in concentration results in a proportional increase in the peak current measured during the detection of CIP. The regression equation for this relationship is Ip (μA) = 147.7 x (μM) + 46.65, with an R^2 value of 0.9984 (Figure 14b). The limit of quantification (LOQ) and limit of detection (LOD) are essential parameters that determine the sensitivity and performance of an electrochemical sensor. These values are determined by monitoring the changes in response signals as the concentration of the analyte varies. The DPV technique was used to create a reliable calibration curve due to its ability to produce precise results and high

sensitivity. Figure 4.14a shows the DPV response for various concentrations of CIP on AuNPs/CHI/GCE under optimal conditions.

The LOD and LOQ were determined using the formulas 3 σ/m and 10 σ/m, respectively. In this context, σ denotes the standard deviation of the intercept and m denotes the slope of the calibration curve (Figure 4.14b)[173]. The investigation determined that the LOD for this experiment was 0.049 µM, while LOQ was 0.232 µM. Furthermore, the sensitivity of the designed AuNPs/CHI/GCE electrode was 786.72 µA μM^{-1} cm^{-2}. This was achieved by dividing the calibration curve's slope by the sensor's surface area. The performance of the designed electrode was compared with the published data based on their linearity range and LOD as shown in Table 4.7. The AuNPs/CHI/GCE demonstrates outstanding performance, achieving the lowest limit of detection (LOD) and a broader linearity range for quantifying CIP. AuNPs and CHI are highly appropriate for electrochemical detection of CIP in real samples because of their affordability, simplicity, and rapid response.

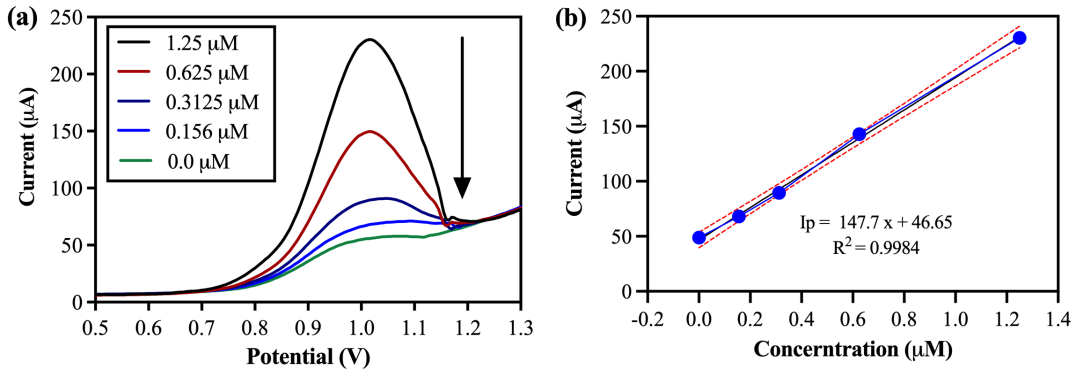


Figure 4.13 (a) DPV responses of AuNPs/CHI/GCE sensor for diverse conc. of CIP in 0.1 M KCl (scan rate: 50 mV/sec), b) CIP's calibration curve.

Table 4.7 Comparison of various developed electrodes and their performance for the determination of CIP.

SL	Sensors	Methods	Sensitivity Range (μM)	LOD (μM)	Electrolyte	Ref
1	$MgFe_2O_4$-MWCNTs/GCE	CV	0.10-1000	0.01	PBS (pH 3.0)	[174]
2	Au/C_3N_4/GN/GCE	SWV	0.6–120	0.42	PBS (pH 7)	[175]
3	NH_2–UiO-66/rGO/GCE	ASV	0.02 -1	0.0067	PBS (pH 4.0)	[176]
4	PEI@Fe_3O_4@CNTS/GCE	DPV	0.03–70	3.0	BR (pH 6)	[34]
5	CHI-AuMIP/GCE	DPV	1.0 –100	0.21	PBS (pH 7.4)	[177]
6	TiO_2/PVA/GCE	DPV	10–120	0.04	PBS (pH 7)	[178]
7	Co-MOFs/PLA/GCE	DPV	0.5–150.0	0.017	PBS (pH 7.0)	[179]
8	Fe@g-C_3N_4/PGE	DPV	0.001–1.0	0.0054	PBS (pH 7.0)	[180]
9	CIMMO/rGO/GCE	DPV	0.00075–0.10	0.0005	PBS (pH 6.5)	[173]
10	AuNPs/CHI/GCE	DPV	0.0 – 1.25	0.049	DI + KCl (pH 5.6)	This study

4.8 QUANTITATIVE ANALYSIS USING DISPOSABLE ELECTRODE

The ability of the AuNPs modified Gr electrode sensor to precisely detect traces of CIP in ultra-pure water samples was assessed. Differential pulse voltammetry (DPV) was used to assess the created electrode's detection and quantification capabilities. To ascertain the concentration of CIP at each level, the experiments were conducted in a 50 mM KCl solution. Specific concentrations were examined at 2.5, 5, 10, 20, and 40 nM, with the analytical concentration range being 2.5–40 nM. The peak current recorded

during the detection of CIP increases proportionately with an increase in concentration, as seen in Figure 4.15a. Ip(μA) = 7524.6 x (μM) + 367.56 is the regression equation for this relationship, and its R^2 value is 0.988 (Figure 4.15b). An electrochemical sensor's sensitivity and performance are largely determined by its limit of quantification (LOQ) and limit of detection (LOD). The formulas 3σ/m and 10σ/m were used to calculate the LOD and LOQ, respectively. Here, σ stands for the intercept's standard deviation and m for the calibration curve's slope [49]. According to the inquiry, the experiment's LOD was 0.0517 nM and its LOQ was 1.723 nM. This was accomplished by dividing the surface area of the sensor by the slope of the calibration curve. For quantifying CIP, the AuNPs/Gr has exceptional performance, reaching the lowest limit of detection (LOD) and a wider linearity range.

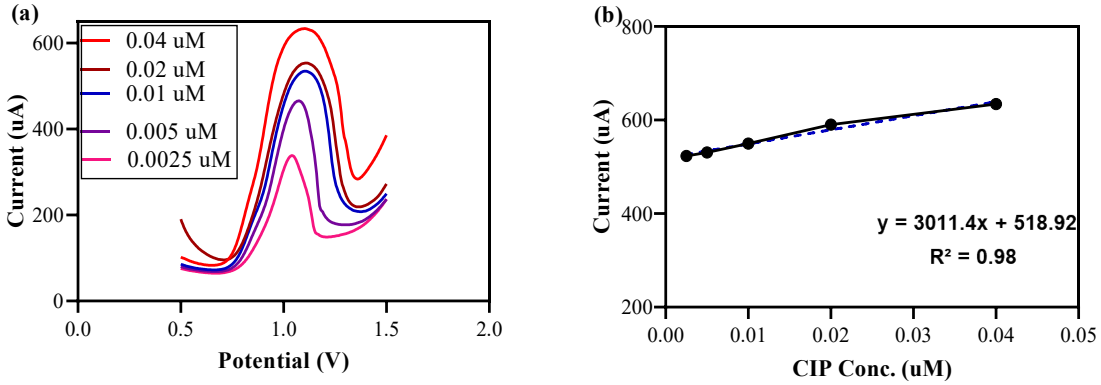


Figure 4.14 (a) Differential pulse voltammetry (DPV) responses of AuNPs/Gr sensor for diverse concentrations of CIP in 0.01 M KCl (scan rate: 25 mV/sec); (b) CIP's calibration curve

Chapter 5: CONCLUSION & RECOMMENDATION

5.1 GENERAL CONCLUSION

In this study, the use of gold nanoparticles and chitosan-modified glassy carbon electrodes enabled the design and evaluation of an ultrasensitive sensor for detecting and measuring the concentration of ciprofloxacin that has not been achieved there before. The sensor displayed significant sensitivity and selectivity for CIP detection through the varied electrochemical parameters; scan rate, pH, temperature or electrode potential that were well optimized. By employing ten machine learning approaches, the predictive ability of the sensor for antibiotics was significantly improved. Of the models, CatBoost was the only one that managed to combine balanced accuracy with low error metrics for training data and testing data, respectively, with R^2 values of 0.9993 and 0.9986, which indicates the high generalization potential of the model. The sensor exhibited a wide linear range of response (0.0 - 1.25 μM) with a low limit of detection (0.049 μM) and limit of quantification (0.232 μM), rendering it extremely appropriate for swift and precise analysis in environmental and clinical contexts. The present study represents a novel approach to quantification in water systems of antibiotics and solves urgent environmental and industrial challenges. However, this technology faces some limitations. Developing highly selective sensors for complex water matrices was challenging because of the possible interference from co-existing pollutants, which can reduce their accuracy. Besides, while machine learning has definitely enhanced data interpretation and predictive modelling, generalizing it requires extensive and high-quality datasets that can be resource-intensive to acquire. Other important challenges involve sensor durability and scalability for large applications; prolonged exposure to harsh environmental conditions could compromise the sensor performance. Some limitations still hail from advancements in nanomaterial-based sensors and data-driven approaches. With further development and cross-disciplinary collaboration, electrochemical sensors can easily be embedded in environmental and industrial

samples for better operational efficiencies, supporting regulatory compliances, and giving a robust framework for sustainable water quality management.

5.2 KEY FINDINGS

- AuNP and CHI modified electrode show better conductivity and faster electron transport than the bare electrode.
- The developed electrode exhibits greater electroactive surface area (0.025291 cm^2) in comparison of all other electrode (0.022179 and 0.018561 cm^2)
- Electrochemical behaviour of CIP showed irreversibility and the process entailed the transfer of two electrons and two protons.
- Sensor showed superior performance in acidic, neutral and alkaline condition.
- Higher temperature helps in creating the noble catalytic pathway to carry out CIP
- Out of ten ML models CatBoost showed better performance to determine the optimum parameter.
- The value of LOD and LOQ are 0.049 μM and 0.232 μM respectively
- Disposable graphite electrode is also capable in detecting CIP.

5.3 LIMITATION OF THE STUDY

The limitation of the study is this study carried out only on a lab-scale base experiment.

5.4 RECOMMENDATION FOR FURTHER STUDY

Reusing and treating wastewater could be an affordable, sustainable, and long-term solution given the severe global water shortage. Numerous contaminants are released by living things, endangering human health by contaminating water supplies. Thus, this raises serious concerns about components of the future. Without knowing the amount of antibiotic properly effective steps can't be taken to remove it from the water bodies completely. To detect the trace amount of antibiotics, electrochemical processes will be cost-effective and sustainable. As our prepared disposable electrode shows a great result, further study should continue to see its effectiveness in real wastewater and also investigate the long-term stability, reproducibility, durability to assess its practical applicability as well as integrate more advance ML models such as neural networks or hybrid models to enhance the detection of ultra-trace level of antibiotics.

REFERENCES

1. M. J. Focazio, D. W. Kolpin, K. K. Barnes, E. T. Furlong, M. T. Meyer, S. D. Zaugg, L. B. Barber, and M. E. Thurman, "A national reconnaissance for pharmaceuticals and other organic wastewater contaminants in the United States — II) Untreated drinking water sources," *Science of The Total Environment*, vol. 402, no.2, pp. 201-216, 2008.
2. M. Bilal, S. Mehmood, T. Rasheed, and H. M. N. Iqbal, "Antibiotics traces in the aquatic environment: persistence and adverse environmental impact," *Current Opinion in Environmental Science & Health*, vol. 13, 68-74, 2020.
3. J. Guo, Y. Wang, Y. Ahmed, M. Jin, and J. Li, Control strategies to combat dissemination of antibiotic resistance in urban water systems, in *Antibiotic Resistance in the Environment : A Worldwide Overview*, C. M. Manaia, E. Donner, I. Vaz-Moreira, and P. Hong, Editors. Springer International Publishing: Cham. pp. 147-187,2020.
4. P. Dadgostar, "Antimicrobial resistance: implications and costs," *Infection and drug resistance*, 3903-3910, 2019.
5. Y. Ahmed, J. Zhong, Z. Yuan, and J. Guo, "Roles of reactive oxygen species in antibiotic resistant bacteria inactivation and micropollutant degradation in Fenton and photo-Fenton processes," *Journal of Hazardous Materials*, vol. 430, 128408, 2022.
6. J. Zhong, Y. Ahmed, Z. Yu, J. F. Mueller, and J. Guo, "Synergistic combination of graphitic carbon nitride and peroxymonosulfate for efficient photocatalytic destruction of emerging contaminants under simulated solar irradiation," *ACS ES&T Water*, vol. 3, no.1, pp. 6-15, 2023.
7. Y. Ahmed, J. Lu, Z. Yuan, P. L. Bond, and J. Guo, "Efficient inactivation of antibiotic resistant bacteria and antibiotic resistance genes by photo-Fenton process under visible LED light and neutral pH," *Water Research*, vol. 179, 115878, 2020.
8. L. O. Omuferen, B. Maseko, and J. Olowoyo, "Occurrence of antibiotics in wastewater from hospital and convectional wastewater treatment plants and their impact on the effluent receiving rivers: current knowledge between 2010 and 2019," *Environmental Monitoring and Assessment*, vol. 194, no.4, pp. 306, 2022.
9. T. P. Van Boeckel, J. Pires, R. Silvester, C. Zhao, J. Song, N. G. Criscuolo, M. Gilbert, S. Bonhoeffer, and R. Laxminarayan, "Global trends in

antimicrobial resistance in animals in low-and middle-income countries," *Science*, vol. 365, no.6459, pp. eaaw1944, 2019.

10. I. Sanseverino, R. Loos, A. Navarro Cuenca, D. Marinov, and T. Lettieri, State of the art on the contribution of water to antimicrobial resistance. 2018: European Commission: Joint Research Centre, EUR 29592 EN, Publications Office of the European Union, Luxembourg.

11. M. Girmatsion, H. Dong, B. Abraha, A. Mahmud, M. Kasimala, H. Gebremedhin, A. Adhanom, G. Lu, F. Yang, and Y. Guo, "A natural fluorescent protein for ciprofloxacin sensing and mechanism study using molecular docking and circular dichroism," *Analytica Chimica Acta*, vol. 1221, 340082, 2022.

12. Y. Ahmed, A. A. S. Maya, P. Akhtar, H. AlMohamadi, A. W. Mohammad, S. M. Ashekuzzaman, A. I. Olbert, and M. G. Uddin, "Advancements and challenges in Fenton-based advanced oxidation processes for antibiotic removal in wastewater: From the laboratory to practical applications," *Journal of Environmental Chemical Engineering*, 115068, 2024.

13. O. A. Alharbi, E. Jarvis, A. Galani, N. S. Thomaidis, M.-C. Nika, and D. V. Chapman, "Assessment of selected pharmaceuticals in Riyadh wastewater treatment plants, Saudi Arabia: Mass loadings, seasonal variations, removal efficiency and environmental risk," *Science of The Total Environment*, vol. 882, 163284, 2023.

14. N. Hareesha, J. G. Manjunatha, P. A. Pushpanjali, N. P. Subbaiah, M. M. Charithra, N. Sreeharsha, S. M. B. Asdaq, and M. K. Anwer, "Electrochemical sensing of antibiotic drug amoxicillin in the presence of dopamine at simple and selective carbon paste electrode activated with cetyltrimethylammonium bromide surfactant," *Monatshefte für Chemie - Chemical Monthly*, vol. 153, no.1, pp. 31-38, 2022.

15. M. K. Matta, A. Chockalingam, A. Gandhi, S. Stewart, L. Xu, K. Shea, V. Patel, and R. Rouse, "LC-MS/MS based quantitation of ciprofloxacin and its application to antimicrobial resistance study in Balb/c mouse plasma, urine, bladder and kidneys," *Analytical methods*, vol. 10, no.10, pp. 1237-1246, 2018.

16. Y. Ahmed, J. Zhong, Z. Wang, L. Wang, Z. Yuan, and J. Guo, "Simultaneous removal of antibiotic resistant bacteria, antibiotic resistance genes, and miicropollutants by FeS_2@GO-based heterogeneousphoto-Fenton process," *Environmental Science & Technology*, vol. 56, no.21, pp. 15156-15166, 2022.

17. Y. Ahmed, J. Zhong, Z. Yuan, and J. Guo, "Simultaneous removal of antibiotic resistant bacteria, antibiotic resistance genes, and

micropollutants by a modified photo-Fenton process," *Water Research*, vol. 197, 117075, 2021.

18. J. Zhong, Y. Ahmed, G. Carvalho, Z. Wang, L. Wang, J. F. Mueller, and J. Guo, "Simultaneous removal of micropollutants, antibiotic resistant bacteria, and antibiotic resistance genes using graphitic carbon nitride under simulated solar irradiation," *Chemical Engineering Journal*, vol. 433, 133839, 2022.
19. R. Bosma, J. Devasagayam, A. Singh, and C. M. Collier, "Microchip capillary electrophoresis dairy device using fluorescence spectroscopy for detection of ciprofloxacin in milk samples," *Scientific Reports*, vol. 10, no.1, pp. 13548, 2020.
20. S. Palamy and W. Ruengsitagoon, "Reverse flow injection spectrophotometric determination of ciprofloxacin in pharmaceuticals using iron from soil as a green reagent," *Spectrochimica Acta Part A: Molecular and Biomolecular Spectroscopy*, vol. 190, 129-134, 2018.
21. Y.-M. Liu, L. Mei, H.-Y. Yue, Y.-M. Shi, and L.-J. Liu, "Highly sensitive chemiluminescence detection of norfloxacin and ciprofloxacin in CE and its applications," *Chromatographia*, vol. 72, 337-341, 2010.
22. P. K. Jiwanti, B. Y. Wardhana, L. G. Sutanto, and M. F. Chanif, "A review on carbon-based electrodes for electrochemical sensor of quinolone Antibiotics," *ChemistrySelect*, vol. 7, no.15, pp. e202103997, 2022.
23. B. Krajewska, "Application of chitin-and chitosan-based materials for enzyme immobilizations: a review," *Enzyme and microbial technology*, vol. 35, no.2-3, pp. 126-139, 2004.
24. R. Khan and M. Dhayal, "Chitosan/polyaniline hybrid conducting biopolymer base impedimetric immunosensor to detect ochratoxin-A," *Biosensors and Bioelectronics*, vol. 24, no.6, pp. 1700-1705, 2009.
25. K. R. Reddy, P. K. Brahman, and L. Suresh, "Fabrication of high performance disposable screen printed electrochemical sensor for ciprofloxacin sensing in biological samples," *Measurement*, vol. 127, 175-186, 2018.
26. J. Lin, C. He, Y. Zhao, and S. Zhang, "One-step synthesis of silver nanoparticles/carbon nanotubes/chitosan film and its application in glucose biosensor," *Sensors and Actuators B: Chemical*, vol. 137, no.2, pp. 768-773, 2009.
27. Y. Wang, W. Wei, J. Zeng, X. Liu, and X. Zeng, "Fabrication of a copper nanoparticle/chitosan/carbon nanotube-modified glassy carbon electrode for electrochemical sensing of hydrogen peroxide and glucose," *Microchimica Acta*, vol. 160, 253-260, 2008.

28. H. Teymourinia, A. Al-nayili, H. A. Alshamsi, R. Mohammadi, E. Sohouli, and M. Gholami, "Development of CNOs/PANI-NTs/AuNPs nanocomposite as an electrochemical sensor and Z-scheme photocatalyst for determination and degradation of ciprofloxacin," *Surfaces and Interfaces*, vol. 42, 103412, 2023.

29. A. Al-nayili and A. H. Idan, "Environmentally friendly production, characterization, and utilization of ZrO_2 nanoparticles for the adsorption of amoxicillin in water solutions," *Journal of Molecular Liquids*, vol. 389, 122875, 2023.

30. H. Teymourinia, H. A. Alshamsi, A. Al-nayili, and M. Gholami, "Photocatalytic degradation of chlorpyrifos using Ag nanoparticles-doped g-C_3N_5 decorated with dendritic CdS," *Chemosphere*, vol. 344, 140325, 2023.

31. S. Zhong, K. Zhang, M. Bagheri, J. G. Burken, A. Gu, B. Li, X. Ma, B. L. Marrone, Z. J. Ren, J. Schrier, W. Shi, H. Tan, T. Wang, X. Wang, B. M. Wong, X. Xiao, X. Yu, J.-J. Zhu, and H. Zhang, "Machine learning: New ideas and tools in environmental science and engineering," *Environmental Science & Technology*, vol. 55, no.19, pp. 12741-12754, 2021.

32. Y. Ahmed, K. R. Dutta, S. N. C. Nepu, M. Prima, H. AlMohamadi, and P. Akhtar, "Optimizing photocatalytic dye degradation: A machine learning and metaheuristic approach for predicting methylene blue in contaminated Water," *Results in Engineering*, 103538, 2024.

33. Y. Ahmed, A. A. Siddiqua Maya, P. Akhtar, M. S. Alam, H. AlMohamadi, M. N. Islam, O. A. Alharbi, and S. M. Rahman, "A novel interpretable machine learning and metaheuristic-based protocol to predict and optimize ciprofloxacin antibiotic adsorption with nano-adsorbent," *Journal of Environmental Management*, vol. 370, 122614, 2024.

34. G. Ke, Q. Meng, T. Finley, T. Wang, W. Chen, W. Ma, Q. Ye, and T.-Y. Liu, LightGBM: a highly efficient gradient boosting decision tree, in Proceedings of the 31st International Conference on Neural Information Processing Systems. Curran Associates Inc.: Long Beach, California, USA. pp. 3149–3157, 2017.

35. M. S. Alam, A. A. Akinpelu, M. K. Nazal, and S. M. Rahman, "Removal of N-nitrosodiphenylamine from contaminated water: A novel modeling framework using metaheuristic-based ensemble models," *Journal of Environmental Management*, vol. 365, 121503, 2024.

36. L. Prokhorenkova, G. Gusev, A. Vorobev, A. V. Dorogush, and A. Gulin, "CatBoost: unbiased boosting with categorical features," *Advances in neural information processing systems*, vol. 31, 2018.

37. Z. Yang, H. Qiu, L. Gao, L. Chen, and X. Cai, "Constraint boundary pursuing-based surrogate-assisted differential evolution for expensive optimization problems with mixed constraints," *Structural and Multidisciplinary Optimization*, vol. 66, no.2, pp. 40, 2023.

38. S. Das and P. N. Suganthan, "Differential evolution: A survey of the State-of-the-Art," *IEEE Transactions on Evolutionary Computation*, vol. 15, no.1, pp. 4-31, 2011.

39. B. Feier, I. Ionel, C. Cristea, and R. Săndulescu, "Electrochemical behaviour of several penicillins at high potential," *New Journal of Chemistry*, vol. 41, no.21, pp. 12947-12955, 2017.

40. J. M. Beale, J. Block, and R. Hill, Organic medicinal and pharmaceutical chemistry. 2010: Philadelphia: Lippincott Williams & Wilkins.

41. N. Sebastian, W.-C. Yu, and D. Balram, "Electrochemical detection of an antibiotic drug chloramphenicol based on a graphene oxide/hierarchical zinc oxide nanocomposite," *Inorganic chemistry frontiers*, vol. 6, no.1, pp. 82-93, 2019.

42. R. I. Aminov, "The role of antibiotics and antibiotic resistance in nature," *Environmental microbiology*, vol. 11, no.12, pp. 2970-2988, 2009.

43. H. Karimi-Maleh, A. Khataee, F. Karimi, M. Baghayeri, L. Fu, J. Rouhi, C. Karaman, O. Karaman, and R. Boukherroub, "A green and sensitive guanine-based DNA biosensor for idarubicin anticancer monitoring in biological samples: A simple and fast strategy for control of health quality in chemotherapy procedure confirmed by docking investigation," *Chemosphere*, vol. 291, 132928, 2022.

44. S. M. Siddeeg, M. A. Tahoon, N. S. Alsaiari, M. Shabbir, and F. B. Rebah, "Application of functionalized nanomaterials as effective adsorbents for the removal of heavy metals from wastewater: a review," *Current Analytical Chemistry*, vol. 17, no.1, pp. 4-22, 2021.

45. H. Sohrabi, O. Arbabzadeh, P. Khaaki, M. R. Majidi, A. Khataee, and S. Woo Joo, "Emerging electrochemical sensing and biosensing approaches for detection of Fumonisins in food samples," *Critical Reviews in Food Science and Nutrition*, vol. 62, no.31, pp. 8761-8776, 2022.

46. H. Sohrabi, M. R. Majidi, O. Arbabzadeh, P. Khaaki, S. Pourmohammad, A. Khataee, and Y. Orooji, "Recent advances in the highly sensitive determination of zearalenone residues in water and environmental resources with electrochemical biosensors," *Environmental Research*, vol. 204, 112082, 2022.

47. Đ. Tadić, M. J. B. Hernandez, F. Cerqueira, V. Matamoros, B. Piña, and J. M. Bayona, "Occurrence and human health risk assessment of antibiotics

and their metabolites in vegetables grown in field-scale agricultural systems," *Journal of Hazardous Materials*, vol. 401, 123424, 2021.

48. H. Y. Kim, R. Y. K. Chang, S. Morales, and H.-K. Chan, "Bacteriophage-delivering hydrogels: current progress in combating antibiotic resistant bacterial infection," *Antibiotics*, vol. 10, no.2, pp. 130, 2021.

49. S. Amann, K. Neef, and S. Kohl, "Antimicrobial resistance (AMR)," *European Journal of Hospital Pharmacy*, vol. 26, no.3, pp. 175-177, 2019.

50. C. Lindmeier, "High levels of antibiotic resistance found worldwide, new data shows," *World Health Organization: Geneva, Switzerland*, 2018.

51. D. M. Whitacre, Reviews of environmental contamination and toxicology. Vol. 202. 2008: Springer.

52. A. J. Abdulghani, H. H. Jasim, and A. S. Hassan, "Determination of tetracycline in pharmaceutical preparation by molecular and atomic absorption spectrophotometry and high performance liquid chromatography via complex formation with Au (III) and Hg (II) ions in solutions," *International Journal of Analytical Chemistry*, vol. 2013, no.1, pp. 305124, 2013.

53. A. S. Mendez, V. Weisheimer, T. P. Oppe, M. Steppe, and E. E. Schapoval, "Microbiological assay for the determination of meropenem in pharmaceutical dosage form," *Journal of pharmaceutical and biomedical analysis*, vol. 37, no.4, pp. 649-653, 2005.

54. H. Liu, H. Wang, and V. B. Sunderland, "An isocratic ion exchange HPLC method for the simultaneous determination of flucloxacillin and amoxicillin in a pharmaceutical formulation for injection," *Journal of pharmaceutical and biomedical analysis*, vol. 37, no.2, pp. 395-398, 2005.

55. S. O. Bekoe, S. A. Bak, E. Björklund, K. A. Krogh, N. N. Okine, R. K. Adosraku, B. Styrishave, and M. Hansen, "Determination of thirteen antibiotics in drug products–A new LC-MS/MS tool for screening drug product quality," *Analytical Methods*, vol. 6, no.15, pp. 5847-5855, 2014.

56. V. K. Gupta, R. Jain, K. Radhapyari, N. Jadon, and S. Agarwal, "Voltammetric techniques for the assay of pharmaceuticals—a review," *Analytical biochemistry*, vol. 408, no.2, pp. 179, 2011.

57. A. K. Srivastava, S. S. Upadhyay, C. R. Rawool, N. S. Punde, and A. S. Rajpurohit, "Voltammetric techniques for the analysis of drugs using nanomaterials based chemically modified electrodes," *Current Analytical Chemistry*, vol. 15, no.3, pp. 249-276, 2019.

58. S. Tursynbolat, Y. Bakytkarim, J. Huang, and L. Wang, "Ultrasensitive electrochemical determination of metronidazole based on polydopamine/carboxylic multi-walled carbon nanotubes

nanocomposites modified GCE," *Journal of pharmaceutical analysis*, vol. 8, no.2, pp. 124-130, 2018.

59. U. J. Pandit, G. A. Naikoo, M. U. D. Sheikh, G. A. Khan, K. Raj, and S. Limaye, "Electrochemical determination of an anti-hyperlipidimic drug pitavastatin at electrochemical sensor based on electrochemically pre-treated polymer film modified GCE," *Journal of pharmaceutical analysis*, vol. 7, no.4, pp. 258-264, 2017.

60. O. Farghaly, R. A. Hameed, and H. Abd Alhakeem, "Electrochemical analysis techniques: a review on recent pharmaceutical applications," *International Journal of Pharmaceutical Sciences Review and Research*, vol. 25, no.2, pp. 37-45, 2014.

61. A. A. Al-rashdi, O. Farghaly, and A. Naggar, "Voltammetric determination of pharmaceutical compounds at bare and modified solid electrodes: a review," *J. Chem. Pharm. Res*, vol. 10, 21-43, 2018.

62. A. Amari, M. K. Al Mesfer, N. S. Alsaiari, M. Danish, A. M. Alshahrani, M. A. Tahoon, and F. B. Rebah, "Electrochemical and optical properties of tellurium dioxide (TeO2) nanoparticles," *International Journal of Electrochemical Science*, vol. 16, no.2, pp. 210235, 2021.

63. A. Amari, B. Alalwan, S. M. Siddeeg, M. A. Tahoon, N. S. Alsaiari, and F. B. Rebah, "Biomolecules behavior on a surface of boron doped/un-doped graphene nanosheets," *International Journal of Electrochemical Science*, vol. 15, no.11, pp. 11427-11436, 2020.

64. S. Das, L. Ngashangva, and P. Goswami, Carbon Dots: An Emerging Smart Material for Analytical Applications. Micromachines 2021, 12, 84. s Note: MDPI stays neutral with regard to jurisdictional claims in published …2021.

65. M. A. Tahoon, S. M. Siddeeg, N. Salem Alsaiari, W. Mnif, and F. Ben Rebah, "Effective heavy metals removal from water using nanomaterials: A review," *Processes*, vol. 8, no.6, pp. 645, 2020.

66. L. Qian, A. R. Thiruppathi, R. Elmahdy, J. van der Zalm, and A. Chen, "Graphene-oxide-based electrochemical sensors for the sensitive detection of pharmaceutical drug naproxen," *Sensors*, vol. 20, no.5, pp. 1252, 2020.

67. L. Lan, Y. Yao, J. Ping, and Y. Ying, "Recent advances in nanomaterial-based biosensors for antibiotics detection," *Biosensors and Bioelectronics*, vol. 91, 504-514, 2017.

68. J. Xue, J. Liu, C. Wang, Y. Tian, and N. Zhou, "Simultaneous electrochemical detection of multiple antibiotic residues in milk based on aptamers and quantum dots," *Analytical methods*, vol. 8, no.9, pp. 1981-1988, 2016.

69. M. Labib, E. H. Sargent, and S. O. Kelley, "Electrochemical methods for the analysis of clinically relevant biomolecules," *Chemical reviews*, vol. 116, no.16, pp. 9001-9090, 2016.

70. X. Liu, D. Huang, C. Lai, G. Zeng, L. Qin, C. Zhang, H. Yi, B. Li, R. Deng, and S. Liu, "Recent advances in sensors for tetracycline antibiotics and their applications," *TrAC Trends in Analytical Chemistry*, vol. 109, 260-274, 2018.

71. H. Aleixo, L. L. Okumura, A. Gurgel, A. F. S. Silva, and J. A. Diniz, "Multiwalled carbon nanotube/ionic liquid paste electrode for voltammetric determination of sulfachlorpyridazine," *Analytical Methods*, vol. 11, no.13, pp. 1743-1750, 2019.

72. C. S. Gondim, G. M. Durán, A. M. Contento, and Á. Ríos, "Development and validation of an electrochemical screening methodology for sulfonamide residue control in milk samples using a graphene quantum dots@ Nafion modified glassy carbon electrode," *Food Analytical Methods*, vol. 11, 1711-1721, 2018.

73. M. Jacobs, V. J. Nagaraj, T. Mertz, A. P. Selvam, T. Ngo, and S. Prasad, "An electrochemical sensor for the detection of antibiotic contaminants in water," *Analytical Methods*, vol. 5, no.17, pp. 4325-4329, 2013.

74. L. Hermouche, M. Bendany, K. Abbi, Y. El Hamdouni, N. Labjar, M. El Mahi, E. M. Lotfi, M. Dalimi, D. Dhiba, and S. El Hajjaji, "Electrochemical sensors for tetracycline antibiotics detection based on carbon electrode materials modified by biological and chemical compounds: A review," *International Journal of Environmental Analytical Chemistry*, vol. 103, no.17, pp. 5887-5909, 2023.

75. A. Ricci, G. P. Parpinello, N. Teslić, P. A. Kilmartin, and A. Versari, "Suitability of the cyclic voltammetry measurements and DPPH• spectrophotometric assay to determine the antioxidant capacity of food-grade oenological tannins," *Molecules*, vol. 24, no.16, pp. 2925, 2019.

76. N. Elgrishi, K. J. Rountree, B. D. McCarthy, E. S. Rountree, T. T. Eisenhart, and J. L. Dempsey, "A practical beginner's guide to cyclic voltammetry," *Journal of chemical education*, vol. 95, no.2, pp. 197-206, 2018.

77. B. Uslu and S. A. Ozkan, "Electroanalytical methods for the determination of pharmaceuticals: a review of recent trends and developments," *Analytical letters*, vol. 44, no.16, pp. 2644-2702, 2011.

78. V. Mirceski, S. Komorsky-Lovric, and M. Lovric, Square-wave voltammetry: theory and application. 2007: Springer Science & Business Media.

79. Y. M. Reddy, S. J. Kumar, K. Saritha, P. Gopal, T. M. Reddy, and J. Simal-Gandara, "Phytochemical profiling of methanolic fruit extract of Gardenia latifolia Ait. by LC-MS/MS analysis and evaluation of its antioxidant and antimicrobial activity," *Plants*, vol. 10, no.3, pp. 545, 2021.

80. L. Percevault, E. Limanton, P. Nicolas, L. Paquin, and C. Lagrost, "Electrochemical determination and antioxidant capacity modulation of polyphenols in deep eutectic solvents," *ACS Sustainable Chemistry & Engineering*, vol. 9, no.2, pp. 776-784, 2020.

81. M. David, A. Serban, C. Radulescu, A. F. Danet, and M. Florescu, "Bioelectrochemical evaluation of plant extracts and gold nanozyme-based sensors for total antioxidant capacity determination," *Bioelectrochemistry*, vol. 129, 124-134, 2019.

82. J. Klans, Technical Scale of Electrochemistry, in *Encyclopedia of Electrochemistry*. Wiley-VCH Verlag GmbH & Co. KGaA2007.

83. J. Agrisuelas, C. Gabrielli, J. García-Jareño, H. Perrot, R. Sanchis-Gual, O. Sel, and F. Vicente, "Evaluation of the electrochemical anion recognition of NO_3^--imprinted poly (Azure A) in NO_3^-/Cl^- mixed solutions by ac-electrogravimetry," *Electrochimica Acta*, vol. 194, 292-303, 2016.

84. K. Z. Brainina, D. Varzakova, and E. Gerasimova, "A chronoamperometric method for determining total antioxidant activity," *Journal of analytical chemistry*, vol. 67, 364-369, 2012.

85. X. Guo, J. Li, M. Arabi, X. Wang, Y. Wang, and L. Chen, "Molecular-imprinting-based surface-enhanced Raman scattering sensors," *Acs Sensors*, vol. 5, no.3, pp. 601-619, 2020.

86. L. Feng, Q. Xue, F. Liu, Q. Cao, J. Feng, L. Yang, and F. Zhang, "Voltammetric determination of ofloxacin by using a laser-modified carbon glassy electrode," *Microchimica Acta*, vol. 187, 1-8, 2020.

87. A. Abou Taka, M. C. Babin, X. Sheng, J. A. DeVine, and H. P. Hratchian, "Unveiling the coexistence of cis-and trans-isomers in the hydrolysis of ZrO_2: A coupled DFT and high-resolution photoelectron spectroscopy study," *The Journal of Chemical Physics*, vol. 153, no.24, pp. 2020.

88. S. Bonyadi, K. Ghanbari, and M. Ghiasi, "All-electrochemical synthesis of a three-dimensional mesoporous polymeric gC_3N_4/PANI/CdO nanocomposite and its application as a novel sensor for the simultaneous determination of epinephrine, paracetamol, mefenamic acid, and ciprofloxacin," *New Journal of Chemistry*, vol. 44, no.8, pp. 3412-3424, 2020.

89. M. Yadav, V. Ganesan, R. Gupta, and P. K. Sonkar, "CoO nanocrystals anchored on graphene sheets for electrochemical determination of chloramphenicol," *Microchemical Journal*, vol. 146, 881-887, 2019.

90. X. Cui, D. Cao, R. Djellabi, M. Qiao, Y. Wang, S. Zhao, R. Mao, Y. Gong, X. Zhao, and B. Yang, "Enhancement of Ni/NiO/graphitized carbon and β-Cyclodextrin/reduced graphene oxide for the electrochemical detection of norfloxacin in water sample," *Journal of Electroanalytical Chemistry*, vol. 851, 113407, 2019.

91. C. Fenzl, P. Nayak, T. Hirsch, O. S. Wolfbeis, H. N. Alshareef, and A. J. Baeumner, "Laser-scribed graphene electrodes for aptamer-based biosensing," *Acs Sensors*, vol. 2, no.5, pp. 616-620, 2017.

92. Y. Zhu, C. Li, L. Wang, M. Chen, J. Yu, Q. Liu, and X. Chen, "Differential Pulse Voltammetry Determination of Ofloxacin in Human Serum and Urine Based on a Novel Tryptophan-graphene Oxide-carbon Nanotube Electrochemical Sensor," *Electroanalysis*, vol. 31, no.8, pp. 1429-1436, 2019.

93. L. Fotouhi and M. Alahyari, "Electrochemical behavior and analytical application of ciprofloxacin using a multi-walled nanotube composite film-glassy carbon electrode," *Colloids and Surfaces B: Biointerfaces*, vol. 81, no.1, pp. 110-114, 2010.

94. T.-S. Chen, K.-L. Huang, and J.-L. Chen, "An electrochemical approach to simultaneous determination of acetaminophen and ofloxacin," *Bulletin of environmental contamination and toxicology*, vol. 89, 1284-1288, 2012.

95. W. Wen, D.-M. Zhao, X.-H. Zhang, H.-Y. Xiong, S.-F. Wang, W. Chen, and Y.-D. Zhao, "One-step fabrication of poly (o-aminophenol)/multi-walled carbon nanotubes composite film modified electrode and its application for levofloxacin determination in pharmaceuticals," *Sensors and Actuators B: Chemical*, vol. 174, 202-209, 2012.

96. X. Zhang, Y. Wei, and Y. Ding, "Electrocatalytic oxidation and voltammetric determination of ciprofloxacin employing poly (alizarin red)/graphene composite film in the presence of ascorbic acid, uric acid and dopamine," *Analytica chimica acta*, vol. 835, 29-36, 2014.

97. S. Liu, G. Lai, H. Zhang, and A. Yu, "Amperometric aptasensing of chloramphenicol at a glassy carbon electrode modified with a nanocomposite consisting of graphene and silver nanoparticles," *Microchimica Acta*, vol. 184, 1445-1451, 2017.

98. J. Sun, T. Gan, H. Zhu, Z. Shi, and Y. Liu, "Direct electrochemical sensing for oxytetracycline in food using a zinc cation-exchanged montmorillonite," *Applied clay science*, vol. 101, 598-603, 2014.

99. S. Jafari, M. Dehghani, N. Nasirizadeh, and M. Azimzadeh, "An azithromycin electrochemical sensor based on an aniline MIP film electropolymerized on a gold nano urchins/GO modified glassy carbon electrode," *Journal of Electroanalytical Chemistry*, vol. 829, 27-34, 2018.

100. Z. Jiang, Q. Liu, Y. Tang, and M. Zhang, "Electrochemical sensor based on a novel Pt− Au bimetallic nanoclusters decorated on reduced graphene oxide for sensitive detection of ofloxacin," *Electroanalysis*, vol. 29, no.2, pp. 602-608, 2017.

101. F.-D. Munteanu, A. M. Titoiu, J.-L. Marty, and A. Vasilescu, "Detection of antibiotics and evaluation of antibacterial activity with screen-printed electrodes," *Sensors*, vol. 18, no.3, pp. 901, 2018.

102. A. Veseli, F. Mullallari, F. Balidemaj, L. Berisha, Ľ. Švorc, and T. Arbneshi, "Electrochemical determination of erythromycin in drinking water resources by surface modified screen-printed carbon electrodes," *Microchemical Journal*, vol. 148, 412-418, 2019.

103. A. M. Santos, A. Wong, F. C. Vicentini, and O. Fatibello-Filho, "Simultaneous voltammetric sensing of levodopa, piroxicam, ofloxacin and methocarbamol using a carbon paste electrode modified with graphite oxide and β-cyclodextrin," *Microchimica Acta*, vol. 186, 1-9, 2019.

104. S. Jahanbani and A. Benvidi, "Comparison of two fabricated aptasensors based on modified carbon paste/oleic acid and magnetic bar carbon paste/Fe3O4@ oleic acid nanoparticle electrodes for tetracycline detection," *Biosensors and Bioelectronics*, vol. 85, 553-562, 2016.

105. N. S. Alsaiari, K. M. M. Katubi, F. M. Alzahrani, S. M. Siddeeg, and M. A. Tahoon, "The application of nanomaterials for the electrochemical detection of antibiotics: A review," *Micromachines*, vol. 12, no.3, pp. 308, 2021.

106. Z. Peng, X. Liu, W. Zhang, Z. Zeng, Z. Liu, C. Zhang, Y. Liu, B. Shao, Q. Liang, and W. Tang, "Advances in the application, toxicity and degradation of carbon nanomaterials in environment: A review," *Environment international*, vol. 134, 105298, 2020.

107. Z. Liu, M. Jin, J. Cao, J. Wang, X. Wang, G. Zhou, A. van den Berg, and L. Shui, "High-sensitive electrochemical sensor for determination of Norfloxacin and its metabolism using MWCNT-CPE/pRGO-ANSA/Au," *Sensors and Actuators B: Chemical*, vol. 257, 1065-1075, 2018.

108. B.-S. He and X.-H. Yan, "Modifications of Au nanoparticle-functionalized graphene for sensitive detection of sulfanilamide," *Sensors*, vol. 18, no.3, pp. 846, 2018.

109. A. M. Santos, A. Wong, A. A. Almeida, and O. Fatibello-Filho, "Simultaneous determination of paracetamol and ciprofloxacin in biological fluid samples using a glassy carbon electrode modified with graphene oxide and nickel oxide nanoparticles," *Talanta*, vol. 174, 610-618, 2017.

110. A. Wong, T. A. Silva, F. C. Vicentini, and O. Fatibello-Filho, "Electrochemical sensor based on graphene oxide and ionic liquid for ofloxacin determination at nanomolar levels," *Talanta*, vol. 161, 333-341, 2016.

111. X. Zhang, Y.-C. Zhang, and J.-W. Zhang, "A highly selective electrochemical sensor for chloramphenicol based on three-dimensional reduced graphene oxide architectures," *Talanta*, vol. 161, 567-573, 2016.

112. M. Parmeggiani, P. Zaccagnini, S. Stassi, M. Fontana, S. Bianco, C. Nicosia, C. F. Pirri, and A. Lamberti, "PDMS/polyimide composite as an elastomeric substrate for multifunctional laser-induced graphene electrodes," *ACS applied materials & interfaces*, vol. 11, no.36, pp. 33221-33230, 2019.

113. T. S. Munonde and P. N. Nomngongo, "Nanocomposites for electrochemical sensors and their applications on the detection of trace metals in environmental water samples," *Sensors*, vol. 21, no.1, pp. 131, 2020.

114. B. He, L. Wang, X. Dong, X. Yan, M. Li, S. Yan, and D. Yan, "Aptamer-based thin film gold electrode modified with gold nanoparticles and carboxylated multi-walled carbon nanotubes for detecting oxytetracycline in chicken samples," *Food chemistry*, vol. 300, 125179, 2019.

115. A. G. Fá, F. Pignanelli, I. López-Corral, R. Faccio, A. Juan, and M. S. Di Nezio, "Detection of oxytetracycline in honey using SERS on silver nanoparticles," *TRAC Trends in Analytical Chemistry*, vol. 121, 115673, 2019.

116. M. Roushani, Z. Rahmati, S. J. Hoseini, and R. H. Fath, "Impedimetric ultrasensitive detection of chloramphenicol based on aptamer MIP using a glassy carbon electrode modified by 3-ampy-RGO and silver nanoparticle," *Colloids and Surfaces B: Biointerfaces*, vol. 183, 110451, 2019.

117. H. Song, L. Zhang, F. Yu, B.-C. Ye, and Y. Li, "Molecularly imprinted polymer functionalized nanoporous Au-Ag alloy microrod: Novel supportless electrochemical platform for ultrasensitive and selective sensing of metronidazole," *Electrochimica Acta*, vol. 208, 10-16, 2016.

118. S. Shahrokhian, N. Hosseini-Nassab, and Z. Kamalzadeh, "Fabrication of an electrochemical sensor based on the electrodeposition of Pt nanoparticles on multiwalled carbon nanotubes film for voltammetric determination of ceftriaxone in the presence of lidocaine, assisted by factorial-based response-surface methodology," *Journal of Solid State Electrochemistry*, vol. 18, 77-88, 2014.

119. X. Liu, S. Zheng, Y. Hu, Z. Li, F. Luo, and Z. He, "Electrochemical immunosensor based on the chitosan-magnetic nanoparticles for detection of tetracycline," *Food Analytical Methods*, vol. 9, 2972-2978, 2016.

120. D. J. Tranchemontagne, J. L. Mendoza-Cortés, M. O'keeffe, and O. M. Yaghi, "Secondary building units, nets and bonding in the chemistry of metal–organic frameworks," *Chemical Society Reviews*, vol. 38, no.5, pp. 1257-1283, 2009.

121. Z. Wang and S. M. Cohen, "Postsynthetic modification of metal–organic frameworks," *Chemical Society Reviews*, vol. 38, no.5, pp. 1315-1329, 2009.

122. M. Bougrini, A. Florea, C. Cristea, R. Sandulescu, F. Vocanson, A. Errachid, B. Bouchikhi, N. El Bari, and N. Jaffrezic-Renault, "Development of a novel sensitive molecularly imprinted polymer sensor based on electropolymerization of a microporous-metal-organic framework for tetracycline detection in honey," *Food Control*, vol. 59, 424-429, 2016.

123. W. Zhang, Z. Zhang, Y. Li, J. Chen, X. Li, Y. Zhang, and Y. Zhang, "Novel nanostructured MIL-101 (Cr)/XC-72 modified electrode sensor: A highly sensitive and selective determination of chloramphenicol," *Sensors and Actuators B: Chemical*, vol. 247, 756-764, 2017.

124. J. Li, X. Li, R. Yang, L. Qu, and P. d. B. Harrington, "A sensitive electrochemical chlorophenols sensor based on nanocomposite of ZnSe quantum dots and cetyltrimethylammonium bromide," *Analytica chimica acta*, vol. 804, 76-83, 2013.

125. Q. Liu, X. Lu, J. Li, X. Yao, and J. Li, "Direct electrochemistry of glucose oxidase and electrochemical biosensing of glucose on quantum dots/carbon nanotubes electrodes," *Biosensors and Bioelectronics*, vol. 22, no.12, pp. 3203-3209, 2007.

126. S. Khene and T. Nyokong, "Redox activity of CdTe quantum dots linked to nickel tetraaminophthalocyanine: Effects of adsorption versus electrodeposition on the catalytic oxidation of chlorophenols," *Microchemical Journal*, vol. 99, no.2, pp. 478-485, 2011.

127. D. Vijian, S. V. Chinni, L. S. Yin, B. Lertanantawong, and W. Surareungchai, "Non-protein coding RNA-based genosensor with quantum dots as electrochemical labels for attomolar detection of multiple pathogens," *Biosensors and Bioelectronics*, vol. 77, 805-811, 2016.

128. M. Pedrero, S. Campuzano, and J. M. Pingarrón, "Quantum dots as components of electrochemical sensing platforms for the detection of environmental and food pollutants: a review," *Journal of AOAC International*, vol. 100, no.4, pp. 950-961, 2017.

129. J. Shan, R. Li, K. Yan, Y. Zhu, and J. Zhang, "In situ anodic stripping of Cd (II) from CdS quantum dots for electrochemical sensing of ciprofloxacin," *Sensors and Actuators B: Chemical*, vol. 237, 75-80, 2016.

130. J.-Y. Huang, T. Bao, T.-X. Hu, W. Wen, X.-H. Zhang, and S.-F. Wang, "Voltammetric determination of levofloxacin using a glassy carbon electrode modified with poly (o-aminophenol) and graphene quantum dots," *Microchimica Acta*, vol. 184, 127-135, 2017.

131. A. M. Santos, A. Wong, F. H. Cincotto, F. C. Moraes, and O. Fatibello-Filho, "Square-wave adsorptive anodic stripping voltammetric determination of norfloxacin using a glassy carbon electrode modified with carbon black and CdTe quantum dots in a chitosan film," *Microchimica Acta*, vol. 186, 1-10, 2019.

132. X. Que, B. Liu, L. Fu, J. Zhuang, G. Chen, and D. Tang, "Molecular imprint for electrochemical detection of streptomycin residues using enzyme signal amplification," *Electroanalysis*, vol. 25, no.2, pp. 531-537, 2013.

133. F. Conzuelo, M. Gamella, S. Campuzano, A. J. Reviejo, and J. M. Pingarrón, "Disposable amperometric magneto-immunosensor for direct detection of tetracyclines antibiotics residues in milk," *Analytica chimica acta*, vol. 737, 29-36, 2012.

134. Z.-g. Yu, A. L. Sutlief, and R. Y. Lai, "Towards the development of a sensitive and selective electrochemical aptamer-based ampicillin sensor," *Sensors and Actuators B: Chemical*, vol. 258, 722-729, 2018.

135. H.-Y. Chen, J. Wang, L. Meng, T. Yang, and K. Jiao, "Thin-layered MoS2/polyaniline nanocomposite for highly sensitive electrochemical detection of chloramphenicol," *Chinese Chemical Letters*, vol. 27, no.2, pp. 231-234, 2016.

136. K. Zarei and A. Khodadadi, "Very sensitive electrochemical determination of diuron on glassy carbon electrode modified with reduced graphene oxide–gold nanoparticle–Nafion composite film," *Ecotoxicology and environmental safety*, vol. 144, 171-177, 2017.

137. K.-J. Huang, X. Liu, W.-Z. Xie, and H.-X. Yuan, "Electrochemical behavior and voltammetric determination of norfloxacin at glassy carbon electrode modified with multi walled carbon nanotubes/Nafion," *Colloids and Surfaces B: Biointerfaces*, vol. 64, no.2, pp. 269-274, 2008.

138. W. Lian, S. Liu, J. Yu, J. Li, M. Cui, W. Xu, and J. Huang, "Determination of oxytetracycline with a gold electrode modified by chitosan-multiwalled carbon nanotube multilayer films and gold nanoparticles," *Analytical Letters*, vol. 46, no.7, pp. 1117-1131, 2013.

139. M. P. Kingsley, P. K. Kalambate, and A. K. Srivastava, "Simultaneous determination of ciprofloxacin and paracetamol by adsorptive stripping voltammetry using copper zinc ferrite nanoparticles modified carbon paste electrode," *RSC advances*, vol. 6, no.18, pp. 15101-15111, 2016.

140. L. V. Faria, J. F. Pereira, G. C. Azevedo, M. A. Matos, R. A. Munoz, and R. C. Matos, "Square-wave voltammetry determination of ciprofloxacin in pharmaceutical formulations and milk using a reduced graphene oxide sensor," *Journal of the Brazilian Chemical Society*, vol. 30, 1947-1954, 2019.

141. J. Shan, Y. Liu, R. Li, C. Wu, L. Zhu, and J. Zhang, "Indirect electrochemical determination of ciprofloxacin by anodic stripping voltammetry of Cd (II) on graphene-modified electrode," *Journal of Electroanalytical Chemistry*, vol. 738, 123-129, 2015.

142. Y. Du, X.-L. Luo, J.-J. Xu, and H.-Y. Chen, "A simple method to fabricate a chitosan-gold nanoparticles film and its application in glucose biosensor," *Bioelectrochemistry*, vol. 70, no.2, pp. 342-347, 2007.

143. A. Benvidi, A. Dehghani-Firouzabadi, M. Mazloum-Ardakani, B.-B. F. Mirjalili, and R. Zare, "Electrochemical deposition of gold nanoparticles on reduced graphene oxide modified glassy carbon electrode for simultaneous determination of levodopa, uric acid and folic acid," *Journal of Electroanalytical Chemistry*, vol. 736, 22-29, 2015.

144. B. J. Sanghavi, P. K. Kalambate, S. P. Karna, and A. K. Srivastava, "Voltammetric determination of sumatriptan based on a graphene/gold nanoparticles/Nafion composite modified glassy carbon electrode," *Talanta*, vol. 120, 1-9, 2014.

145. Y. Ahmed, M. M. Rahman, M. S. Alam, M. I. Miah, M. S. H. Choudhury, O. A. Alharbi, P. Akhtar, and S. M. Rahman, "Harnessing neural network model with optimization for enhanced ciprofloxacin antibiotic adsorption from contaminated water: A transparent and objective framework," *Journal of Water Process Engineering*, vol. 65, 105724, 2024.

146. Z. H. Jaffari, A. Abbas, C.-M. Kim, J. Shin, J. Kwak, C. Son, Y.-G. Lee, S. Kim, K. Chon, and K. H. Cho, "Transformer-based deep learning models for adsorption capacity prediction of heavy metal ions toward biochar-based adsorbents," *Journal of Hazardous Materials*, vol. 462, 132773, 2024.

147. A. Casas, D. Rodríguez-Llorente, G. Rodríguez-Llorente, J. García, and M. Larriba, "Machine learning screening tools for the prediction of extraction yields of pharmaceutical compounds from wastewaters," *Journal of Water Process Engineering*, vol. 62, 105379, 2024.

148. A. Natekin and A. Knoll, "Gradient boosting machines, a tutorial," *Frontiers in Neurorobotics*, vol. 7, 2013.

149. L. Xia, P. Zheng, J. Li, X. Huang, and R. X. Gao, "Histogram-based Gradient boosting tree: A federated learning approach for collaborative fault diagnosis," *IEEE/ASME Transactions on Mechatronics*, 1-12, 2023.

150. T. Chen and C. Guestrin. *XGBoost: A scalable tree boosting system*. in *Proceedings of the 22nd acm sigkdd international conference on knowledge discovery and data mining*. 2016.

151. L. Breiman, "Bagging predictors," *Machine Learning*, vol. 24, no.2, pp. 123-140, 1996.

152. L. Breiman, "Random Forests," *Machine Learning*, vol. 45, no.1, pp. 5-32, 2001.

153. P. Geurts, D. Ernst, and L. Wehenkel, "Extremely randomized trees," *Machine Learning*, vol. 63, no.1, pp. 3-42, 2006.

154. P. Geurts, A. Irrthum, and L. Wehenkel, "Supervised learning with decision tree-based methods in computational and systems biology," *Molecular Biosystems*, vol. 5, no.12, pp. 1593-1605, 2009.

155. D. Opitz and R. Maclin, "Popular ensemble methods: An empirical study," *Journal of artificial intelligence research*, vol. 11, 169-198, 1999.

156. S. Pattaweepaiboon, W. Hirunpinyopas, P. Iamprasertkun, K. Pimphor, S. Roddecha, D. Dirayanti, A. Boonchun, and W. Sirisaksoontorn, "Upcycling electrode materials from spent single-use zinc-carbon/alkaline batteries into rechargeable lithium-ion battery application," *Journal of Energy Storage*, vol. 76, 109755, 2024.

157. W. D. Adane, B. S. Chandravanshi, and M. Tessema, "A simple, ultrasensitive and cost-effective electrochemical sensor for the determination of ciprofloxacin in various types of samples," *Sensing and Bio-Sensing Research*, vol. 39, 100547, 2023.

158. H. Ali, E. Khan, and I. Ilahi, "Environmental chemistry and ecotoxicology of hazardous heavy metals: environmental persistence, toxicity, and bioaccumulation," *Journal of chemistry*, vol. 2019, no.1, pp. 6730305, 2019.

159. H. S. Magar, R. Y. A. Hassan, and A. Mulchandani, "Electrochemical impedance spectroscopy (EIS): Principles, construction, and biosensing applications," *Sensors*, vol. 21, no.19, pp. 6578, 2021.

160. H. S. Magar, R. Y. Hassan, and A. Mulchandani, "Electrochemical impedance spectroscopy (EIS): Principles, construction, and biosensing applications," *Sensors*, vol. 21, no.19, pp. 6578, 2021.

161. M. Ahsan, M. M. Rahman, A. E. Alsafrani, M. A. Aziz, A. Almahri, H. M. Marwani, M. M. Rahman, and M. A. Hasnat, "Immobilization of poly (o-

aminophenol) film on Pt surface: A robust sensor for detecting As (III) in an acidic medium," *Surfaces and Interfaces*, vol. 39, 102976, 2023.

162. M. Ahsan, M. M. Rahman, A. E. Alsafrani, M. A. Aziz, A. Almahri, H. M. Marwani, M. M. Rahman, and M. A. Hasnat, "Immobilization of poly(o-aminophenol) film on Pt surface: A robust sensor for detecting As(III) in an acidic medium," *Surfaces and Interfaces*, vol. 39, 102976, 2023.

163. A. Chaabani, T. Ben Jabrallah, and N. Belhadj Tahar, "Electrochemical oxidation of ciprofloxacin on COOH-Functionalized multi-walled carbon nanotube–coated vitreous carbon electrode," *Electrocatalysis*, vol. 13, no.4, pp. 402-413, 2022.

164. R. Chauhan, A. A. S. Gill, Z. Nate, and R. Karpoormath, "Highly selective electrochemical detection of ciprofloxacin using reduced graphene oxide/poly(phenol red) modified glassy carbon electrode," *Journal of Electroanalytical Chemistry*, vol. 871, 114254, 2020.

165. S. A. C. Carabineiro, T. Thavorn-Amornsri, M. F. R. Pereira, and J. L. Figueiredo, "Adsorption of ciprofloxacin on surface-modified carbon materials," *Water Research*, vol. 45, no.15, pp. 4583-4591, 2011.

166. L. Yang and A. Shami, "On hyperparameter optimization of machine learning algorithms: Theory and practice," *Neurocomputing*, vol. 415, 295-316, 2020.

167. F. Nogueira, "Bayesian optimization: Open source constrained global optimization tool for Python," 2014.

168. A. H. Victoria and G. Maragatham, "Automatic tuning of hyperparameters using Bayesian optimization," *Evolving Systems*, vol. 12, no.1, pp. 217-223, 2021.

169. D. Chicco, M. J. Warrens, and G. Jurman, "The coefficient of determination R-squared is more informative than SMAPE, MAE, MAPE, MSE and RMSE in regression analysis evaluation," *Peerj computer science*, vol. 7, e623, 2021.

170. R. Selvaraj, S. Jogi, G. Murugesan, N. R. Srinivasan, L. C. Goveas, T. Varadavenkatesan, A. Samanth, R. Vinayagam, M. Ali Alshehri, and A. Pugazhendhi, "Machine learning and statistical physics modeling of tetracycline adsorption using activated carbon derived from *Cynometra ramiflora* fruit biomass," *Environmental Research*, vol. 252, 118816, 2024.

171. R. Antonelli, G. R. P. Malpass, M. G. C. da Silva, and M. G. A. Vieira, "Adsorption of ciprofloxacin onto thermally modified bentonite clay: Experimental design, characterization, and adsorbent regeneration," *Journal of Environmental Chemical Engineering*, vol. 8, no.6, pp. 104553, 2020.

172. N. Watanabe, S. Horikoshi, H. Hidaka, and N. Serpone, "On the recalcitrant nature of the triazinic ring species, cyanuric acid, to degradation in Fenton solutions and in UV-illuminated TiO_2 (naked) and fluorinated TiO_2 aqueous dispersions," *Journal of Photochemistry and Photobiology A: Chemistry*, vol. 174, no.3, pp. 229-238, 2005.

173. J. Chuiprasert, S. Srinives, N. Boontanon, C. Polprasert, N. Ramungul, A. Karawek, and S. K. Boontanon, "Ciprofloxacin electrochemical sensor using copper–iron mixed metal oxides nanoparticles/reduced graphene oxide composite," *ACS Omega*, vol. 9, no.22, pp. 23172-23183, 2024.

174. A. A. Ensafi, A. R. Allafchian, and R. Mohammadzadeh, "Characterization of $MgFe_2O_4$ nanoparticles as a novel electrochemical sensor: Application for the voltammetric determination of ciprofloxacin," *Analytical Sciences*, vol. 28, no.7, pp. 705-710, 2012.

175. Y. Yuan, F. Zhang, H. Wang, L. Gao, and Z. Wang, "A sensor based on Au nanoparticles/carbon nitride/graphene composites for the detection of chloramphenicol and ciprofloxacin," *ECS Journal of Solid State Science and Technology*, vol. 7, no.12, pp. M201, 2018.

176. X. Fang, X. Chen, Y. Liu, Q. Li, Z. Zeng, T. Maiyalagan, and S. Mao, "Nanocomposites of Zr(IV)-based metal–organic frameworks and reduced graphene oxide for electrochemically sensing ciprofloxacin in Water," *ACS Applied Nano Materials*, vol. 2, no.4, pp. 2367-2376, 2019.

177. S. G. Surya, S. Khatoon, A. Ait Lahcen, A. T. H. Nguyen, B. B. Dzantiev, N. Tarannum, and K. N. Salama, "A chitosan gold nanoparticles molecularly imprinted polymer based ciprofloxacin sensor," *RSC Advances*, vol. 10, no.22, pp. 12823-12832, 2020.

178. J. Zhao, P. Huang, and W. Jin, "Electrochemical sensor based on TiO2/polyvinyl alcohol nanocomposite for detection of ciprofloxacin in rainwater," *International Journal of Electrochemical Science*, vol. 16, no.10, pp. 211018, 2021.

179. M. Yahyapour, M. Ranjbar, and A. Mohadesi, "Determination of ciprofloxacin drug with molecularly imprinted polymer/co- metal organic framework nanofiber on modified glassy carbon electrode (GCE)," *Journal of Materials Science: Materials in Electronics*, vol. 32, no.3, pp. 3180-3190, 2021.

180. H. S. Vedhavathi, B. P. Sanjay, M. Basavaraju, B. S. Madhukar, and N. K. Swamy, "Development of ciprofloxacin sensor using iron-doped graphitic carbon nitride as transducer matrix: Analysis of ciprofloxacin in blood samples," *Journal of Electrochemical Science and Engineering*, vol. 12, no.1, pp. 59-70, 2022.